# STRUCTURAL CONNECTIVITY ALTERS IN PEDIATRIC SYSTEMIC LUPUS ERYTHEMATOSUS PRIOR TO NEUROPSYCHIATRIC MANIFESTATIONS

A THESIS SUBMITTED TO

THE GRADUATE SCHOOL OF ENGINEERING AND SCIENCE

OF BILKENT UNIVERSITY

IN PARTIAL FULFILLMENT OF THE REQUIREMENTS FOR

THE DEGREE OF

MASTER OF SCIENCE

IN

NEUROSCIENCE

By

Laleh Eskandarian

February 2022

Structural connectivity alters in Pediatric Systemic Lupus Erythematosus prior to neuropsychiatric manifestations

By Laleh Eskandarian

February 2022

We certify that we have read this thesis and that in our opinion it is fully adequate, in scope and in quality, as a thesis for the degree of Master of Science.

Ergin Atalar (Advisor)

Hatice Kader Karlı Oğuz (Co-Advisor)

Sadriye Ebru Çengel Kültür

Emine Ülkü Sarıtaş Çukur

Approved for the Graduate School of Engineering and Science:

Ezhan Karaşan

Director of the Graduate School

# ABSTRACT

## Structural connectivity alters in Pediatric Systemic Lupus Erythematosus prior to neuropsychiatric manifestations

By Laleh Eskandarian
M.S. in Neuroscience
Advisor: Ergin Atalar
Co-advisor: Hatice Kader Karlı Oğuz
February 2022

Systemic lupus erythematosus (SLE) is an autoimmune multi-system disorder affecting the central nervous system which may exhibit neuropsychiatric manifestations. Pediatric-onset SLE is rare and although there is an increased risk of neuropsychiatric symptoms, underlying pathological mechanisms remain poorly understood. This study explored the entire white matter network with brain structural connectivity and DTI tractography analysis to provide a better understanding of the probable connectivity alterations.

Whole-brain structural connectivity and tractography of 17 pediatric-onset SLE patients without neuropsychiatric involvement (non-NPSLE) and 8 age and gender matched healthy controls were explored. To investigate the topological structure, graph theory analysis was applied. Global and nodal network features were derived by estimating structural connectivity matrices between 360 brain regions of the HCP atlas.

Non-NPSLE patients demonstrated higher network characteristic path length and assortativity and lower density and global efficiency compared with healthy controls. The hubs were selected according to the strength of the nodes and their structure and distribution were changed in the patients. According to the altered hubs' network characteristics significant modifications between HCs and non-NPSLE, along with TBSS findings, altered regions were observed in language, visual, auditory, and motor-related areas. These findings are in good agreement with WISC-IV Verbal

Comprehension Index. Compared to healthy controls non-NPSLE patients showed significantly lower scores according to WISC-IV score components.

To conclude, from a network and connectivity perspective, our research demonstrated an altered topological structure of the brain in non-NPSLE patients. The findings of this study provide a better understanding of the structural alterations underlying pediatric-onset non-NPSLE patients' functional and neurocognitive abnormalities.

*Keywords*: Non-Neuropsychiatric Pediatric Systemic Lupus Erythematosus (Pediatric non-NPSLE), Structural brain connectivity, Diffusion Tensor Imaging (DTI), Probabilistic tractography, Graph theory, WISC-IV

# ÖZET

## Nöropsikiyatrik Belirtilerden Önce Pediatrik Sistemik Lupus Eritematozus'ta Yapısal Bağlantı Değişiklikleri

Laleh Eskandarian
Nörobilim, Yüksek Lisans
Danışman: Ergin Atalar
Eş danışman: Hatice Kader Karlı Oğuz
Şubat 2022

Sistemik lupus eritematozus (SLE), merkezi sinir sistemini etkileyen ve nöropsikiyatrik belirtiler gösterebilen otoimmün, multisistemik bir hastalıktır. Çocukluk çağı başlangıçlı SLE nadirdir ve nöropsikiyatrik tutulumun yüksek oluşuna karşın, altta yatan patolojik mekanizmalar tam olarak anlaşılamamıştır. Bu çalışma, olası bağlantısallık değişikliklerinin daha iyi anlaşılmasını sağlamak için difüzyon tensör görüntüleme (DTI) traktografi analizi ile tüm beyaz madde ağını araştırdı.

Nöropsikiyatrik tutulumu olmayan (NPSLE olmayan) 17 pediatrik başlangıçlı SLE hastası ve 8 yaş ve cinsiyet uyumlu sağlıklı kontrolün tüm beyin yapısal bağlantısı ve traktografisi araştırıldı. Topolojik yapıyı araştırmak için graf (çizge) teorisi analizi uygulandı. Küresel ve düğümsel ağ özellikleri, HCP atlasının 360 beyin bölgesi arasındaki yapısal bağlantı matrisleri ile elde edildi.

NPSLE olmayan hastalar, sağlıklı kontrollerle karşılaştırıldığında daha yüksek ağ karakteristik yol uzunluğu ve sınıflandırılması ve daha düşük yoğunluk ve global verimlilik gösterdi. Hublar düğümlerin gücüne göre seçilmiş ve hastalarda yapıları ve dağılımları değişmiştir. Değişen Hubların ağ özelliklerine göre, önemli değişiklikler TBSS bulguları ve değişen bölgeler ile birlikte sağlıklı kontroller ve NPSLE olmayanlar arasında, dil, görsel, işitsel ve motorla ilgili alanlarda gözlendi. Bu bulgular WISC-IV Sözel Anlama İndeksi ile iyi bir uyum içindedir. Sağlıklı kontrollerle karşılaştırıldığında, NPSLE olmayan hastalar, WISC-IV skor bileşenlerine göre anlamlı derecede daha düşük skorlar gösterdi.

Sonuç olarak, ağ ve bağlantısallık perspektifinden, araştırmamız NPSLE olmayan hastalarda beynin belirtilerin ortaya çıkmasından önce ortaya çıkmış topolojik yapısını gösterdi. Difüzyon tensör görüntüleme ile bağlantısallık çalışmaları, çocukluk çağında başlayan SLE'de gelişen fonksiyonel ve nörobilişsel anormalliklerinin altında yatan yapısal değişikliklerin daha iyi anlaşılmasını sağlar.

*Anahtar Kelimeler*: Pediatrik Sistemik Lupus Eritematozus (NPSLE olmayan Pediatrik), Beyin, MRG, Difüzyon Tensör Görüntüleme (DTI), Olasılıksal traktografi, Graf (çizge) teorisi, WISC-IV

# Acknowledgment

I could not have hoped for a better advisor than Prof. Kader Karli Oguz. I would like to express my sincere gratefulness to Kader Hoca for the great opportunities, continued guidance, and infinite support throughout my MSc studies. Without her knowledge, encouragement, enthusiasm, patience, and perfection I would not be able to put my effort into my research. My appreciation also extends to Prof. Ergin Atalar for his incredibly generous support, valuable guidance, help, and advice over the past years. I would like to thank him for providing such a professional, great, and motivating research environment at UMRAM. I am fortunate, honored, and privileged to be a student of Kader Hoca and Ergin Hoca.

I am indebted to my thesis jury members, Prof. Ebru Cengel Kültür and Prof. Emine Ülkü Sarıtaş for their guidance and eagerness to serve on my MSc committee. Thanks for their precious time and effort in assessing this thesis.

I would like to extend my special thanks to all my lab mates and colleagues at UMRAM and all UMRAM family, especially Hacer Daşgın, Meltem Karataş, Aydan Ercingoz, and Cemre Ariyurek for providing such a professional and friendly environment and my dearest friends Bahram, Sepideh, Elnaz, Maryam, Gamze, Naeimeh, Fatemeh, Fariba, Zeinab, Aysan, Reza, Amir, Alireza, Sina, Wiria and many others for their friendliness and favors who made my time in Bilkent unforgettable episode of my life.

My greatest gratitude and love go to my lovely parents, grandmothers, my dearest sister Ladan and my family for their enduring support, encouragement, and love. I am forever indebted to you for the love and support you have shown me.

Finally, and above all, I would like to thank Ehsan, the love of my life and my best and dearest friend. Words fail to extend my gratitude for your love and support during this journey. I thank and love you with every nerve of my body.

# Content

# List of Figures

# List of Tables

# List of Abbreviations

| Abbreviation | Definition |
|---|---|
| 1 | Primary somatosensory cortex |
| 4 | M1, or primary motor cortex |
| 52 | Medial belt, transitional auditory area |
| 10d | Part of prefrontal cortical area |
| 23c | Part of posterior cingulate cortex (PCC) |
| 3b | Primary sensory cortex |
| 5mv | Subdivision of the parietal cortex, medial ventral |
| 6a | Premotor cortex and supplementary motor cortex anterior |
| 6ma | Part of premotor regions (anterior supplementary motor areas) |
| 6mp | Part of premotor regions (posterior supplementary motor areas) |
| 8BL | Part of lateral frontal lobe |
| 8BM | Part of medial frontal lobe |
| 9-46d | Part of dorsolateral prefrontal cortex |
| 9a | Anterior portion of Dorsolateral prefrontal cortex |
| 9m | Medial portion of Dorsolateral prefrontal cortex |
| A | Anterior |
| a24 | Part of medial frontal lobe |
| a32pr | Anterior subdivision of dorsal anterior cingulate area |

| | |
|---|---|
| ACR | American College of Rheumatology |
| ADC | Apparent diffusion coefficient |
| BC | Betweenness centrality |
| CC | Clustering coefficient |
| CNS | Central nervous system |
| pSLE | Pediatric onset systemic lupus erythematosus |
| d32 | Part of dorsal anterior cingulate area |
| DVT | Dorsal visual transitional area |
| FA | Fractional anisotropy |
| FFC | Fusiform face complex |
| fMRI | Functional magnetic resonance imaging |
| GE | Global efficiency |
| H | Hippocampus |
| HC | Healthy controls |
| Ig | Insular granular complex |
| IP0 | intraparietal 0 |
| IP1 | Intraparietal 1 |
| IPS1 | Intraparietal sulcus 1 |
| L | Left |
| LE | Local efficiency |
| MBelt | Medial belt complex |
| MS | Multiple sclerosis |
| n.s. | Not significant |
| NA | Not applicable |
| NCD | Neurocognitive dysfunction |
| NP | Neuropsychiatric |

| | |
|---|---|
| P | Posterior |
| p10p | Lateral frontal lobe |
| p24 | Posterior subdivisions of anterior cingulate cortex |
| PGp | Parietal area G, posterior |
| PGs | Parietal area G, superior |
| PH | Part of lateral occipital lobe |
| PHA1 | Parahippocampal area 1 |
| PHA3 | Parahippocampal area 3 |
| PHT | Part of middle temporal gyrus |
| PoI1 | Posterior Insular 1 |
| PoI2 | Posterior Insular 2 |
| POS2 | Parieto-occipital sulcus 2 |
| PreS | Presubiculum |
| R | Right |
| SCEF | Supplementary and cingulate eye field |
| SD | Standard deviation |
| SLF | Superior longitudinal fasciculus |
| SLE | Systemic lupus erythematosus |
| SLEDAI | Systemic lupus disease activity index |
| SLICC | Systemic lupus erythematosus international collaborating clinics |
| STAI State | State anxiety inventory |
| STAI Trait | State-trait anxiety inventory |
| TBSS | Tract-based spatial statistics |
| TE1p | Area TE1 posterior, part of middle temporal gyrus |
| V1 | Primary visual cortex |

| | |
|---|---|
| V2 | Second visual area |
| V3 | Third visual area |
| V4 | Fourth visual area |
| V6 | Sixth visual area |
| V7 | Seventh visual area |
| V8 | Eighth visual area |
| VMV1 | Ventro medial visual area 1 |
| VVC | Ventral visual complex |
| WICSIVNS | WISC-IV Number sequencing |
| WISCIVFS | WISC-IV Full Scale Intelligence Quotient |
| WISCIVPR | WISC-IV Perceptual Reasoning score |
| WISCIVPS | WISC-IV Processing Speed score |
| WISCIVVC | WISC-IV Verbal Comprehension score |
| WISCIVVOC | WISC-IV Vocabulary |
| WISCIVWM | WISC-IV Working Memory score |
| WM | White matter |

# Chapter 1

# Introduction and background

Systemic lupus erythematosus (SLE, lupus) is a multi-system autoimmune disease clinically characterized by flare and remissions. Widespread inflammation and tissue damage are seen in various organ systems, including the brain. The disease is distinguished at the molecular level by an inflammatory process that is directed against the self and is modulated by autoantibodies. Females are affected about ten times more frequently than males [1]. Ethnicity plays a role in the prevalence of SLE, overall estimated to affect about one out of every 1,000 persons [1]. The disease presents three to four times less in people of European ancestry than in those of Asian, African, Caribbean, and Hispanic descent [2].

Initial SLE symptoms usually appear between the ages of 20 and 40 [3][4]; however, approximately 15-20% of the patients have their initial symptoms in childhood [5]. As with other diseases, onset under the age of 18 years is referred to as 'pediatric-onset systemic lupus erythematosus' (pSLE) [6]. pSLE is very rare, with an annual incidence and prevalence of 0.3-0.9 and 3.3-24 per 100,000 in Asian and Native American children, respectively [7]. The mean age of presentation is between 11 and 12 years old, with pSLE seldom occurring before the age of 5 years [8]. Generally, pSLE presents with a more severe clinical course than adult SLE and tends to have a higher prevalence of nephritis, neuropsychiatric, hematologic abnormalities, photosensitivity, as well as mucocutaneous involvement [7][9][10].

Abnormalities in the central nervous system (CNS) reveal themselves most often within the first year after diagnosis, and they may potentially be a presenting symptom

of pSLE [11]. Headaches, new-onset seizures, mood disorders, psychosis, chorea, and cerebrovascular disease are the reported CNS manifestations [12]. Depression and anxiety constitute prevalent symptoms in adult SLE patients affecting 24 to 57 % of these patients [13]. In a longitudinal study, it was found that although the absence of clinical attack reduced psychological distress, levels of depression did not change between patients with and without the active disease [14]. However, Moorthy LN et al. showed that the life quality and physical functioning of children with SLE did not correlate considerably with disease activity [15]. On the other hand, SLE-related emotional and behavioral disorders in children have received less attention in the medical literature.

Neuropsychiatric systemic lupus erythematosus (NPSLE) is the most prevalent complication of SLE and develops when the pathogenic etiologies affect the CNS. NPSLE has been documented in around 75% of SLE patients with a variety of clinical symptoms, including headaches, mood disorders, cognitive dysfunctions, and seizures [16]. Non-NPSLE patients are those with SLE who have no neuropsychiatric symptoms [17]. Despite the fact that non-NPSLE individuals do not exhibit neuropsychiatric symptoms, neuroimaging studies have revealed that their brains have certain structural and functional abnormalities [17].

Diagnosis of NPSLE is an exclusionary one, meaning that any other possible causes, such as acute or chronic infections, recreational drugs, primary mental illness, cancer, trauma, or metabolic disorders, must be ruled out before moving on with the diagnosis [18]. Magnetic resonance imaging (MRI) of the brain and neurocognitive testing are now frequently employed for assessment. Standard Gd-based contrast-enhanced brain MRI is frequently performed in patients with NPSLE to document disease effects on the brain and also rule out other neurologic diseases or systemic diseases presenting a similar clinical scenario [19][20].

Pediatric-onset disease has a higher-than-average chance of developing NPSLE. However, the processes that underlie the wide variety of NPSLE are still not well understood. It is estimated that NPSLE affects between 22-95% of children with pSLE [21][22]. Studies have shown that up to 60% of all children who develop pSLE experience acquired neurocognitive dysfunction (NCD) later in life [22]. The diagnosis of NCD is made by the use of a range of standardized tests [23]. NCD

without a major neurologic deficit or clinical symptom reveals no abnormality in most of the cases on conventional brain MRI [24]. According to functional magnetic resonance imaging (fMRI) studies, some abnormalities in multiple functional systems, such as learning memory [25], working memory [26][27], language processing functional systems [28], and attention [26], have been observed in non-NPSLE patients groups. In terms of brain structure, the thickness and volume of gray matter as studied by MRI in an adult non-NPSLE group are both normal [29].

An MRI technique, known as diffusion tensor imaging (DTI), allows for the assessment of the microstructure and structural connectivity of white-matter tracts. In adults with diverse symptoms of NPSLE, recent research has indicated alterations in white-matter tracts [30][31]; however, studies explicitly evaluate DTI correlations of SLE with NCD but with neuropsychiatric symptoms in children are sparse. Patients with non-NPSLE were shown to have some abnormalities in the white matter integrity, revealed by the latest DTI studies [32]. It appears that the structure and function of the brain in patients without NPSLE are already affected, and abnormalities/disruption of the white matter plays an important role in this process [32][33].

## 1.1 Magnetic Resonance Imaging

MRI has become a valuable tool in the diagnosis and classification of brain diseases. Apart from overt imaging abnormalities arising from tissue involvement, MRI enabled understanding the structural connectivity patterns via a thorough map of the structural connections of the human brain. Individuals with SLE may exhibit abnormalities on such MRI scans, although these abnormalities are neither sensitive nor specific for SLE. Some individuals have significant neuropsychological involvement yet seem to have normal-appearing MRIs, while others have abnormalities on MRIs despite the lack of neuropsychological symptoms in one or more instances [34][35]. Technological advancements in non-invasive neuroimaging, along with the development of strong network modeling tools, have paved the way for new horizons. This prompted researchers to investigate quantitative imaging approaches such as Diffusion Tensor Imaging (DTI), which may be able to detect more subtle changes in the brain parenchyma prior to their appearance on conventional MRI.

## 1.2 Conventional MRI Sequences

Conventional MRI (cMRI) sequences are fundamental for radiological evaluation of the brain. This term refers to a well-defined collection of common MRI acquisition procedures that enable the capture of in-vivo anatomical images of the brain or, more broadly, the human body. Different sets of MR images may be formed by altering the sequence parameters of applied and collected RF pulses. MRI is a medical imaging modality [36] that is often used to evaluate the soft tissues of the human body. Magnet, radio waves, gradient, and computer are the critical components of MR imaging. Our bodies are composed of 60% water, of which each molecule contains an oxygen atom bonded to two hydrogen atoms (H2O). Small subatomic particles of hydrogen behave as small magnets and are extremely sensitive to magnetic fields. Usually, the water molecules inside the body are randomly distributed, but when the body is surrounded by a magnetic field, the majority of the water molecules move at the same rhythm or frequency as that of the magnetic field. Low-energy water molecules are those that do not move in the direction of the magnetic field. The low-energy water molecules are targeted by the MRI scanner in order to build an image of body sections. By transmitting radio waves that resonate with the magnetic field, the low-energy water molecules absorb the energy required to move in the magnetic field's direction. When the MRI scanner stops generating radio waves, the water molecules that have been moving alongside the magnetic field directions release the energy that they have absorbed and return to their original position. The MRI scanner detects this movement and transmits the signal to a computer, utilizing imaging software to translate the data into a body image. By imaging the body in different sections of the magnetic field, the MRI scanner creates a three-dimensional image of the organs that need to be evaluated for a diagnosis. In an MRI scanner, multiple transmitted radio waves in sequence (called RF pulses) can be emitted to the patient body to highlight specific tissues or abnormalities [36]. A distinct emphasis could occur in MRI images because various tissues relax at diverse rates when the MRI scanner stops generating RF pulse. By changing the sequence of transmitted and received RF pulses, an MRI scanner can generate different body image sets featuring various soft tissue characteristics. Repetition Time (TR) is the time interval between consecutive RF pulse sequences emitted to the same body slice. The time interval between the delivery of the RF pulse and the receiving of the echo signal is referred to as the Time to Echo (TE).

Almost all brain MRI studies include T1-weighted (W) and T2-W sequences, as well as Fluid Attenuated Inversion Recovery (FLAIR) sequence in which cerebrospinal fluid signal is suppressed using an inversion recovery pulse and increased tissue water caused by pathological disturbances, is exaggerated, thus more amenable to visual detection. Apart from these MRI sequences, additional imaging sequences are used according to the problem in patients' management or scientific research. In addition to the advantages of high resolution multiplanar soft tissue imaging, the lack of X-ray radiation, unlike other imaging modalities such as conventional x-ray or computed tomography (CT) imaging, enables repeatability of studies.

### 1.2.1 T1-Weighted Imaging

The T1-weighted sequences are generated by setting the TR parameter to a value less than T1 time (~500 ms) and the TE parameter to a value less than T2 time (~14 ms). For paramagnetic contrast agents (e.g., gadolinium-containing compounds), the T1-weighted sequence is especially advantageous since it provides the best contrast possible. This characteristic is critical, even more so in clinical contexts where contrast agents are required to provide an accurate diagnosis, most notably in brain-related disorders.

### 1.2.2 Diffusion MRI

Diffusion MRI (dMRI), and more precisely, Diffusion Tensor Imaging (DTI), are used to visualize the diffusion of water in the brain. The fundamental notion of diffusion is based on the premise that water is always in motion [37]. Water movement within a perfectly homogeneous environment has an equal probability throughout all directions, defined as 'isotropic diffusion'. The human body environment, on the other hand, has complicated structural properties; thus, diffusion characteristics so called 'anisotropic', and pathologic changes change the relative proportion of water distributed between intracellular and extracellular compartments [37].

The water molecules in our body are constantly moving in random directions under normal physiologic conditions. This type of motion is referred to as 'Brownian

Motion', the principal event of 'Diffusion' in physics. The magnetic resonance (MR) images can be responsive to this motion if proper diffusion-encoding gradients are employed. Diffusion weighted imaging (DWI) is the name given to this method. Water molecules in the body do not have free diffusion because they are constrained by cell membranes and impeded by macromolecules and proteins. Magnetic resonance imaging (MRI) can be used to estimate the diffusion coefficient by using diffusion sensitive gradients.

The calculated diffusion coefficient D is influenced by the microstructural environment because water molecules diffusion in biological tissue is inhibited and confined. The biological tissue features such as axon diameters and fiber bundle orientations can both be inferred from the estimation of D [38]. As a result, the brain's microstructure can be obtained from measurements of water molecule mobility in the brain. The apparent diffusion coefficient (ADC) is the estimated value of D that is lower than the actual diffusion coefficient (D) because of the tissue hindrances [39]. The Stejskal-Tanner pulsed gradient spin-echo (PGSE) is a common sequence in diffusion MRI. To tag the spin of water molecules with their spatial location, a diffusion gradient induces a phase shift along the gradient's path, which results in a dispersion of phase.

Once the diffusion time has elapsed, a second gradient with the exact same amplitude and length is applied in order to rephase the spins. Second gradients will restore the water molecules' phase if they haven't been displaced. Alternatively, if any water molecules have migrated, the spins' phase will not be fully recovered. Typically, three gradients are applied. The b-value determines how much diffusion affects the image's weighting. As a result, images are not weighted by diffusion when the b-value = 0. As long as the b-value is above zero (e.g., b=1,000), the images are weighted by diffusion.

DWI is a technique that permits non-invasive mapping of the diffusion process of molecules in biological tissues. It is possible to get both quantitative and qualitative information on diffusion characteristics using DWI. The contribution of DWI to radiologic diagnosis, in turn, neurology practices, is tremendous, especially in acute stroke and infections.

### 1.2.3 Diffusion Tensor Imaging

Similar to DWI, DTI is based on the diffusion of water molecules by their inherent thermal energy in the brain [40][41]. DWI is raw data which means it consists of diffusion maps in different directions, while DTI uses raw data to calculate tensors that contain matrices that present each voxels diffusion pattern which later can be used in white matter fiber tractography [41]. DTI data are obtained using diffusion weighting using at least six directions. This is used to compute the diffusion tensor and may be seen as an ellipsoid with a diffusion tensor, as seen in Figure 1.1. The diffusion tensor contains three orthogonal eigenvectors ($\varepsilon_1$, $\varepsilon_2$, and $\varepsilon_3$) that correspond to the tensor's principal axes [42]. They are scaled according to the amount of diffusion along the direction, which is represented by the diffusion tensor's eigenvalues ($\lambda_1$, $\lambda_2$, and $\lambda_3$) [42]. A significant benefit of measuring diffusion in this manner is that it is rotationally.

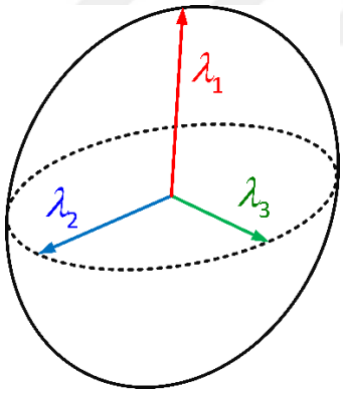


**Figure 1.1** - Diffusion Tensor Schematic Representation The three orthogonal eigenvectors are shown by arrows, which indicate their direction. The axes are scaled in accordance with the eigenvalues $\lambda_1$, $\lambda_2$, and $\lambda_3$, which are shown in the figure.

The ADC is a measure of the amount to which diffusion has occurred. In free water, molecules may flow around freely, resulting in a high ADC. ADC is dependent on biological barriers to water transport in the brain, such as cell walls and nerve fibers, with increased barriers resulting in decreased ADC [42].

In a given voxel, ADC defines the mean diffusivity (MD), which is determined as the average diffusion values along with three orthogonal directions, as explained in Equation 1.1 [42].

$$ADC = MD = \frac{(ADC_X + ADC_Y + ADC_Z)}{3} \tag{1.1}$$

The fractional anisotropy (FA) is used to measure the directionality of diffusion. Depending on the directional nature of the tissue, diffusion anisotropy might be affected [43]. Diffusion happens preferentially along rather than across long thin fibers, such as white matter tracts in the brain. As a result, diffusion within white matter is anisotropic, and its FA coefficient is a larger one. Gray matter diffusion, on the other hand, is not confined in any specific direction, resulting in greater isotropic diffusion and a lower FA than white matter [44].

FA is a scalar number between zero and one, where zero denotes isotropic diffusion (diffusion that is equal in all directions), and bigger values imply more anisotropy [44]. FA is derived from the diffusion tensor's eigenvalues [43].

$$FA = \sqrt{\frac{3}{2}} \frac{\sqrt{(\lambda_1 - \hat{\lambda})^2 + (\lambda_2 - \hat{\lambda})^2 + (\lambda_3 - \hat{\lambda})^2}}{\sqrt{{\lambda_1}^2 + {\lambda_2}^2 + {\lambda_3}^2}} \tag{1.2a}$$

$$\hat{\lambda} = \frac{(\lambda_1 + \lambda_2 + \lambda_3)}{3} \tag{1.2b}$$

The diffusion tensor is affected by anything that modifies the molecular environment, such as changes in the tissue compartments in the brain, and this impact may be measured quantitatively [45].

Diffusion magnitude parallel to fiber tracts is referred to as axial diffusivity (AD). A decrease in AD could be the result of axonal damage, a reduction in axonal diameter, or a less coherent axonal orientation [46].

Diffusion perpendicular to axonal fibers is referred to as radial diffusivity (RD). Demyelination, dysmyelination, and glial cell dysfunction are likely to be more closely associated with RD. In addition, RD may be affected by changes in axonal density or diameter [47].

The diffusion parameters can be determined within a specific region of interest or within a whole brain. This may be expressed as a mean value or shown graphically as a histogram [48].

Diffusion features have also been studied in SLE patients, showing higher mean ADC [31], [49]–[52], and lower mean FA in patients [30][50][31][52] compared with the healthy controls. Despite this overall finding of elevated ADC, one study reported that the amygdala of SLE patients had considerably lower ADC levels than those of healthy controls [53].

Different studies compared adult SLE patients with and without neuropsychiatric manifestations. It was found that NPSLE patients differed from their non-NPSLE counterparts in several regions; however, these differences were less pronounced compared to controls [32]. On the other hand, Emmer et al. examined mean ADC across the entire grey and white matter; they observed no significant differences between the NPSLE and SLE patient groups [53].

#### 1.2.3.1 Tractography

To get an idea of the white matter tracts' path through the brain, a technique termed "tractography" is frequently used in DTI [54]. Tractography is a non-invasive method that uses DTI to estimate and visualize fiber pathways. Although tractography enables mapping the connections in the brain, it does not offer physiological information about the connections, such as latency and conduction velocity, as opposed to electromyography. To categorize tractography algorithms, we can say that there are two main approaches: the deterministic method [54][55] and the probabilistic approach [56][57][58].

Tractography algorithms that are deterministic in nature [59][60] produce a streamline by following the primary direction in each voxel, with no consideration for any ambiguities, mostly due to crossing fibers. Deterministic tractography, on the other hand, always yields the same outcome, implying that the most likely direction would always be chosen in regions of high uncertainty. Deterministic algorithms are relatively rapid and enable the generation of quite reliable findings in WM fiber reconstruction when compared to other methods. The correctness of the path taken by the fibers is a limitation of this sort of tractography. These algorithms simply follow

one of the main routes without considering alternative approaches that might produce better results. A new class of probabilistic algorithms was created to get around this problem [61].

A method called probabilistic tractography was created to measure the degree of uncertainty in a voxel to estimate brain connections. Streamlines are generated using a probabilistic tractography algorithm which models the uncertainty degree within a voxel according to the direction from the estimated diffusion orientations' probability density function. Streamlines are repeated a few thousand times in order to produce a uniform distribution of fibers. A streamline count map is created once all streamlines are calculated using the number of streamlines that enter each voxel. A streamline count map in conjunction with a connectivity matrix provides information about the number of streamlines that connect two regions of interest together. The number of streamlines produced depends on a variety of factors, including the local variability in fiber orientation, the number of fibers aligned in a given orientation, the length of the pathway, fiber diameters, and uncertainty in each voxel. If one of the voxels along the trajectory is noisy, for example, the number of streamlines connecting two regions can be drastically reduced [62]. Connection maps can be generated using probabilistic algorithms that repeat the deterministic version multiple times by producing maps and randomly perturbing the principal fiber directions. These maps show the likelihood that a given voxel is related to a reference location [63].

## 1.3 Brain Connectivity Analysis using Graph Theory

It has been known that the neuronal elements of the brain constituted a formidably complicated structural network since the nineteenth century. Modern non-invasive imaging techniques applied to the human brain allow mapping its intricate networks of anatomical regions and neural pathways at near-millimeter resolution. The resulting large-scale networks provide a comprehensive description of the brain's structural connectivity, also called the human connectome [64].

### 1.3.1 Graph Theory

In mathematics, a graph may be used to analyze organized data and study them in the form of networks. To address the Konigsberg bridges problem (The Königsberg bridge

problem tests whether all seven bridges in the city of Königsberg could be visited in a single trip without requiring a retrace of any kind, with an additional restriction that the travel must finish up in the exact location as it started), Euler presented graph theory in 1735, which was the first time it had been used [65]. Graphs are mostly used to represent pairwise relationships between different objects [66]. A graph is made up of vertices (also known as nodes), which are linked by edges (also called links) and form a network. To put it another way, a graph is an ordered pair $G = (V, E)$, wherein V represents the set of vertices and E represents the set of edges defined as follows: $E \subseteq \{\{x, y\} \mid (x, y) \in V \times V\}$, where (x, y) represents non-ordered pairs of vertices [67]. To be more specific, this form of an object is referred to as an undirected graph. In contrast, a directed graph is a graph where the edges possess orientations. A graph, taking a broader view, is an ordered triple $G = (V, E, \omega)$, where each edge is associated with a value by the function $\omega$ (e.g., $\omega: E \rightarrow R$) [67]. These quantities are referred to as weights. As a result, graphs may be either weighted or unweighted [67].

Because graphs represent relationships, they are very strong models. By employing edges between nodes, a graph likely represents any form of relationship. Each node in the network is linked to a subset of the other nodes in the graph that define its neighborhood [67].

**Degree:** The degree of a node corresponds to the number of edges that link that node to the others. This degree represents the number of nodes that are adjacent to each other in an undirected graph, the number of incoming/outcoming edges in a directed graph, and the sum of weights associated with linked edges in a weighted graph [68].

The degree is considered a good metric for reflecting the importance level of nodes in a network. The degree distribution is made up of the degrees of all nodes in the network, and it is a crucial indicator of the durability of the network [68]. The mean network degree, often known as the global degree, represents the density of the network [64]. Nodes with a high degree value connect with many other nodes in the network both functionally and structurally, making them critical nodes from a neurobiological perspective [64]. Furthermore, it has been demonstrated that most neurobiological systems contain a wide degree distribution, with a small but significant proportion of nodes that are highly connected and others that are considerably less interconnected [68].

**Strength:** In a binary network, node degree is a numerical representation of the total number of edges that pass through a node. It is possible for edges in weighted networks (a network in which the edges between nodes are allocated weights) to take on a variety of distinct values. The range of values in weighted networks may be rather big in certain circumstances [68]. For instance, in diffusion MRI generated structural connectivity networks, connectivity weights are commonly expressed as the number of reconstructed streamlines connecting pairs of brain regions [66]. In weighted networks, the equivalent of node degree is node strength [68]. The strength of a node is defined analogously as the summation of the weights of the edges on the node. Generally, degree (or strength) is an acceptable metric for finding hubs [68].

**Path:** A path in a graph is made up of a series of edges that can be either finite or infinite, each of which is connected to the next. To put it another way, the set of all paths in a graph G = (V, E) is defined as Paths = $\{P \in V+|1 \leq I < |P|, (Pi, Pi+1) \in E\}$, where V+ represents all sequences of edges with length $\geq 1$ [67]. In a network, paths are made up of edges that can only be visited once [66].

### 1.3.2 DTI Based Structural Connectivity

The functionality and structure of the brain are inherently linked through numerous levels of brain connection. This finding underscores the importance of the connectome [69]. These forms of brain connection give different sorts of information, each of which reflects a different feature of the brain network architecture. Structural connectivity mainly characterizes the anatomical interconnections combining a group of neural elements. In the scope of the human brain, these connections are most often represented by the trajectories of white matter pathways derived from DTI data sets [70]. Functional connectivity (as determined by functional MRI) is often generated from time-series measurements and depicts patterns of statistical dependency among neuronal components in the brain. Brain connectivity is represented as a network in the formal framework of graph theory, consisting of a collection of nodes, which correspond to segmented cortical areas, and edges, which represent their mutual connections [70]. Structural brain connectivity may be converted into network form using a complicated task comprising numerous phases and a large number of computational resources [69]. Nodes are typically formed by parcellating cortical/subcortical gray matter regions into equally sized and spaced voxel clusters.

Once the nodes have been specified, estimation of their structural couplings and combination of the whole set of all pairwise couplings into a connection matrix are possible [69]. The tools and techniques derived from graph theory can be used to detect, analyze, and visualize network topologies. One of the most promising aspects of human connectomics is that it contributes to the understanding of the biological underpinnings that underlie the normal brain dynamics and abnormalities in neuropsychiatric diseases [69][71].

### 1.3.3 Complex Network Analysis

Complex Network Analysis is a novel interdisciplinary approach to the analysis of complex systems that aims to characterize brain networks via the use of a minimal number of neurobiologically significant and simply computed measurements [72]. Graph metrics are calculated to quantify the attributes of brain networks, which in turn provide a complete picture of brain networks.

Graph metrics, which are used to describe the features of a network, may be classified into four categories [72]:

- Integration measurements, which quantify how easy a region of the brain can transfer information to the other regions, giving the fundamental concepts of the path and shortest path.
- Segregation measurements, which quantify the existence of such groupings, referred to as clusters or modules, inside the network.
- Centrality measurements, which evaluate the relevance of nodes as hubs for facilitating functional integration.
- Resilience measurements, which quantify the network's functional integration vulnerability.

#### 1.3.3.1 Measures of Integration

**Shortest Path Length:** Between nodes i and j (two nodes assumed), the Shortest Path Length (SPL) is the shortest route from i to j. For directed and undirected graphs, SPL would be the smallest number of vertices (edges) between the nodes i and j. For a weighted graph, SPL would be the summation of all the edge weights along the shortest path between nodes i and j [67].

Short path lengths facilitate functional integration by allowing communication to occur with minimal intermediary stages, limiting the impacts of noise or signal deterioration. The Characteristic Path Length (CPL) is the most essential integration measurement that uses SPL as a baseline metric [73].

**Global Efficiency:** The concept of the Global Efficiency (GE) of a network in a graph is linked to the average shortest path, which is defined as the inverse of the average shortest path lengths between all nodes. The global efficiency of a fully connected network is the highest, while the global efficiency of a totally disconnected network is the lowest. This measure is impacted by short pathways; as a result, the shorter the paths are, the lower the value is calculated [73].

**Local Efficiency:** Local Efficiency (LE) is a numeric number between 0 and 1, which 1 signifies the network's highest LE. High LE in functional brain networks indicates a topological architecture suggestive of segregated neural processing. LE measures how efficiently information is being integrated between a network node's local neighbors, while global efficiency measures how effectively information is integrated over the whole network [74].

#### 1.3.3.2 Measures of Segregation

**Clustering Coefficient**: A clustering coefficient (CC) is a quantity used in graph theory that quantifies the degree to which nodes tend to cluster together in a graph. In fact, the CC measures the density of linked triangles in a graph, and it is a significant descriptive statistic of graphs. The global CC is calculated using triplets of nodes. A triplet is a collection of three nodes which are linked either by two (open triplet) or three undirected connections (closed triplet). As a result, a triangular graph consists of three closed triplets, one of which is centered on each of the nodes. This indicates that the three triplets in a triangle are formed by selecting nodes from different sets of nodes. The global CC is equal to the ratio of closed triplets to total triplets including both open and closed triplets. The CC of a network may be thought of as a network segregation index [75].

**Small-worldness properties:** Networks' small-world features represent an appropriate balance of local specialization and global integration. In order to assess the brain's small-worldness attribute, the characteristic path length and CC of the

network must be compared to the mean values obtained from the null random networks [76].

#### 1.3.3.3 Measures of Centrality

**Betweenness Centrality:** The Betweenness Centrality (BC) of a node is a measure of how well it connects to other nodes. BC of a vertex (node) is the number of all-pairs shortest paths that pass through that vertex [64]. This metric is important for finding bridging nodes that link different regions of the network (hubs) since these types of nodes have a high level of BC. The mean of the BC metrics, referred to as Global Betweenness Centrality (GBC), indicates the degree with which the node is capable of maintaining a hub [77].

#### 1.3.3.4 Measures of Resilience

**Assortativity Coefficient:** A network's Assortativity Coefficient (AC) is the Pearson correlation coefficient across the degrees of all nodes on two opposing endpoints of a connection [78]. Networks with a positive AC are more likely to contain a fairly durable core of high-degree hubs that are mutually coupled. Networks which experience a negative coefficient are more likely to contain high-degree hubs that are broadly distributed.

The measures for networks listed above do not represent a complete list of all possible measures but rather the most informative metrics, which can be used to define the prominence of brain regions in the human connectome. The node degree is one of the most immediately available graph metrics, and it is also one of the most informative and commonly used in the reported studies. There are several instances in which a node's degree is significantly correlated with other more complex metrics such as the BC. This measure is connected to communication processes, but it is often observed to be substantially associated with the "closeness centrality" metric, which quantifies each node's proximity to the rest of the network [79].

Another category of measurements is concerned with the vulnerability of networks. For example, when seeking to identify the network’s crucial areas, the drop (or rise) in global efficiency caused by the deletion of a single edge or node, or the change in

assortativity, in combination with a fall (or rise) in network density, should be employed [69].

Further investigation of brain networks revealed that modules are network communities of highly linked neuronal elements that share similar input and output projections and display comparable physiological responses [80]. Therefore, hubs are critical components of structural networks since they serve as crucial integrative elements. It should be highlighted that there is no unique approach to finding these hubs using graph theory techniques. Nodes that serve as bridging points between modules are often distinguished by their high degree, high centrality, and a diversified set of connection profiles that span the borders between modules [81]. According to a comprehensive investigation of the human brain structural connectivity, the brain has a club of densely connected hub regions, which include parts of the superior parietal cortex, superior frontal cortex, and precuneus, in addition to multiple subcortical regions, comprising the hippocampus, thalamus, and a portion of the basal ganglia [82].

The investigation of brain networks is a potential new field of inquiry. The development of new analytic tools and modeling techniques, together with ongoing methodological advances in neuroimaging, has enabled ever more thorough assessments of human structural and functional networks. Graph approaches have been shown to be effective in capturing how networks differ across people, how they grow over time, and how they function in the presence of a range of neuropsychiatric diseases.

## 1.4 Wechsler intelligence scale fourth edition

In order to measure intelligence, the WISC-IV is designed to assess a child's intellectual abilities between the ages of 6 and 18 [83]. The WISC-IV consists of ten core components and four extra subtests, which are combined to provide four index scores plus one full-scaled IQ (FSIQ), with scores ranging from lowest (40 points) to highest (160 points). The index has an average standard score of 100 points and a standard deviation of 15 points. The verbal comprehension index (VCI) is comprised of score tests of vocabulary, comprehension, and similarity (an additional subtest of

VCI is the common sense test). The perceptual reasoning index (PRI) consists of three score tests: picture concept, block design, and matrix reasoning (an additional subtest of PRI is the mapping test). The working memory index (WMI) consists of tests of alphabetic ranking and numerical breadth (an additional subtest of WMI is the arithmetic test). The processing speed index (PSI) is comprised of scores from symbol and coding search examinations (a supplemental subtest of PSI is the cancellation test). Clinical psychologists administered all assessments. A high level of reliability has been demonstrated for the FSIQ, four indicators, and subtests [84].

## 1.5 Purpose

This study aimed to investigate the structural connectivity alterations of the white matter networks in pediatric-onset non-NPSLE patients and these alterations differences compare to HCs and correlation with clinical disease severity, disease onset age, duration of the disease, and WISC-IV scores. The thesis is organized into four chapters. Chapter 2 gives information about the material and methods which we used in this thesis. Chapter 3 demonstrates the results of this work along with the results of the statistical analysis, and chapter 4 discusses the results of our analysis, compares our findings with the other existing works in the literature and concludes our work.

# Chapter 2

# Materials and methods

## 2.1 Ethics committee approval

The local institutional ethical committee (#16969557-2209) approved this study, and all the participants signed the informed consent.

## 2.2 Subjects

The current study involved 17 pediatric-onset SLE patients (F/M:11/6) (mean age ± SD: 16.44 ± 2.37; range:11-20 years), and 8 healthy controls (F/M:4/4) (mean age ± SD: 17.38 ± 1.69; range:15-20 years). All patients were diagnosed in Hacettepe University Pediatric Rheumatology Clinics and categorized in line with the American College of Rheumatology [17][85]. Exclusion criteria were presence of (1) history of psychiatric, neuropsychiatric disorders; (2) any abnormalities on cMRI; (3) hypertension, epilepsy, diabetes, and cardiovascular illnesses; (4) any condition that can be a contraindication for MRI, such as neural stimulators, cardiac pacemakers or prosthesis, pregnancy, and claustrophobia. Following that, all of the participants were given a standardized clinical examination that comprised a medical record, standard laboratory assessment, and physical examination. Afterward, a full neurological examination, psychiatric and cognitive records, State-Trait Anxiety Inventory, and depression scale were applied and individuals with no abnormality on these examinations were defined as non-NPSLE patients.

## 2.3 Clinical evaluation and neuropsychological tests

The period between the diagnosis of SLE (disease onset age) and the MRI acquisition time was used to calculate the disease duration. Systemic lupus disease activity index (SLEDAI) was calculated. The cumulative damage was calculated using the Systemic Lupus International Collaborating Clinics' damage index score (SLICC).

Demographic features (age and gender) and clinical features including disease onset age, duration of disease, Neurocognitive Dysfunction score (NCD), Wechsler Intelligence Scale for Children-IV (WISC-IV) scores with four main components (Verbal Comprehension index (WISCIVVC), Perceptual Reasoning Index (WISCIVPR), Working Memory Index (WISCIVWM), and Processing Speed Index (WISCIVPS) and three subcomponents of Number sequencing (WISCIVNS), Vocabulary subset (WISCIVVOC), and Full Scale Intelligence Quotient (WISCIVFS)), State-Trait Anxiety Inventory (STAI Trait) score for children, State Anxiety Inventory (STAI state) score for Children, Systemic Lupus Erythematosus Disease Activity Index score, and Systemic Lupus International Collaborating Clinics scores of the patients were documented. All MRI and tests were performed within a 4-week time period.

## 2.4 Image Acquisition

All participants underwent MR imaging on a 3.0 T scanner (Trio, Magnetom, Siemens, Germany) at the National Magnetic Resonance Research Center (UMRAM) of Bilkent University. Imaging protocol included structural T1-weighted (W) three-dimensional magnetization-prepared recalled gradient-echo sequence (MPRAGE) (TR/TE = 1900 / 3.41 ms, FA: $9^0$, 0.9 mm slice thickness, field of view (FoV), 230 mm; acquisition matrix, 256×256), and single shell diffusion tensor imaging (DTI) (TR/TE = 8020 / 83 ms; slice thickness, 2 mm; max b-values 700 s/mm$^2$; diffusion gradient directions, 60 independent directions; field of view (FoV), 256 mm; acquisition matrix, 128×128; voxel size 2×2×2 mm) of the whole brain. Additional axial FLAIR images were also obtained and reviewed on-site by an experienced neuroradiologist, for confirmation that the patients had no lesion in the brain.

## 2.5 Data Processing and Analysis

Image processing and analysis were carried out on a MacBook pro and UMRAM server which runs both Ubuntu 18.4 Linux operating system and Windows 10.

Prior to preprocessing, participants' images (both T1 and DTI) stored in Dicom format at the magnetic resonance scanner's computer, were converted to NIFTI by using dcm2nii software (https://people.cas.sc.edu/rorden/mricron/dcm2nii.html).

## 2.6 Diffusion Tensor Imaging (DTI)/Tract-Based Spatial Statistics (TBSS)

1. DTI analysis was conducted using the FSL toolkit (http://www.fmrib.ox.ac.uk/fsl) version 5.9. As the first stage of the preprocessing, BET (Brain Extraction Tool) of the FSL software was employed to remove the non-brain tissues from the head images to create a binary mask of the brain by using T1-W images of the subjects.

2. In the second step of preprocessing, the eddy correct function of FSL was applied on images to correct distortions caused by subjects' movements, head motions, or eddy current effects during DTI acquisition. This function works by aligning each diffusion-weighted image to the non-diffusion b0 image with an affine alignment [86] and adjusting the gradient orientations [87].

3. To calculate the tensors, the Mean Diffusivity (MD), Fractional Anisotropy (FA), Axial Diffusivity (AD), and the Radial Diffusivity (RD) maps, DTIFIT function of FSL was applied on the eddy-corrected data. The eigenvalues calculated from the DTIFIT function were used in the formula to calculate the values for the MD, FA, AD, and RD. Each abovementioned step was repeated individually for all 31 participants of this study. The Stejskal and Tanner equations were used to calculate the diffusion tensor models [88].

4. In the next step, to find the anatomical connectivity in the brain, TBSS was used. As a first stage, the TBSS method was applied on FA images which were calculated in the previous step. Preprocessing function of TBSS was applied on FA images to remove outlier slices by changing the end slices to zero. In this step,

an overview webpage was created by a preprocessing script that included a static view of input images individually that could be helpful in recognizing obvious problems quickly.

5. In the following steps of TBSS analysis, the script applied nonlinear registration and aligned all FA maps to the MNI152 space of 1x1x1mm. Once this was done, all participants had their transformation of the original FA image into MNI152 space, which is the result of the two combined transformations of nonlinear transform and affine transformation to the MNI152 space. At the end of these steps all the participant's FA images were merged into a single 4D image and then the script created the mean of the abovementioned "all FA" images and to create a "mean FA" skeleton, the FA skeletonization program was used according to the enhanced mean FA image.

6. The prestat script of TBSS applied the threshold (which was chosen as 0.2) to the "mean FA skeleton" image which led to a binary skeleton mask. Then a distance map was prepared according to the binary skeleton mask. In the last step of the prestat script, the projection of the FA maps was done on the previously prepared distance map and the 4D all FA image was taken to project FA maps onto "mean FA skeleton" and as a result, the projected skeletonized FA data has been created.

7. In this step voxelwise statistics was applied on the skeletonized FA data which was calculated in the previous step, to find significantly different FA skeleton between healthy controls and patients. First of all, GLM GUI was used to generate contrast file and design matrix. Then to find the voxelwise statistics, a randomize tool was used, according to the generated design matrix and contrast file, and by using skeletonized all FA images.

8. In order to apply TBSS analysis and find voxelwise statistics for MD, AD, and RD the same steps were applied.

## 2.7 Graph Analysis/ Network Construction

The construction of the structural network requires the following basic elements: nodes and connection edges. Fiber density determined the edges, and anatomical

regions were defined as nodes. Graph analysis was conducted using DSI Studio software (http://dsi-studio.labsolver.org/)[89]. The data processing for the brain structural connectivity extraction and network analysis consisted of five steps.

1. The first step was a reconstruction step that is converting the Dicom file to the FIB file which in turn was used for fiber tracking. The subjects' DTI Dicom images were used to prepare the src file, which DSI Studio software needs for the reconstruction stage. Then, using the src file, a mask was created for each individual separately to filter out the background region, improve reconstruction efficiency, and make future viewing easier. Afterward, Q-Space diffeomorphic reconstruction (QSDR) [90] was used to recreate the DTI images in the MNI space in order to ascertain the function of the spin distribution [91]. Quantitative anisotropy (QA) mapping was calculated by DSI Studio in the native space before normalizing it to the MNI QA map in QSDR. At the end of this step, the FIB files were created by DSI Studio.

2. Then, fiber tracking was applied to the image to get the whole brain fiber tracts. The deterministic fiber tracking technique in the DSI Studio that improves accuracy by utilizing quantitative anisotropy was used for the whole-brain tractography [92]. The entire brain was used as a seeding region. In this study, 100,000 seeds were used for fiber tracking. The seeding points, which served as the tracking's beginning points, were uniformly spread within a defined region. In order to place the seeds, a constant random generator was used by DSI Studio. This implies that, although if the seeding site is picked at random from the seeding regions, the seeding sequence is "deterministic," and each tracking cycle will have identical results. Since we chose to use the deterministic fiber tracking technique of this software, the angular threshold, anisotropy threshold, and step size random generator were also deterministically random [92]. The threshold for anisotropy was set at 0.055. It was chosen at random from 15 degrees to 90 degrees as the angular threshold. The voxel size ranged from 0.5 to 1.5 voxels chosen at random. The DSI studio's tractography was implemented based on the streamline tracking algorithm which has been using the Eulerian integration [93]. In tractography, first, subjects' images were registered non-linearly to the MNI space; second, seeds were inserted in each voxel associated with Human Connectome Project (HCP) tractography atlas tract.

3. To generate the connectivity matrix, DSI Studio needs a brain parcellation framework. In order to get the parcellation map, we used the HCP atlas to segment the entire brain into 360 regions (180 regions per hemisphere). A total of 360 ROIs were thus used as the brain parcellation. In the structural network, each node represents one of the anatomical regions of the selected ROIs.

4. Next, the connectivity matrix was calculated based on counting the number of tracts that pass two ROIs. As a result, a symmetric 360*360 weighted matrix was generated for each participant to represent the created network. Connecting tracks with a length shorter than 30 mm and longer than 300 mm were eliminated as the software guide recommended.

5. According to the connectivity matrix and selected ROIs, network analysis was done by DSI Studio. Graph theoretical analysis looks at brain connections as a graph and analyzes them using graph-based metrics. These metrics consist of a vast range of measurements including network strength, CC, path length, LE, global efficiency, small-worldness as described in the introduction (page 14 - 16) [94][76][95]. In terms of regional characteristics, we used the nodal degree [57]. Network analysis tool was implemented as guided by the brain connectivity toolbox (https://sites.google.com/site/bctnet/) on DSI Studio. Furthermore, a network hub is a brain region that connects to a lot of others and plays a vital role in the integration of different brain functions. If a brain region's strength was at least one standard deviation greater than the mean of the entire network, it was considered as a hub.

## 2.8 Statistical Analysis

The two-sample t-test was used to find out differences between non-NPSLE patients and healthy controls for demographic, clinical, and MRI-based variables. In the non-NPSLE patients, the correlations between the clinical variables and demographic features were assessed using Pearson’s correlation coefficient.

Regional network metrics (strength, BC, CC, and LE) were compared between patients and healthy controls in identified structural brain hubs using the two-sample t-test. Correlations between the above-mentioned network metrics and clinical

findings were evaluated by Spearman's rank correlation coefficient. P-values < 0.05 were considered significant. Statistical analysis was performed by R, using R Studio version 1.2.1335 [96] on Mac.

# Chapter 3

# Results

## 3.1 Demographic, MRI and Clinical Findings

Table 3.1 summarizes demographic and clinical findings from HCs and pediatric-onset non-NPSLE patients. There was no significant difference in terms of gender and age between the patients and HCs (two-sample t-tests, p: 0.5 and 0.32, respectively). Compared to HCs, patients showed significantly lower scores in WISCIVVC, WISCIVPR, WISCIVWM, and WISCIVFS (two-sample t-test, p: 0.02, p: 0.006, p: 0.049, and 0.001, respectively). Patients had also lower WISCIVPS scores than HCs although the difference was not significant ($p > 0.05$, two-sample t-test). No correlation was found between the disease duration with age, and gender in the patients ($p > 0.05$, Pearson product-moment correlation coefficient test). Neither there was a correlation between the NCD score and disease duration or age ($p > 0.05$, Pearson product-moment correlation coefficient test). None of the WISCIVVC, WISCIVPR, WISCIVWM, WISCIVPS, WISCIVFS scores showed a correlation with age ($p > 0.05$, Pearson product-moment correlation coefficient test). Additionally, no correlation was observed between WISCIVVC, WISCIVPR, WISCIVWM, WISCIVFS scores with gender ($p > 0.05$, Pearson product-moment correlation coefficient test). A strong negative correlation has been found between the WISCIVPR, WISCIVWM, WISCIVFS scores, and disease duration (r from -0.5 to -0.45 and p from 0.01 to 0.02). However, disease duration did not have a correlation with WISCIVVC, WISCIVPS scores ($p > 0.05$, Pearson product-moment correlation coefficient test).

**Table 3.1** - Demographic and Clinical features of the HCs and non-NPSLE Patients

| Subject | Patients Mean ± SD | Healthy Controls Mean ± SD | P-Value |
|---|---|---|---|
| **Gender** | 0.65 ± 0.49 | 0.5 ± 0.53 | 0.5 |
| **Age (years)** | 16.44 ± 2.37 | 17.38 ± 1.69 | 0.32 |
| **Age at disease onset (years)** | 11.82 ± 3.43 | NA | NA |
| **Disease duration (years)** | 4.56 ± 3.69 | NA | NA |
| **SLEDAI** | 4.18 ± 2.96 | NA | NA |
| **SLICC** | 3.18 ± 1.24 | NA | NA |
| **NCD** | 1.71 ± 0.47 | NA | NA |
| **WISCIVVC** | 91.76 ± 13.93 | 107.75 ± 15.62 | 0.02* |
| **WISCIVPR** | 87.12 ± 10.29 | 99.88 ± 9.37 | 0.006* |
| **WISCIVWM** | 84.82 ± 13.74 | 96.75 ± 13.40 | 0.049* |
| **WISCIVPS** | 90.06 ± 12.40 | 98.12 ± 12.21 | 0.14 |
| **WISCIVNS** | 6.82 ± 2.53 | 9.5 ± 3.21 | 0.03* |
| **WISCIVVOC** | 7.58 ± 3.28 | 12.5 ± 3.96 | 0.003* |
| **WISCIVFS** | 84.47 ± 11.55 | 102.00 ± 10.41 | 0.001* |
| **STAI Trait** | 32.29 ± 7.10 | 30.50 ± 6.37 | 0.69 |
| **STAI state** | 31.71 ± 7.14 | 33.62 ± 6.32 | 0.52 |

* Statistically significant p-value. P-value calculated according to two-sample t-test, R: Right, L: Left, SD: Standard Deviation, For abbreviations, see page xiv.

## 3.2 TBSS Analysis

As presented in Figure 3.1, compared with HCs, the patients exhibited a significant decrease in FA maps throughout the genu and the body of the corpus callosum, the left anterior corona radiata, and the forceps minor (p-value < 0.05).

In non-NPSLE patients, TBSS maps revealed significantly higher MD and RD values prominent in the genu and body of the corpus callosum, the forceps minor, the right external capsule, cingulum, anterior and superior corona radiata, anterior

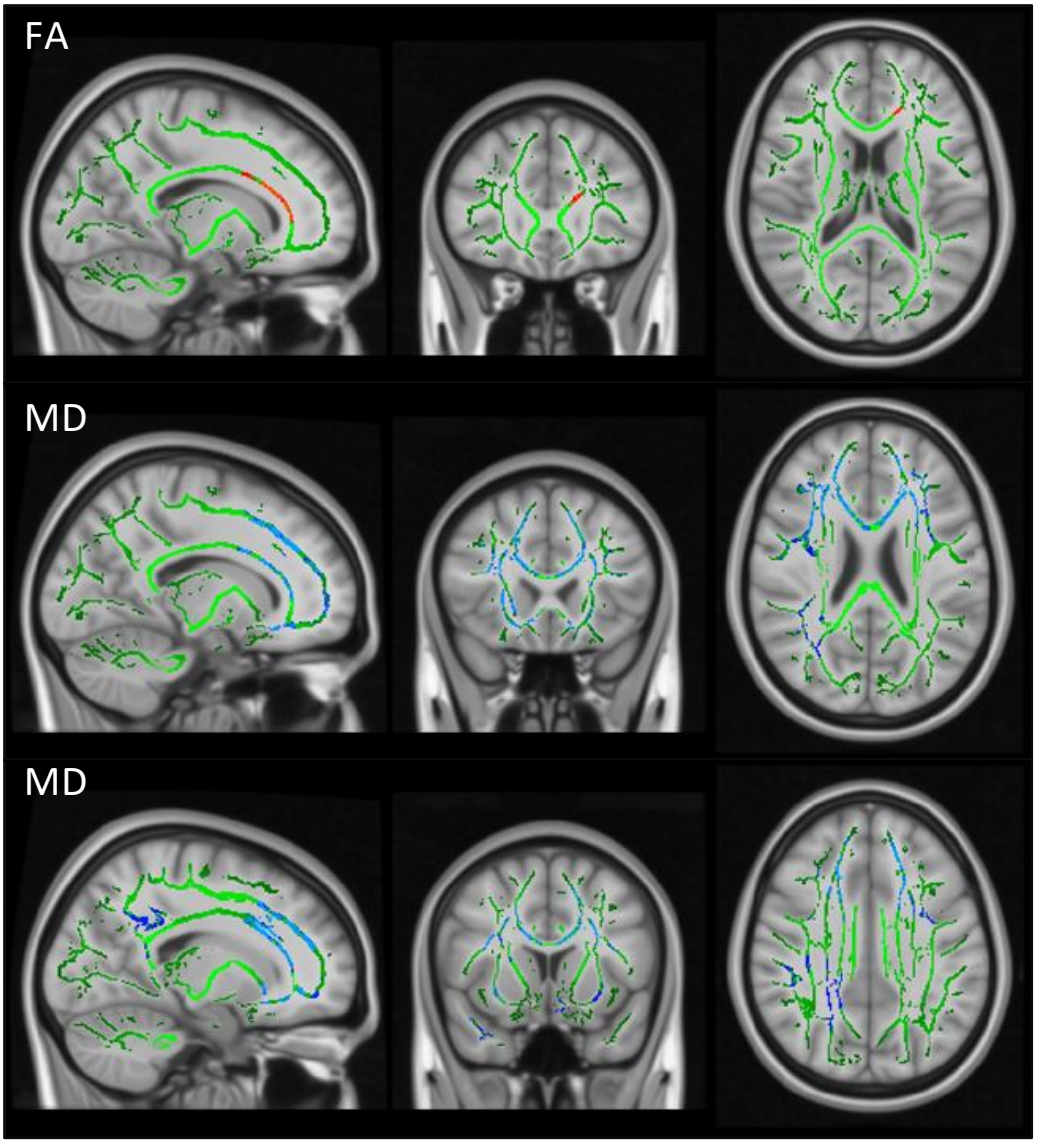


**Figure 3.1 -** TBSS-DTI shows the comparison of WM tracts in pSLE and HCs. Yellow-Red highlighted areas represent the regions where pSLE had significantly lower FA, while blue and dark red highlighted areas show regions with significantly increased MD and RD, respectively ($p < 0.05$). There is no significant change in AD. Patients with pSLE have significantly lower FA, and higher MD and RD as shown in the genu and body of corpus callosum, and tracts of forceps minor. The first row shows FA maps, the second and third row show MD maps.

thalamic radiation, the superior longitudinal fasciculus, the uncinate fasciculus, and the inferior fronto-occipital fasciculus bilaterally with additional increment in the splenium of the corpus callosum, the right posterior corona radiata, anterior limb of

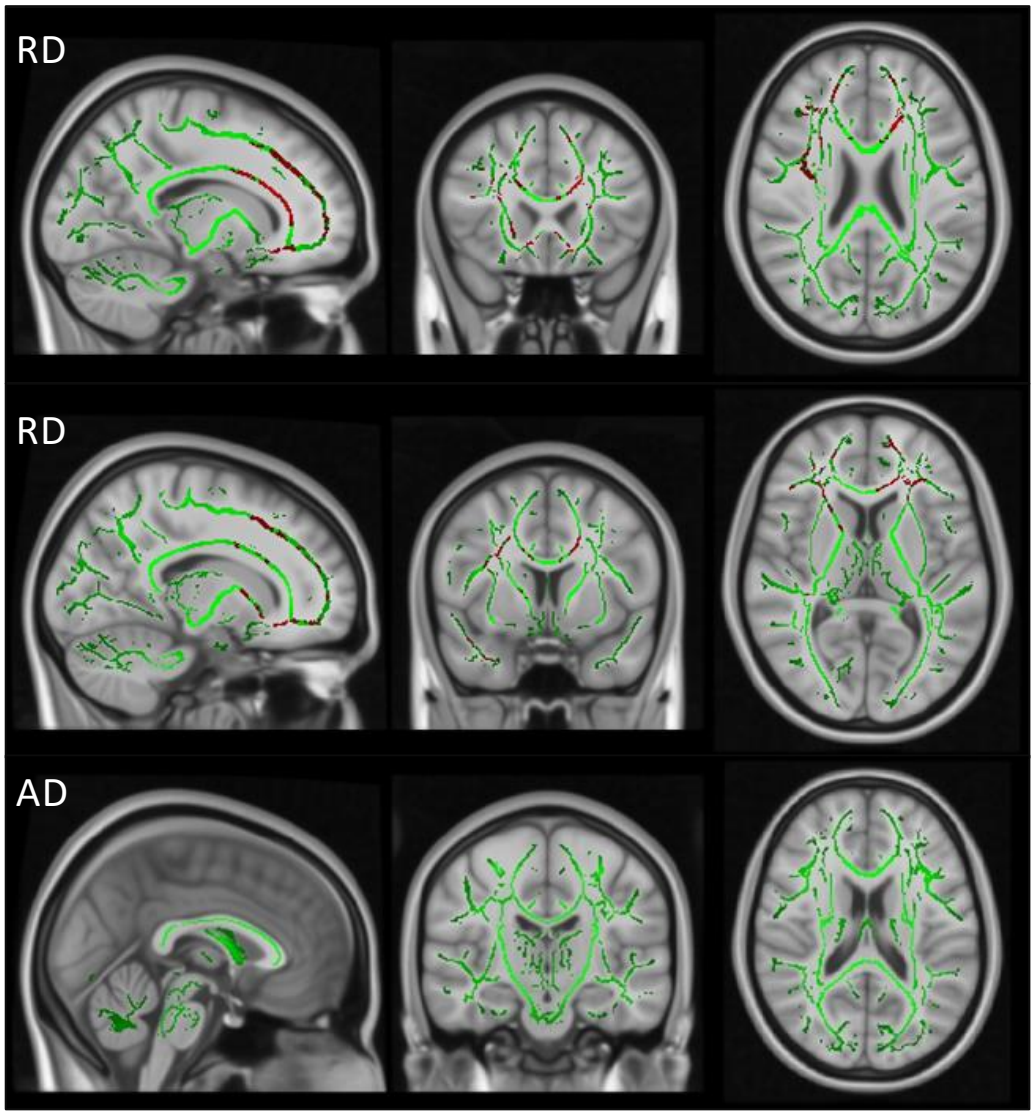


**Figure 3.1** (continued) - TBSS-DTI shows the comparison of WM tracts in pSLE and HCs. Yellow-Red highlighted areas represent the regions where pSLE had significantly lower FA, while blue and dark red highlighted areas show regions with significantly increased MD and RD, respectively ($p < 0.05$). There is no significant change in AD. Patients with pSLE have significantly lower FA, and higher MD and RD as shown in the genu and body of corpus callosum, and tracts of forceps minor. The first and second rows show RD maps and the third row shows AD map.

the internal capsule, and inferior longitudinal fasciculus (p-value < .05) in comparison with HCs. In terms of AD maps, the patients did not have any significant elevation or reduction compared with HCs (Figure 3.1).

## 3.3 Global Network Analyses

Compared to HCs, structural network density, transitivity, and global efficiency were lower in non-NPSLE patients as represented in Table 2. In addition, network characteristic path length and assortativity coefficient were higher in patients than HCs as shown in Table 2. However, none of them reached statistical significance.

**Table 3.2** - Global structural network parameters in HCs and non-NPSLE patients

| Global network metrics | Patients (n=17) Mean ± SD | Healthy Controls (n=8) Mean ± SD | p-value |
|---|---|---|---|
| **Density** | 0.14 ± 0.02 | 0.16 ± 0.03 | 0.3 |
| **Transitivity** | 0.07 ± 0.01 | 0.08 ± 0.02 | 0.89 |
| **Global efficiency** | 0.53 ± 0.03 | 0.54 ± 0.03 | 0.46 |
| **Small worldness** | 0.27 ± 0.01 | 0.28 ± 0.02 | 0.59 |
| **Network characteristic path length** | 2.09 ± 0.12 | 2.05 ± 0.12 | 0.56 |
| **Assortativity** | 0.05 ± 0.04 | 0.04 ± 0.04 | 0.65 |

## 3.4 Hub regions

Graph analysis revealed 64 and 59 brain network hubs in HCs and non-NPSLE patients, respectively. Patients and HCs shared the same 44 brain network hubs which were dispersed throughout the entire brain (Figure 3.2 and Table 3.3). Right VVC, V4, V1, a32pr, 6mp, and left VMV1, V8, V4, V1, PreS, PHA3, PHA1, PH, MBelt, Ig, H, a32pr, 9a, 52 and 6a hubs disappeared in non-NPSLE patients. On the other hand, 15 new hubs showed up in patients consisting of PHT, p10p, MBelt, IPS1, IP1, 8BM, and 8BL hubs in the right hemisphere and V7, TE1p, PGs, IPS1, IP1, a24, 5mv, and 23c hubs in the left hemisphere. The abbreviation list of the network hubs is presented on page xiv.

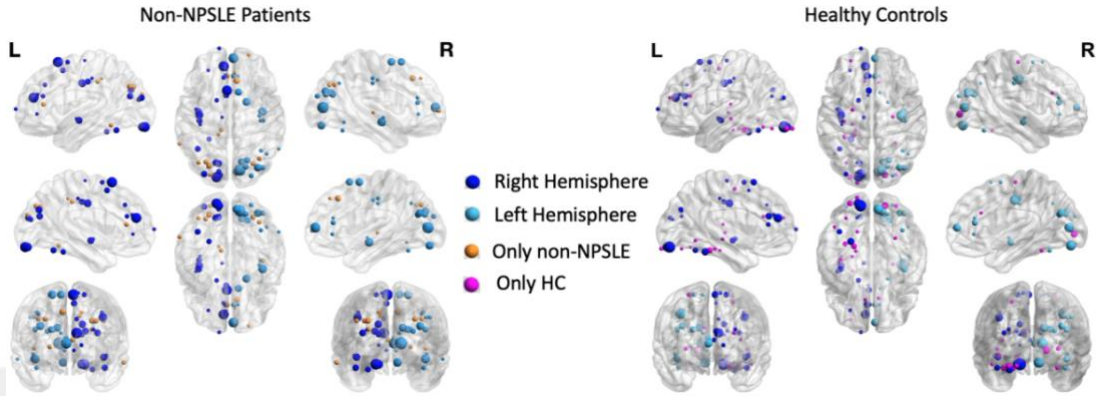


**Figure 3.2 -** Structural brain hubs in non-NPSLE patients and HCs with diameters in relation to hub strength. There are fewer hubs in patients compared to HCs. R for right, L for left; Figure prepared using BrainNet Viewer (https://www.nitrc.org/projects/bnv/).

**Table 3.3 -** Hub regions common in non-NPSLE patients and HCs, mean values showing the hubs mean strength and standard deviation

| Brain structural hubs | Patients (n=17) Mean ± SD | Healthy Controls (n=8) Mean ± SD |
|---|---|---|
| **L_1** | 2.25 ± 1 | 1.9 ± 0.82 |
| **R_1** | 2.28 ± 1.06 | 2.26 ± 1.78 |
| **L_3b** | 3.05 ± 0.99 | 2.6 ± 1.17 |
| **R_3b** | 2.19 ± 0.92 | 2.05 ± 1 |
| **L_4** | 3.58 ± 1.56 | 3.6 ± 1.55 |
| **R_4** | 3.51 ± 1.56 | 4.23 ± 2.45 |
| **L_6ma** | 2.32 ± 1.45 | 2.56 ± 0.82 |
| **R_6ma** | 2.23 ± 1.26 | 2.1 ± 1.74 |
| **L_9m** | 4.06 ± 1.37 | 3.93 ± 1.28 |
| **R_9m** | 3.88 ± 1.36 | 3.56 ± 1.66 |
| **L_d32** | 2.47 ± 1.17 | 3.18 ± 1.86 |
| **R_d32** | 2.19 ± 0.9 | 1.99 ± 1.1 |
| **L_DVT** | 2.9 ± 1.01 | 2.05 ± 1.2 |
| **R_DVT** | 3.15 ± 0.95 | 2.98 ± 1.6 |

| Brain structural hubs | Patients (n=17) Mean ± SD | Healthy Controls (n=8) Mean ± SD |
|---|---|---|
| **L_FFC** | 2.72 ± 1.1 | 2.71 ± 1.3 |
| **R_FFC** | 2.18 ± 1.02 | 2.29 ± 0.59 |
| **L_IP0** | 3.01 ± 1.67 | 2.39 ± 1.38 |
| **R_IP0** | 3.41 ± 1.17 | 3.04 ± 1.21 |
| **L_p24** | 2.48 ± 1.01 | 2.37 ± 0.76 |
| **R_p24** | 2.46 ± 0.9 | 2.76 ± 1.12 |
| **L_PoI1** | 3.08 ± 1.1 | 2.94 ± 0.59 |
| **R_PoI1** | 3.55 ± 1.19 | 3.07 ± 1.1 |
| **L_PoI2** | 2.02 ± 0.81 | 2.48 ± 0.82 |
| **R_PoI2** | 1.88 ± 0.83 | 1.97 ± 1.17 |
| **L_POS2** | 3.17 ± 1.43 | 2.75 ± 1.77 |
| **R_POS2** | 3.42 ± 1.27 | 3.49 ± 1.81 |
| **L_SFL** | 4.02 ± 2.39 | 3.07 ± 1.31 |
| **R_SFL** | 2.92 ± 1.3 | 1.95 ± 1.03 |
| **L_V2** | 3.35 ± 1.14 | 4.87 ± 2.45 |
| **R_V2** | 3.22 ± 1.25 | 4.29 ± 2.5 |
| **L_V3** | 3.85 ± 1.45 | 3.95 ± 1.88 |
| **R_V3** | 4.27 ± 1.83 | 4.23 ± 2.01 |
| **L_V6** | 2.52 ± 1.21 | 1.94 ± 1.33 |
| **R_V6** | 2.72 ± 1.28 | 2.21 ± 1.27 |
| **L_10d** | 2.17 ± 1 | 2.18 ± 0.96 |
| **L_6mp** | 1.96 ± 1.14 | 2.16 ± 1.66 |
| **L_8BM** | 2.47 ± 1.15 | 1.94 ± 1.21 |
| **L_9-46d** | 2.14 ± 0.96 | 2.15 ± 0.98 |
| **L_SCEF** | 2.94 ± 2.62 | 1.88 ± 0.98 |

| Brain structural hubs | Patients (n=17) Mean ± SD | Healthy Controls (n=8) Mean ± SD |
|---|---|---|
| **L_VVC** | 2.43 ± 1.22 | 3.31 ± 0.79 |
| **R_a24** | 2.2 ± 0.95 | 2.05 ± 0.81 |
| **R_PGp** | 2.65 ± 1.06 | 2.93 ± 1.79 |
| **R_PGs** | 2.33 ± 1.34 | 1.91 ± 0.95 |
| **R_V7** | 2.6 ± 1.12 | 2.1 ± 0.9 |
| **L_a32pr** | NA | 2.09 ± 1.17 |
| **R_a32pr** | NA | 1.96 ± 0.92 |
| **L_V1** | NA | 2.25 ± 1.24 |
| **R_V1** | NA | 3.23 ± 1.71 |
| **L_V4** | NA | 2.75 ± 1.16 |
| **R_V4** | NA | 2.25 ± 1.32 |
| **L_52** | NA | 2.05 ± 1.43 |
| **L_6a** | NA | 2.13 ± 1.48 |
| **L_9a** | NA | 1.98 ± 1.26 |
| **L_H** | NA | 1.94 ± 0.54 |
| **L_Ig** | NA | 1.91 ± 1.22 |
| **L_MBelt** | NA | 2.02 ± 0.95 |
| **L_PH** | NA | 1.92 ± 1 |
| **L_PHA1** | NA | 2.76 ± 1.48 |
| **L_PHA3** | NA | 2.61 ± 1.1 |
| **L_PreS** | NA | 2.05 ± 1.46 |
| **L_V8** | NA | 1.95 ± 0.92 |
| **L_VMV1** | NA | 1.98 ± 0.87 |
| **R_6mp** | NA | 2.21 ± 1.51 |
| **R_VVC** | NA | 2.07 ± 1.0 |

| Brain structural hubs | Patients (n=17) Mean ± SD | Healthy Controls (n=8) Mean ± SD |
|---|---|---|
| **L_IPS1** | 2.81 ± 1.71 | NA |
| **R_IPS1** | 2.61 ± 1.16 | NA |
| **L_IP1** | 2.53 ± 1.89 | NA |
| **R_IP1** | 2.52 ± 1.3 | NA |
| **L_23c** | 2.29 ± 0.92 | NA |
| **L_PGs** | 2.47 ± 1 | NA |
| **L_TE1p** | 2.14 ± 0.95 | NA |
| **L_V7** | 2.4 ± 1.32 | NA |
| **R_p10p** | 2.18 ± 1.55 | NA |
| **R_MBelt** | 2.05 ± 0.66 | NA |
| **L_a24** | 2.08 ± 1.09 | NA |
| **L_5mv** | 2.02 ± 1.22 | NA |
| **R_8BM** | 2.61 ± 1.55 | NA |
| **R_8BL** | 1.9 ± 1.25 | NA |
| **R_PHT** | 1.69 ± 1.1 | NA |

R: Right, L: Left, NA: Not Applicable, SD: Standard Deviation, for abbreviations, see page xiv.

## 3.5 Nodal Network Analyses

Compared with HCs, non-NPSLE patients showed lower strength bilaterally in the second visual area (V2) and area 4 (M1, or primary motor cortex), and also in the left hemisphere's VVC (ventral visual vomplex), 6ma (anterior supplementary motor areas), d32 (part of dorsal anterior cingulate area), 10d (prefrontal cortical area), 9-46d (part of dorsolateral prefrontal cortex), PoI2 (posterior insular 2), and 6mp (posterior supplementary motor areas) areas. Additionally, POS2 (left parieto-occipital sulcus 2), DVT (dorsal visual transitional area), PGp (parietal area G, posterior), p24 (posterior subdivisions of anterior cingulate cortex), and 1 (primary somatosensory cortex) areas of the right hemisphere showed a lower strength in patients compared to HCs. Right

FFC (fusiform face complex) showed the same strength in both HCs and patients. The remaining shared hubs in non-NPSLE patients and HCs showed increased strength. The results are displayed in Figure 3.3 and Table 3.4.

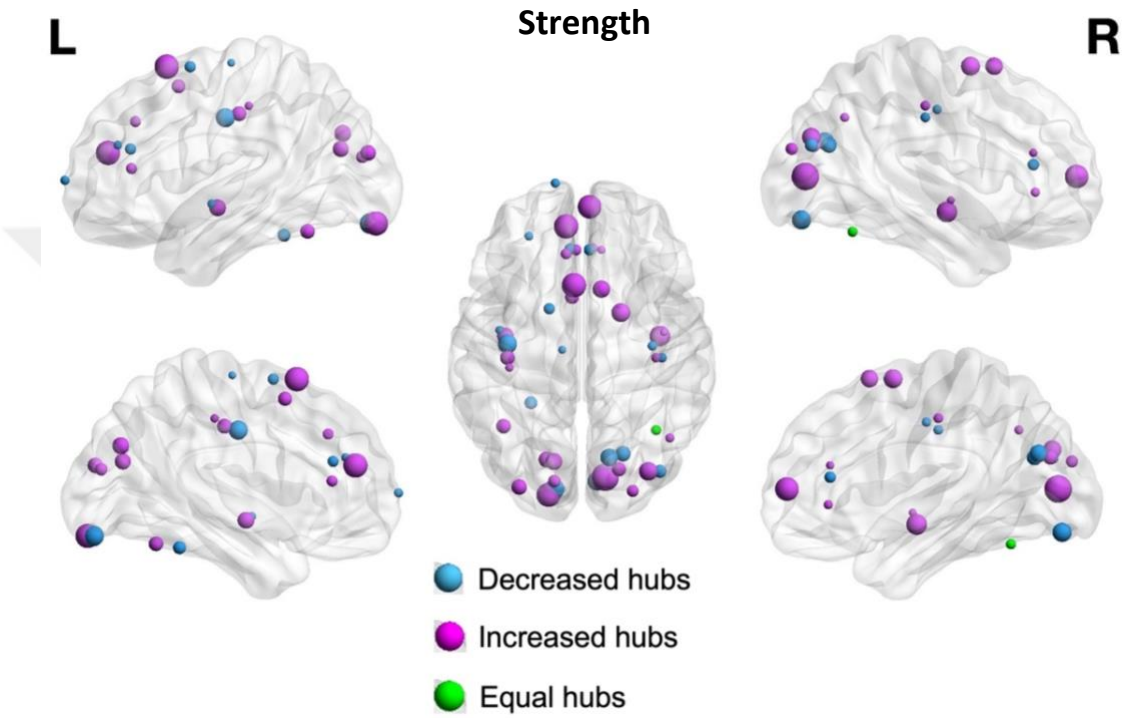


**Figure 3.3 -** Comparison of the structural brain nodes in non-NPSLE patients and HCs according to nodal strength. Compared to HCs, patients show decreased nodal strength in the blue highlighted nodes, increased nodal strength in pink colored ones, and equal strength in the green nodes. R for right, L for left; Figure prepared using BrainNet Viewer (https://www.nitrc.org/projects/bnv/).

**Table 3.4** - Strength mean values and standard deviations of the structural hubs in HCs and non-NPSLE patients

| Brain structural hubs | Patients (n=17) Mean ± SD | Healthy Controls (n=8) Mean ± SD | P-values |
|---|---|---|---|
| **R_V3** | 4.23 ± 2.01 | 4.44 ± 1.91 | 0.8↑ |
| **L_SFL** | 3.07 ± 1.31 | 4.08 ± 2.38 | 0.27↑ |
| **L_9m** | 3.93 ± 1.28 | 4.06 ± 1.33 | 0.81↑ |
| **L_V3** | 3.95 ± 1.88 | 4.04 ± 1.61 | 0.89↑ |
| **R_9m** | 3.56 ± 1.66 | 3.97 ± 1.34 | 0.51↑ |

| Brain structural hubs | Patients (n=17) Mean ± SD | Healthy Controls (n=8) Mean ± SD | P-values |
|---|---|---|---|
| **R_PoI1** | 3.07 ± 1.1 | 3.61 ± 1.17 | 0.28↑ |
| **L_V2** | 4.87 ± 2.45 | 3.59 ± 1.76 | 0.14↓ |
| **L_4** | 3.6 ± 1.55 | 3.41 ± 1.55 | 0.77↓ |
| **R_V2** | 4.29 ± 2.5 | 3.4 ± 1.65 | 0.29↓ |
| **R_4** | 4.23 ± 2.45 | 3.38 ± 1.5 | 0.29↓ |
| **R_IP0** | 3.04 ± 1.21 | 3.33 ± 1.23 | 0.57↑ |
| **R_POS2** | 3.49 ± 1.81 | 3.23 ± 1.39 | 0.69↓ |
| **R_SFL** | 1.95 ± 1.03 | 3.2 ± 1.38 | 0.03↑* |
| **L_POS2** | 2.75 ± 1.77 | 3.14 ± 1.8 | 0.62↑ |
| **L_PoI1** | 2.94 ± 0.59 | 3.13 ± 1.07 | 0.64↑ |
| **L_DVT** | 2.05 ± 1.2 | 3.02 ± 1.74 | 0.16↑ |
| **L_IP0** | 2.39 ± 1.38 | 2.96 ± 1.85 | 0.44↑ |
| **R_DVT** | 2.98 ± 1.6 | 2.95 ± 1 | 0.95↓ |
| **L_3b** | 2.6 ± 1.17 | 2.87 ± 1.05 | 0.56↑ |
| **L_FFC** | 2.71 ± 1.3 | 2.85 ± 1.23 | 0.8↑ |
| **R_8BM** | 1.57 ± 0.67 | 2.81 ± 1.72 | 0.06↑ |
| **R_V6** | 2.21 ± 1.27 | 2.79 ± 1.43 | 0.33↑ |
| **L_SCEF** | 1.88 ± 0.98 | 2.77 ± 2.41 | 0.32↑ |
| **L_IPS1** | 1.54 ± 1.04 | 2.73 ± 1.79 | 0.09↑ |
| **R_PGp** | 2.93 ± 1.79 | 2.66 ± 1.14 | 0.65↓ |
| **L_VVC** | 3.31 ± 0.79 | 2.64 ± 1.38 | 0.21↓ |
| **L_V6** | 1.94 ± 1.33 | 2.58 ± 1.42 | 0.29↑ |
| **L_IP1** | 1.6 ± 1.18 | 2.53 ± 1.87 | 0.21↑ |
| **R_V7** | 2.1 ± 0.9 | 2.52 ± 1.09 | 0.34↑ |
| **R_IPS1** | 1.62 ± 0.78 | 2.46 ± 1.1 | 0.06↑ |

| Brain structural hubs | Patients (n=17) Mean ± SD | Healthy Controls (n=8) Mean ± SD | P-values |
|---|---|---|---|
| **R_p24** | 2.76 ± 1.12 | 2.46 ± 0.88 | 0.46↓ |
| **L_6ma** | 2.56 ± 0.82 | 2.44 ± 1.41 | 0.81↓ |
| **L_d32** | 3.18 ± 1.86 | 2.41 ± 1.07 | 0.19↓ |
| **L_p24** | 2.37 ± 0.76 | 2.4 ± 0.97 | 0.92↑ |
| **L_8BM** | 1.94 ± 1.21 | 2.39 ± 1.12 | 0.36↑ |
| **R_IP1** | 1.68 ± 0.89 | 2.38 ± 1.22 | 0.16↑ |
| **L_23c** | 1.64 ± 0.65 | 2.36 ± 1.08 | 0.09↑ |
| **L_PGs** | 1.54 ± 1.13 | 2.32 ± 1.07 | 0.11↑ |
| **R_6ma** | 2.1 ± 1.74 | 2.31 ± 1.32 | 0.73↑ |
| **L_TE1p** | 1.57 ± 0.86 | 2.3 ± 1.09 | 0.11↑ |
| **R_FFC** | 2.29 ± 0.59 | 2.29 ± 1.15 | 1 |
| **L_V7** | 1.82 ± 1.33 | 2.24 ± 1.33 | 0.46↑ |
| **R_1** | 2.26 ± 1.78 | 2.23 ± 1.06 | 0.96↓ |
| **R_p10p** | 1.35 ± 0.62 | 2.19 ± 1.4 | 0.12↑ |
| **R_3b** | 2.05 ± 1 | 2.18 ± 0.96 | 0.75↑ |
| **L_10d** | 2.18 ± 0.96 | 2.16 ± 0.92 | 0.78↓ |
| **R_a24** | 2.05 ± 0.81 | 2.16 ± 1.03 | 0.96↑ |
| **R_PGs** | 1.91 ± 0.95 | 2.15 ± 1.28 | 0.63↑ |
| **L_9-46d** | 2.15 ± 0.98 | 2.12 ± 0.87 | 0.21↑ |
| **R_MBelt** | 1.71 ± 0.91 | 2.12 ± 0.65 | 0.92↑ |
| **L_PoI2** | 2.48 ± 0.82 | 2.11 ± 0.79 | 0.29↓ |
| **L_1** | 1.9 ± 0.82 | 2.08 ± 1.01 | 0.67↑ |
| **L_a24** | 1.76 ± 0.72 | 2.07 ± 1.13 | 0.48↑ |
| **L_5mv** | 1.12 ± 0.42 | 2.06 ± 1.2 | 0.04↑* |
| **R_d32** | 1.99 ± 1.1 | 2.04 ± 0.88 | 0.18↑ |

| Brain structural hubs | Patients (n=17) Mean ± SD | Healthy Controls (n=8) Mean ± SD | P-values |
|---|---|---|---|
| **R_8BL** | 1.29 ± 0.69 | 2.04 ± 1.48 | 0.92↑ |
| **R_PHT** | 1.51 ± 0.63 | 2.01 ± 1.46 | 0.36↑ |
| **L_6mp** | 2.16 ± 1.66 | 2 ± 1.06 | 0.77↓ |
| **R_PoI2** | 1.97 ± 1.17 | 2 ± 0.82 | 0.95↑ |

*Hubs with the statistically significantly changed p-value. P-value calculated according to two-sample t-test. Arrows with p-values show whether patients show higher (↑) or lower (↓) than the HCs. R: Right, L: Left, SD: Standard Deviation, For abbreviations, see page xiv.

As presented in Figure 3.4 and Table 3.5, compared to HCs, patients showed lower BC bilaterally in V3 (third visual area), 9m (medial portion of dorsolateral prefrontal cortex), 4 (M1, or primary motor cortex), POS2 (left parieto-occipital sulcus 2), 1 (primary somatosensory cortex), 6ma (anterior supplementary motor areas), p24 (posterior subdivisions of anterior cingulate cortex), a24 (anterior subdivisions of anterior cingulate cortex), and d32 (Part of dorsal anterior cingulate area). Moreover, V2 (second visual area), PoI1 (posterior insular 1), 3b (primary sensory cortex), V6 (sixth visual area), PoI2 (posterior insular 2), VVC (ventral visual complex), 10d (prefrontal cortical area), 9-46d (Part of dorsolateral prefrontal cortex), and 6mp (posterior supplementary motor areas) areas of the left hemisphere and DVT (dorsal visual transitional area), V7(seventh visual area), and PHT (Part of middle temporal gyrus) areas in the right hemisphere presented lower BC in patients than in HCs. Other 29 hubs showed higher BC in non-NPSLE patients compared to HCs. On the other hand, patients' BC showed a significant decrease in the left medial portion of the dorsolateral prefrontal cortex and posterior supplementary motor areas (p: 0.005 and p: 0.01 respectively) and in the right anterior subdivisions of the anterior cingulate cortex (p: 0.01) and a significant increase in the left posterior TE1, which is part of middle temporal gyrus (p: 0.02) compared to HCs.

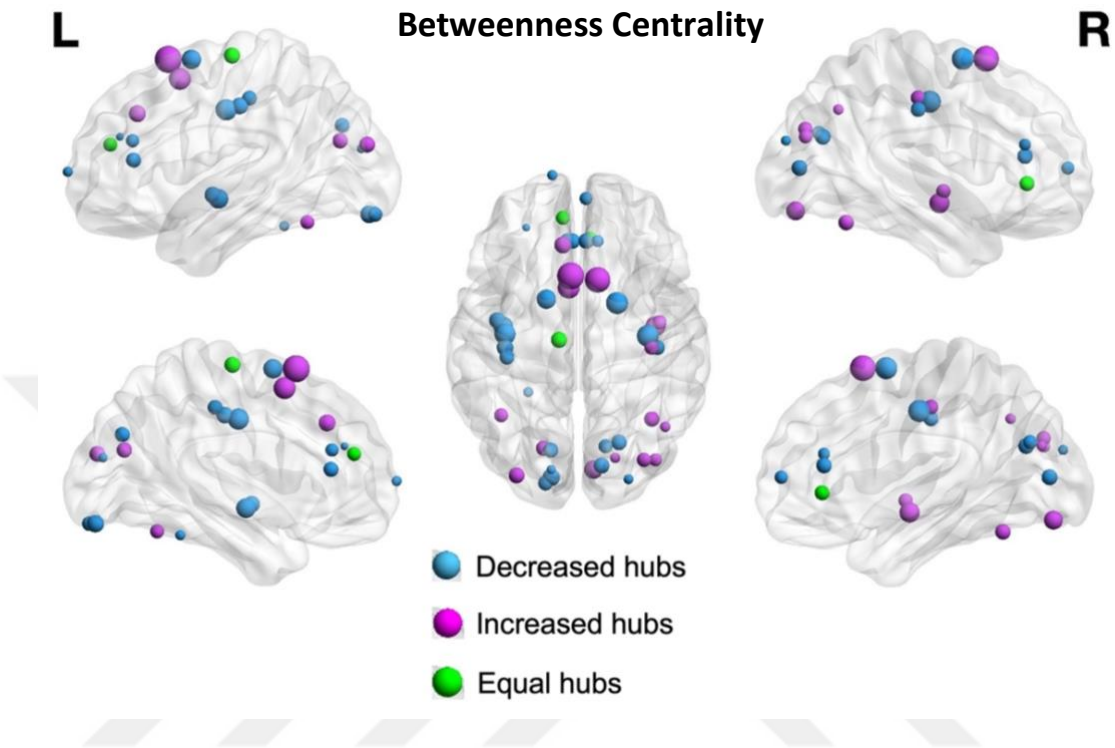


**Figure 3.4 -** Comparison of the structural brain nodes in non-NPSLE patients and HCs according to betweenness centrality (BC). Compared to HCs, patients show decreased BC in the blue highlighted nodes, increased BC in pink colored ones, and equal BC in the green nodes. R for right, L for left; Figure prepared using BrainNet Viewer (https://www.nitrc.org/projects/bnv/).

**Table 3.5** - Mean values and standard deviations of BC of the hubs in HCs and non-NPSLE patients

| Brain structural hubs | Patients (n=17) Mean ± SD | Healthy Controls (n=8) Mean ± SD | P-values |
|---|---|---|---|
| **R_V3** | 827.7 ± 513.14 | 1008.48 ± 665.86 | 0.46↓ |
| **L_SFL** | 5684.8 ± 4893.51 | 3425.29 ± 3307.67 | 0.25↑ |
| **L_9m** | 615.25 ± 368.51 | 1523.6 ± 1119.66 | 0.005↓* |
| **L_V3** | 709.46 ± 746.68 | 729.19 ± 517.37 | 0.94↓ |
| **R_9m** | 518.39 ± 498.4 | 876.79 ± 418.13 | 0.09↓ |
| **R_PoI1** | 1725.83 ± 1103.24 | 1162.33 ± 514.81 | 0.18↑ |
| **L_V2** | 1091.16 ± 385.62 | 1444.55 ± 725.99 | 0.12↓ |
| **L_4** | 2086.87 ± 1071.02 | 2776.25 ± 1222.12 | 0.16↓ |

| Brain structural hubs | Patients (n=17) Mean ± SD | Healthy Controls (n=8) Mean ± SD | P-values |
|---|---|---|---|
| **R_V2** | 1351.06 ± 951.35 | 1217.08 ± 354.44 | 0.7↑ |
| **R_4** | 2366.56 ± 1542.04 | 3126.07 ± 2064.21 | 0.31↓ |
| **R_IP0** | 630.16 ± 317.13 | 508.17 ± 353.88 | 0.39↑ |
| **R_POS2** | 607.45 ± 368.35 | 715.31 ± 393.64 | 0.51↓ |
| **R_SFL** | 4376.2 ± 3074.15 | 2020.85 ± 2636.9 | 0.07↑ |
| **L_POS2** | 719.86 ± 577.11 | 728.59 ± 205.23 | 0.96↓ |
| **L_PoI1** | 1588.3 ± 949.09 | 1182.24 ± 879.92 | 0.31↓ |
| **L_DVT** | 765.64 ± 596.73 | 490.7 ± 206.59 | 0.22↑ |
| **L_IP0** | 824.58 ± 500.53 | 571.84 ± 369.48 | 0.21↑ |
| **R_DVT** | 807.37 ± 561.86 | 844.45 ± 508.33 | 0.87↓ |
| **L_3b** | 960.95 ± 804.62 | 1327.15 ± 1220.79 | 0.37↓ |
| **L_FFC** | 608.84 ± 360.94 | 492.91 ± 620 | 0.55↑ |
| **R_8BM** | 1804.09 ± 1792.97 | 490.74 ± 210.32 | 0.05↑* |
| **R_V6** | 315.06 ± 237.39 | 255.93 ± 184.22 | 0.54↑ |
| **L_SCEF** | 2400.68 ± 2777.52 | 1116.13 ± 797.14 | 0.21↑ |
| **L_IPS1** | 596.68 ± 681.64 | 496.45 ± 380.33 | 0.7↑ |
| **R_PGp** | 509.34 ± 486.91 | 400.2 ± 284.58 | 0.56↑ |
| **L_VVC** | 308.28 ± 182.47 | 544.23 ± 470.36 | 0.08↓ |
| **L_V6** | 264.48 ± 222.03 | 290.63 ± 373.89 | 0.82↓ |
| **L_IP1** | 613.53 ± 820.45 | 559.54 ± 539.72 | 0.86↑ |
| **R_V7** | 297.71 ± 176.51 | 578.6 ± 897.44 | 0.21↓ |
| **R_IPS1** | 449.22 ± 363.8 | 281.74 ± 107.01 | 0.21↑ |
| **R_p24** | 757.14 ± 645.48 | 1219.44 ± 845.21 | 0.14↓ |
| **L_6ma** | 1532.62 ± 1608.47 | 2550.87 ± 1930.18 | 0.17↓ |
| **L_d32** | 528.41 ± 580.5 | 1154.64 ± 1011.18 | 0.06↓ |

| Brain structural hubs | Patients (n=17) Mean ± SD | Healthy Controls (n=8) Mean ± SD | P-values |
|---|---|---|---|
| **L_p24** | 721.95 ± 525.59 | 1029.95 ± 747.18 | 0.24↓ |
| **L_8BM** | 1002.52 ± 1112.58 | 680.41 ± 628.25 | 0.45↑ |
| **R_IP1** | 274.24 ± 226.09 | 153.23 ± 154.53 | 0.18↑ |
| **L_23c** | 1661.99 ± 1361.92 | 744.66 ± 492.45 | 0.07↑ |
| **L_PGs** | 471.98 ± 432.34 | 348.73 ± 359.33 | 0.49↑ |
| **R_6ma** | 2381.82 ± 1770.35 | 2653.76 ± 4000.34 | 0.81↓ |
| **L_TE1p** | 910.14 ± 610.06 | 316 ± 421.07 | 0.02↑* |
| **R_FFC** | 765.59 ± 884.6 | 757.58 ± 496.1 | 0.98↑ |
| **L_V7** | 343.83 ± 366.07 | 269.29 ± 276.97 | 0.61↑ |
| **R_1** | 699.08 ± 418.18 | 804.29 ± 566.53 | 0.6↓ |
| **R_p10p** | 714.95 ± 769.28 | 456.29 ± 571.99 | 0.4↑ |
| **R_3b** | 669.53 ± 444.01 | 631.91 ± 303.38 | 0.83↑ |
| **L_10d** | 312.59 ± 362.89 | 815.09 ± 565.58 | 0.11↓ |
| **R_a24** | 709.05 ± 558 | 1201.52 ± 927.87 | 0.01↓* |
| **R_PGs** | 331.01 ± 257.36 | 219.45 ± 155.03 | 0.27↑ |
| **L_9-46d** | 205.19 ± 163.98 | 265.73 ± 399.44 | 0.23↓ |
| **R_MBelt** | 530.06 ± 374.81 | 355.14 ± 209.89 | 0.59↑ |
| **L_PoI2** | 930.48 ± 396.75 | 970.62 ± 590.73 | 0.84↓ |
| **L_1** | 700.78 ± 330.53 | 876.07 ± 705.94 | 0.4↓ |
| **L_a24** | 597.3 ± 455.86 | 712.28 ± 501.92 | 0.61↓ |
| **L_5mv** | 756.03 ± 576.55 | 298.29 ± 199.1 | 0.6↑ |
| **R_d32** | 421.16 ± 425.94 | 631.15 ± 597.23 | 0.4↓* |
| **R_8BL** | 943.54 ± 1900.44 | 428.51 ± 624.74 | 0.83↑ |
| **R_PHT** | 540.81 ± 480.07 | 563.42 ± 827.5 | 0.11↓ |
| **L_6mp** | 866.31 ± 943.01 | 1429.74 ± 1692.57 | 0.01↓* |

| Brain structural hubs | Patients (n=17) Mean ± SD | Healthy Controls (n=8) Mean ± SD | P-values |
|---|---|---|---|
| **R_PoI2** | 650.99 ± 640.07 | 595.9 ± 841.33 | 0.27↑ |

*Hubs with the statistically significantly changed p-value. P-value calculated according to two-sample t-test. Arrows with p-values show whether patients show higher (↑) or lower (↓) than the HCs. R: Right, L: Left, SD: Standard Deviation, For abbreviations, see page xiv.

As demonstrated in Figure 3.5 and Table 3.6, in comparison with HCs, non-NPSLE patients showed lower CC bilaterally in SFL, PoI1, IP0, DVT, 8BM, and PoI2. Additionally, patients showed higher CC bilaterally in 9m, 4, d32, p24, and a24 areas

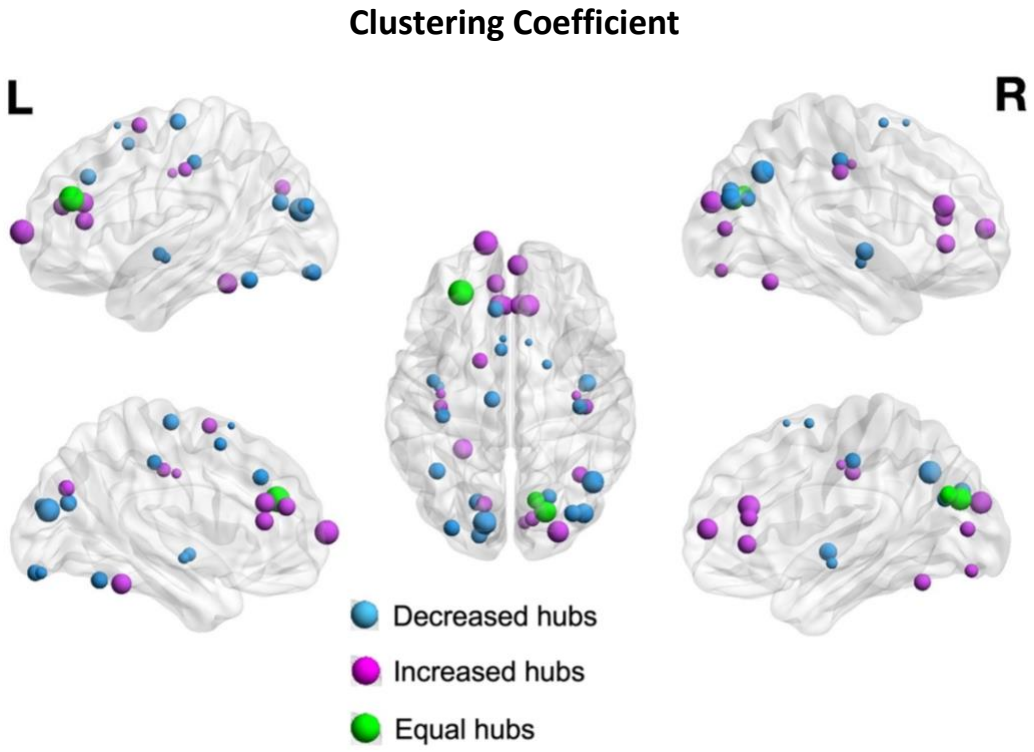


**Figure 3.5 -** Comparison of the structural brain nodes in non-NPSLE patients and HCs according to clustering coefficient (CC). Compared to HCs, patients show decreased CC in the blue highlighted nodes, increased CC in pink colored ones, and equal CC in the green nodes. R for right, L for left; Figure prepared using BrainNet Viewer (https://www.nitrc.org/projects/bnv/).

compared to HCs. Right POS2 and V6 and left 9-46d showed the same CC in both HCs and patients. The left V2, V3, FFC, V6, V7, 1, SCEF, 23C, TE1p, 5mv, and 6mp areas and in the right hemisphere the IPS1, 3b, IP1, PGp, 6ma, p10p, PGs, Mbelt2, 8BL, and PHT area showed lower CC in patients compared to healthy controls. The remaining hubs showed higher CC in patients in comparison with HCs. Moreover, in patients right SFL and left FFC and TE1p showed a significant decrease in CC compared to healthy controls (p: 0.03, p: 0.02, and 0.01, respectively). Compared to HCs, CCs were significantly increased in the left 10d area (part of the prefrontal cortical area) in patients (p: 0.02). The abovementioned hub regions' detailed explanations are represented in the abbreviations page xiv.

**Table 3.6** - Mean values and standard deviations of clustering coefficient (CC) in HCs and non-NPSLE patients

| Brain structural hubs | Patients (n=17) Mean ± SD | Healthy Controls (n=8) Mean ± SD | P-values |
|---|---|---|---|
| **R_V3** | 0.43 ± 0.06 | 0.43 ± 0.07 | 0.84↑ |
| **L_SFL** | 0.31 ± 0.11 | 0.36 ± 0.1 | 0.29↓ |
| **L_9m** | 0.48 ± 0.06 | 0.4 ± 0.06 | 0.005↑* |
| **L_V3** | 0.45 ± 0.06 | 0.46 ± 0.07 | 0.77↓ |
| **R_9m** | 0.51 ± 0.08 | 0.44 ± 0.04 | 0.04↑ |
| **R_PoI1** | 0.37 ± 0.05 | 0.4 ± 0.05 | 0.22↓ |
| **L_V2** | 0.39 ± 0.04 | 0.4 ± 0.06 | 0.76↓ |
| **L_4** | 0.35 ± 0.04 | 0.33 ± 0.03 | 0.4↑ |
| **R_V2** | 0.4 ± 0.07 | 0.39 ± 0.03 | 0.84↑ |
| **R_4** | 0.35 ± 0.05 | 0.34 ± 0.04 | 0.55↑ |
| **R_IP0** | 0.46 ± 0.06 | 0.51 ± 0.08 | 0.15↓ |
| **R_POS2** | 0.47 ± 0.04 | 0.47 ± 0.03 | 0.96 |
| **R_SFL** | 0.31 ± 0.09 | 0.41 ± 0.11 | 0.03↓* |
| **L_POS2** | 0.45 ± 0.06 | 0.44 ± 0.02 | 0.6↑ |
| **L_PoI1** | 0.37 ± 0.06 | 0.41 ± 0.06 | 0.17↓ |
| **L_DVT** | 0.46 ± 0.08 | 0.49 ± 0.07 | 0.24↓ |

| Brain structural hubs | Patients (n=17) Mean ± SD | Healthy Controls (n=8) Mean ± SD | P-values |
|---|---|---|---|
| **L_IP0** | 0.45 ± 0.06 | 0.47 ± 0.07 | 0.43↓ |
| **R_DVT** | 0.44 ± 0.04 | 0.45 ± 0.07 | 0.71↓ |
| **L_3b** | 0.42± 0.06 | 0.4 ± 0.07 | 0.61↑ |
| **L_FFC** | 0.46± 0.06 | 0.53 ± 0.1 | 0.02↓* |
| **R_8BM** | 0.41 ± 0.11 | 0.49 ± 0.08 | 0.08↓ |
| **R_V6** | 0.54 ± 0.1 | 0.54 ± 0.06 | 0.97 |
| **L_SCEF** | 0.4 ± 0.14 | 0.41 ± 0.07 | 0.79↓ |
| **L_IPS1** | 0.49 ± 0.08 | 0.48 ± 0.06 | 0.88↑ |
| **R_PGp** | 0.5 ± 0.06 | 0.54 ± 0.08 | 0.15↓ |
| **L_VVC** | 0.51 ± 0.07 | 0.5 ± 0.1 | 0.81↑ |
| **L_V6** | 0.56 ± 0.09 | 0.59 ± 0.13 | 0.6↓ |
| **L_IP1** | 0.5 ± 0.11 | 0.45 ± 0.07 | 0.2↑ |
| **R_V7** | 0.53 ± 0.08 | 0.52 ± 0.11 | 0.87↑ |
| **R_IPS1** | 0.51 ± 0.08 | 0.54 ± 0.04 | 0.3↓ |
| **R_p24** | 0.46 ± 0.07 | 0.41 ± 0.06 | 0.08↑ |
| **L_6ma** | 0.44 ± 0.16 | 0.37 ± 0.1 | 0.3↑ |
| **L_d32** | 0.51 ± 0.09 | 0.45 ± 0.14 | 0.18↑ |
| **L_p24** | 0.48 ± 0.1 | 0.43 ± 0.08 | 0.24↑ |
| **L_8BM** | 0.45 ± 0.1 | 0.48 ± 0.09 | 0.61↓ |
| **R_IP1** | 0.56 ± 0.08 | 0.64 ± 0.1 | 0.06↓ |
| **L_23c** | 0.39 ± 0.09 | 0.45 ± 0.05 | 0.08↓ |
| **L_PGs** | 0.52 ± 0.1 | 0.5 ± 0.1 | 0.76↑ |
| **R_6ma** | 0.35 ± 0.09 | 0.43 ± 0.16 | 0.09↓ |
| **L_TE1p** | 0.44 ± 0.09 | 0.55 ± 0.1 | 0.01↓ |
| **R_FFC** | 0.45 ± 0.07 | 0.44 ± 0.07 | 0.66↑ |

| Brain structural hubs | Patients (n=17) Mean ± SD | Healthy Controls (n=8) Mean ± SD | P-values |
|---|---|---|---|
| **L_V7** | 0.54 ± 0.09 | 0.55 ± 0.1 | 0.87↓ |
| **R_1** | 0.44 ± 0.06 | 0.45 ± 0.05 | 0.9↑ |
| **R_p10p** | 0.51 ± 0.14 | 0.52 ± 0.12 | 0.92↓ |
| **R_3b** | 0.44 ± 0.06 | 0.45 ± 0.05 | 0.77↓ |
| **L_10d** | 0.57 ± 0.11 | 0.47 ± 0.1 | 0.02↑* |
| **R_a24** | 0.48 ± 0.11 | 0.41 ± 0.06 | 0.08↑ |
| **R_PGs** | 0.54 ± 0.07 | 0.58 ± 0.07 | 0.15↓ |
| **L_9-46d** | 0.59 ± 0.07 | 0.59 ± 0.08 | 0.96 |
| **R_MBelt** | 0.48 ± 0.07 | 0.5 ± 0.06 | 0.45↓ |
| **L_PoI2** | 0.41 ± 0.04 | 0.42 ± 0.05 | 0.61↓ |
| **L_1** | 0.43 ± 0.04 | 0.43 ± 0.07 | 0.84↓ |
| **L_a24** | 0.49 ± 0.09 | 0.45 ± 0.06 | 0.18↑ |
| **L_5mv** | 0.44 ± 0.08 | 0.5 ± 0.05 | 0.07↓ |
| **R_d32** | 0.53 ± 0.09 | 0.49 ± 0.09 | 0.24↑ |
| **R_8BL** | 0.53 ± 0.16 | 0.59 ± 0.18 | 0.44↓ |
| **R_PHT** | 0.49 ± 0.08 | 0.51 ± 0.1 | 0.52↓ |
| **L_6mp** | 0.45 ± 0.1 | 0.46 ± 0.18 | 0.77↓ |
| **R_PoI2** | 0.47 ± 0.07 | 0.49 ± 0.08 | 0.43↓ |

*Hubs with the statistically significantly changed p-value. P-value calculated according to two-sample t-test. Arrows with p-values show whether patients show higher (↑) or lower (↓) than the HCs. R: Right, L: Left, SD: Standard Deviation, For abbreviations, see page xiv.

Figure 3.6 and Table 3.7 illustrated that in comparison to healthy controls, non-NPSLE patients had significantly decreased LE in the left FFC, and TE1p and in the right SFL hubs. Moreover, non-NPSLE patients showed a significant increase in the left 10d and bilateral 9m hubs compared to healthy controls. Furthermore, patients showed reduced LE bilaterally in SFL, PoI1, IP0, DVT, PoI2, and 8BM hubs, and in

the left V2, V3, FFC, SCEF, V6, 1, 5mv, 23c, TE1p, V7, and 6mp regions and in the right 3b, IPS1, IP1, 6ma, PGp, PGs, Mbelt, 8BL, and PHT areas compared with HCs. In addition, the V2, POS2, V6, 1, and p10p hubs of the right hemisphere showed the same LE in both patients and healthy controls. Patients showed increased LE bilaterally in 9m, 4, p24, a24, and d32 areas compared with HCs. The rest of the hubs demonstrated higher LE in patients compared to HCs.

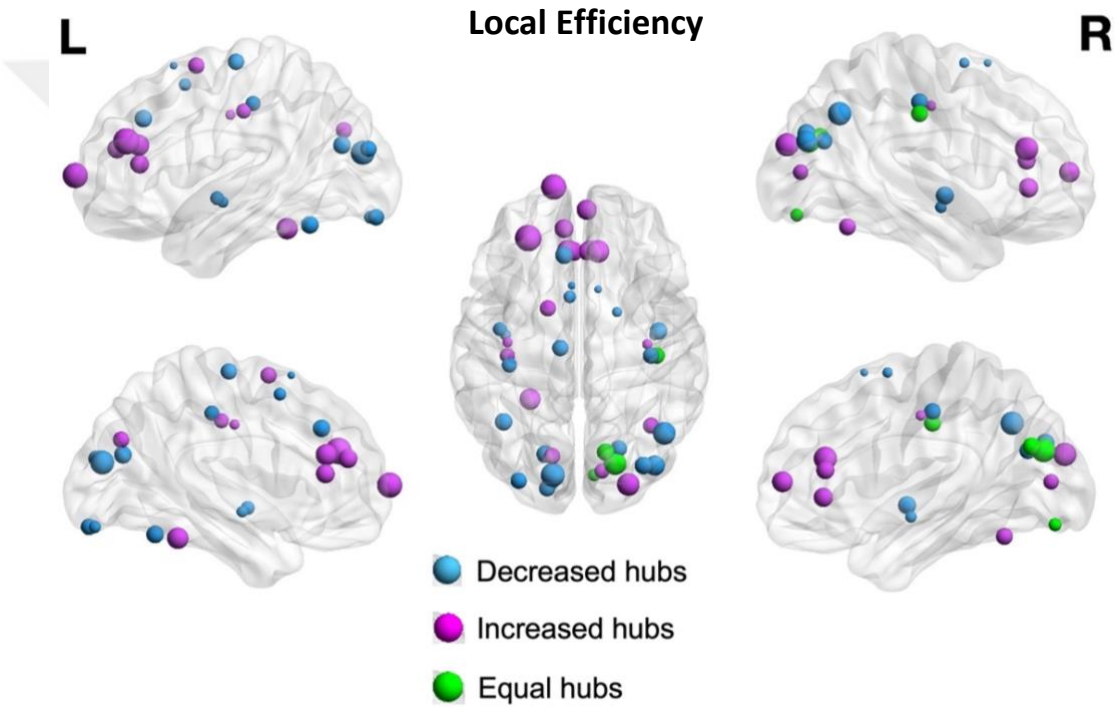


**Figure 3.6 -** Comparison of the structural brain nodes in non-NPSLE patients and HCs according to local efficiency (LE). Compared to HCs, patients exhibited decreased LE in the blue highlighted nodes, increased LE in pink colored ones, and equal LE in the green nodes. R for right, L for left; Figure prepared using BrainNet Viewer (https://www.nitrc.org/projects/bnv/).

**Table 3.7 -** Mean values and standard deviations of local efficiency (LE) in HCs and non-NPSLE patients

| Brain structural hubs | Patients (n=17) Mean ± SD | Healthy Controls (n=8) Mean ± SD | P-values |
|---|---|---|---|
| **R_V3** | 0.71 ±0.03 | 0.7 ± 0.04 | 0.78↑ |
| **L_SFL** | 0.65 ±0.06 | 0.67 ± 0.05 | 0.3↓ |

| Brain structural hubs | Patients (n=17) Mean ± SD | Healthy Controls (n=8) Mean ± SD | P-values |
|---|---|---|---|
| **L_9m** | 0.74 ±0.03 | 0.7 ± 0.03 | 0.006↑* |
| **L_V3** | 0.72 ±0.03 | 0.73 ± 0.04 | 0.67↓ |
| **R_9m** | 0.75 ±0.04 | 0.72 ± 0.02 | 0.03↑* |
| **R_PoI1** | 0.68 ±0.03 | 0.7 ± 0.03 | 0.2↓ |
| **L_V2** | 0.69 ±0.02 | 0.7 ± 0.03 | 0.67↓ |
| **L_4** | 0.67 ±0.02 | 0.66 ± 0.01 | 0.53↑ |
| **R_V2** | 0.69 ±0.04 | 0.69 ± 0.02 | 1 |
| **R_4** | 0.67 ±0.03 | 0.66 ± 0.02 | 0.59↑ |
| **R_IP0** | 0.73 ±0.03 | 0.75 ± 0.04 | 0.15↓ |
| **R_POS2** | 0.73 ±0.02 | 0.73 ± 0.02 | 1 |
| **R_SFL** | 0.65 ±0.05 | 0.7 ± 0.06 | 0.03↓* |
| **L_POS2** | 0.72 ±0.03 | 0.72 ± 0.01 | 0.58↑ |
| **L_PoI1** | 0.68 ±0.03 | 0.7 ± 0.03 | 0.18↓ |
| **L_DVT** | 0.73 ±0.04 | 0.75 ± 0.03 | 0.24↓ |
| **L_IP0** | 0.72 ±0.03 | 0.73 ± 0.03 | 0.42↓ |
| **R_DVT** | 0.72 ±0.02 | 0.73 ± 0.03 | 0.7↓ |
| **L_3b** | 0.71 ±0.03 | 0.7 ± 0.04 | 0.57↑ |
| **L_FFC** | 0.73 ±0.03 | 0.77 ± 0.05 | 0.02↓ |
| **R_8BM** | 0.7 ±0.06 | 0.74 ± 0.04 | 0.08↓ |
| **R_V6** | 0.77 ±0.05 | 0.77 ± 0.03 | 1 |
| **L_SCEF** | 0.69 ±0.07 | 0.7 ± 0.04 | 0.75↓ |
| **L_IPS1** | 0.74 ±0.04 | 0.74 ± 0.03 | 0.88↑ |
| **R_PGp** | 0.75 ±0.03 | 0.77 ± 0.04 | 0.16↓ |
| **L_VVC** | 0.76 ±0.03 | 0.75 ± 0.05 | 0.81↑ |
| **L_V6** | 0.78 ±0.04 | 0.79 ± 0.07 | 0.63↓ |
| **L_IP1** | 0.75 ±0.05 | 0.72 ± 0.03 | 0.18↑ |

| Brain structural hubs | Patients (n=17) Mean ± SD | Healthy Controls (n=8) Mean ± SD | P-values |
|---|---|---|---|
| **R_V7** | 0.77 ±0.04 | 0.76 ± 0.06 | 0.83↑ |
| **R_IPS1** | 0.75 ±0.04 | 0.77 ± 0.02 | 0.32↓ |
| **R_p24** | 0.73 ±0.04 | 0.7 ± 0.03 | 0.08↑ |
| **L_6ma** | 0.72 ±0.08 | 0.68 ± 0.05 | 0.28↑ |
| **L_d32** | 0.76 ±0.04 | 0.73 ± 0.07 | 0.18↑ |
| **L_p24** | 0.74 ±0.05 | 0.71 ± 0.04 | 0.25↑ |
| **L_8BM** | 0.73 ±0.05 | 0.74 ± 0.05 | 0.62↓ |
| **R_IP1** | 0.78 ±0.04 | 0.82 ± 0.05 | 0.06↓ |
| **L_23c** | 0.69 ±0.05 | 0.72 ± 0.02 | 0.1↓ |
| **L_PGs** | 0.76 ±0.05 | 0.75 ± 0.05 | 0.76↑ |
| **R_6ma** | 0.67 ±0.05 | 0.71 ± 0.09 | 0.12↓ |
| **L_TE1p** | 0.72 ±0.05 | 0.78 ± 0.05 | 0.01↓* |
| **R_FFC** | 0.72 ±0.04 | 0.71 ± 0.04 | 0.84↑ |
| **L_V7** | 0.77 ±0.04 | 0.77 ± 0.05 | 0.88↓ |
| **R_1** | 0.72 ±0.03 | 0.72 ± 0.03 | 1 |
| **R_p10p** | 0.76 ±0.07 | 0.76 ± 0.06 | 1 |
| **R_3b** | 0.72 ±0.03 | 0.73 ± 0.02 | 0.74↓ |
| **L_10d** | 0.79 ±0.05 | 0.73 ± 0.05 | 0.02↑* |
| **R_a24** | 0.74 ±0.05 | 0.7 ± 0.03 | 0.08↑ |
| **R_PGs** | 0.77 ±0.04 | 0.79 ± 0.04 | 0.15↓ |
| **L_9-46d** | 0.8 ±0.04 | 0.79 ± 0.04 | 0.94↑ |
| **R_MBelt** | 0.74 ±0.03 | 0.75 ± 0.03 | 0.45↓ |
| **L_PoI2** | 0.7 ±0.02 | 0.71 ± 0.03 | 0.62↓ |
| **L_1** | 0.71 ±0.02 | 0.71 ± 0.04 | 0.87↓ |
| **L_a24** | 0.75 ±0.05 | 0.72 ± 0.03 | 0.18↑ |

| Brain structural hubs | Patients (n=17) Mean ± SD | Healthy Controls (n=8) Mean ± SD | P-values |
|---|---|---|---|
| **L_5mv** | 0.72 ±0.04 | 0.75 ± 0.03 | 0.07↓ |
| **R_d32** | 0.77 ±0.04 | 0.74 ± 0.05 | 0.24↑ |
| **R_8BL** | 0.76 ±0.08 | 0.79 ± 0.09 | 0.45↓ |
| **R_PHT** | 0.74 ±0.04 | 0.75 ± 0.05 | 0.52↓ |
| **L_6mp** | 0.72 ±0.05 | 0.73 ± 0.09 | 0.78↓ |
| **R_PoI2** | 0.73 ±0.03 | 0.74 ± 0.04 | 0.44↓ |

*Hubs with the statistically significantly changed p-value. P-value calculated according to two-sample t-test. Arrows with p-values show whether patients show higher (↑) or lower (↓) than the HCs. R: Right, L: Left, SD: Standard Deviation, For abbreviations, see page xiv.

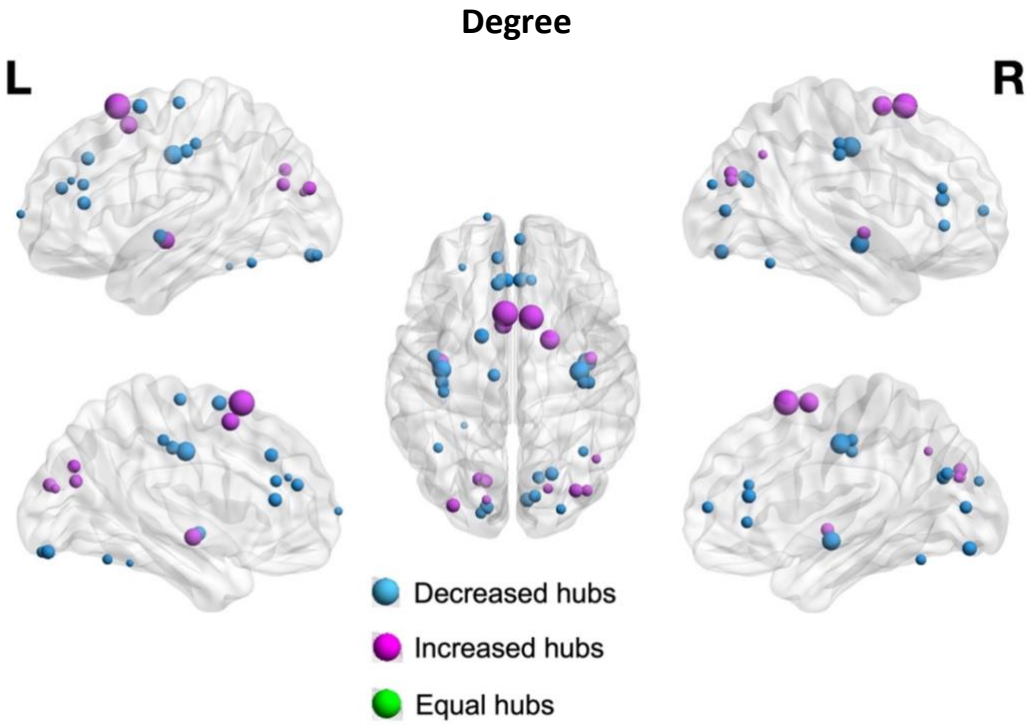


**Figure 3.7 -** Comparison of the structural brain nodes in non-NPSLE patients and HCs according to the nodal degree. Compared to HCs, patients show decreased degree in the blue highlighted nodes, increased nodal degree in pink colored ones. R for right, L for left; Figure prepared using BrainNet Viewer (https://www.nitrc.org/projects/bnv/).

As presented in Figure 3.7 and Table 3.8, non-NPSLE patients' degree reduced significantly in the left 9m, VVC, and 10d areas and in the right a24 hub compared to healthy controls (p: 0.01, p: 0.01, p: 0.03 and p: 0.03 respectively). In comparison with HCs, patients showed a lower degree bilaterally in the V3, 9m, V2, 4, a24, FFC, 1, 3b, d32, and p24. Additionally, in the right PoI1, POS2, DVT, V7, Mbelt, PGp and PHT and in the left PoI2, 9-46d, 6mp, VVC, 6ma, 8BM, and 10d hubs lower degree observed in patients compared with healthy controls. The remaining shared structural hubs showed a higher degree in non-NPSLE patients in comparison to HCs.

**Table 3.8** - Mean value and standard deviation of degree in the Healthy controls and non-NPSLE patients' hubs

| Brain structural hubs | Patients (n=17) Mean ± SD | Healthy Controls (n=8) Mean ± SD | P-values |
|---|---|---|---|
| **R_V3** | 75.88 ± 24.15 | 82 ± 12.34 | 0.5↓ |
| **L_SFL** | 141.41 ± 53.7 | 127.38 ± 46.53 | 0.53↑ |
| **L_9m** | 77.18 ± 22.66 | 106.25 ± 27.58 | 0.01↓* |
| **L_V3** | 70.71 ± 21.48 | 77.5 ± 28.37 | 0.51↓ |
| **R_9m** | 71.53 ± 22.98 | 89.75 ± 22.96 | 0.07↓ |
| **R_PoI1** | 105.88 ± 19.86 | 107.12 ± 20.05 | 0.88↓ |
| **L_V2** | 83.53 ± 17.16 | 104.62 ± 38.38 | 0.06↓ |
| **L_4** | 107.94 ± 31.61 | 128.62 ± 38.45 | 0.1↓ |
| **R_V2** | 85.41 ± 22.9 | 98.88 ± 30.78 | 0.23↓ |
| **R_4** | 113 ± 33.07 | 136.75 ± 50.11 | 0.16↓ |
| **R_IP0** | 81.88 ± 14.6 | 78.88 ± 20.12 | 0.67↑ |
| **R_POS2** | 76.47 ± 23.59 | 79.62 ± 22.93 | 0.75↓ |
| **R_SFL** | 137.29 ± 39.8 | 102.62 ± 50.55 | 0.07↑ |
| **L_POS2** | 78.76 ± 25.04 | 78 ± 24.38 | 0.94↑ |
| **L_PoI1** | 100.59 ± 19.77 | 99.5 ± 15.59 | 0.89↑ |
| **L_DVT** | 80.35 ± 24.39 | 71.38 ± 18.67 | 0.36↑ |
| **L_IP0** | 82.59 ± 25.47 | 75.38 ± 16.99 | 0.47↑ |

| Brain structural hubs | Patients (n=17) Mean ± SD | Healthy Controls (n=8) Mean ± SD | P-values |
|---|---|---|---|
| **R_DVT** | 81.82 ± 23.32 | 84.75 ± 22.54 | 0.77↓ |
| **L_3b** | 81.82 ± 24.92 | 90.25 ± 33.1 | 0.48↓ |
| **L_FFC** | 63.88 ± 21.14 | 65.38 ± 14.75 | 0.85↓ |
| **R_8BM** | 98.88 ± 41 | 72.25 ± 21.24 | 0.09↑ |
| **R_V6** | 63.76 ± 22.34 | 61.75 ± 16.8 | 0.82↑ |
| **L_SCEF** | 102.41 ± 55.99 | 97.12 ± 37.64 | 0.81↑ |
| **L_IPS1** | 73.41 ± 27.96 | 60.88 ± 19.53 | 0.26↑ |
| **R_PGp** | 70.47 ± 15.74 | 70.62 ± 22.98 | 0.98↑ |
| **L_VVC** | 50.47 ± 16.43 | 69 ± 19.09 | 0.01↓* |
| **L_V6** | 60.06 ± 24.74 | 57.12 ± 24.71 | 0.78↑ |
| **L_IP1** | 70 ± 22.54 | 60.38 ± 24.67 | 0.34↑ |
| **R_V7** | 64.59 ± 17.21 | 66.25 ± 12.6 | 0.81↓ |
| **R_IPS1** | 69.29 ± 15.99 | 60.62 ± 14.85 | 0.2↑ |
| **R_p24** | 83.65 ± 24.81 | 104.25 ± 32.74 | 0.09↓ |
| **L_6ma** | 87.71 ± 45.19 | 118.25 ± 40.92 | 0.11↓ |
| **L_d32** | 72.76 ± 24.22 | 95.5 ± 32.57 | 0.06↓ |
| **L_p24** | 81.82 ± 25.25 | 96 ± 24.84 | 0.2↓ |
| **L_8BM** | 80.88 ± 23.2 | 81.12 ± 33.1 | 0.98↓ |
| **R_IP1** | 57.71 ± 15.4 | 48 ± 23.84 | 0.23↑ |
| **L_23c** | 98.41 ± 37.13 | 72.75 ± 31.84 | 0.1↑ |
| **L_PGs** | 64.59 ± 18.06 | 51.25 ± 25.74 | 0.14↑ |
| **R_6ma** | 110.88 ± 33.3 | 99 ± 47.64 | 0.47↑ |
| **L_TE1p** | 80.65 ± 25.79 | 61 ± 20.68 | 0.07↑ |
| **R_FFC** | 66.06 ± 30.47 | 78.62 ± 19.32 | 0.29↓ |
| **L_V7** | 63.24 ± 25.45 | 56.25 ± 21.51 | 0.5↑ |

| Brain structural hubs | Patients (n=17) Mean ± SD | Healthy Controls (n=8) Mean ± SD | P-values |
|---|---|---|---|
| **R_1** | 76.82 ± 23.84 | 86 ± 38.99 | 0.47↓ |
| **R_p10p** | 67.94 ± 26.95 | 60.12 ± 23.17 | 0.48↑ |
| **R_3b** | 74.24 ± 26.44 | 84.62 ± 30.24 | 0.38↓ |
| **L_10d** | 55.18 ± 20.64 | 77.5 ± 26.41 | 0.03↓* |
| **R_a24** | 72.65 ± 23.83 | 95.5 ± 25.89 | 0.03↓* |
| **R_PGs** | 58.71 ± 10.56 | 55.62 ± 18.92 | 0.6↑ |
| **L_9-46d** | 52.76 ± 17.99 | 56.12 ± 27.85 | 0.71↓ |
| **R_MBelt** | 78.18 ± 15.28 | 78.75 ± 24.78 | 0.94↓ |
| **L_PoI2** | 84.47 ± 12.38 | 94.12 ± 12.96 | 0.08↓ |
| **L_1** | 72.41 ± 18.73 | 77.75 ± 24.9 | 0.55↓ |
| **L_a24** | 70 ± 21.11 | 82.38 ± 10.29 | 0.13↓ |
| **L_5mv** | 77.94 ± 32.2 | 56.75 ± 20.35 | 0.1↑ |
| **R_d32** | 68.18 ± 23.44 | 79.25 ± 26.8 | 0.3↓ |
| **R_8BL** | 64.24 ± 33.34 | 55 ± 27 | 0.5↑ |
| **R_PHT** | 71.88 ± 26.09 | 75.75 ± 34.78 | 0.75↓ |
| **L_6mp** | 76 ± 31.24 | 91.38 ± 54.83 | 0.37↓ |
| **R_PoI2** | 80.06 ± 20.12 | 78.5 ± 25.03 | 0.86↑ |

*Hubs with the statistically significantly changed p-value. P-value calculated according to two-sample t-test. Arrows with p-values show whether patients show higher (↑) or lower (↓) than the HCs. R: Right, L: Left, SD: Standard Deviation, For abbreviations, see page xiv.

## 3.6 Correlations between network measures and clinical variables

### 3.6.1 Correlation with demographic features

The results of the correlation between demographic features and network parameters are shown in Figure 3.8 and Table 3.9.

BC of the right V3 and PGp, and left SCEF hubs showed a significantly negative correlation with the age of the patients (r from -0.68 to -0.48, p from 0.007 to 0.04), i.e., as the age increases, the BC decreases. Similarly, CC and LE presented a significant negative correlation with age in R_PoI2 ($r = -0.49$, $p = 0.04$) and a significant positive correlation with R_V3, R_PGp, and L_a24 regions (r from 0.49 to 0.61, and p from 0.008 to 0.04). The results are displayed in Figure 3.8a.

The strength of the right POS2, DVT, PGp, IP1, and left 23c, PGs, POS2, and IPS1 hubs showed a significant positive correlation with age at disease onset (r from 0.48 to 0.68 and p from 0.002 to 0.046). The CC and LE of the R_V3, R_V2, R_4, and R_1 also showed significantly positive correlation with disease onset age (r from 0.52 to 0.7 and p from 0.001 to 0.03). The results are shown in Figure 3.8b.

The results of Spearman's rank correlation coefficient analyses indicated that the strength in the non-NPSLE patients presented a significant negative correlation with disease duration in R_POS2, L_POS2, L_IP0, R_DVT, L_IPS1, R_PGp, and L_IP1 hubs (r from -0.56 to -0.48, and p from 0.002 to 0.036). The BC showed a significant negative correlation with disease duration in L_IP0 ($r = -0.53$, $p = 0.029$). Similarly, the CC and LE of R_4 and L_DVT were significantly negatively correlated with disease duration (r from -0.57 to -0.53, and p from 0.01 to 0.02).

(a) Age

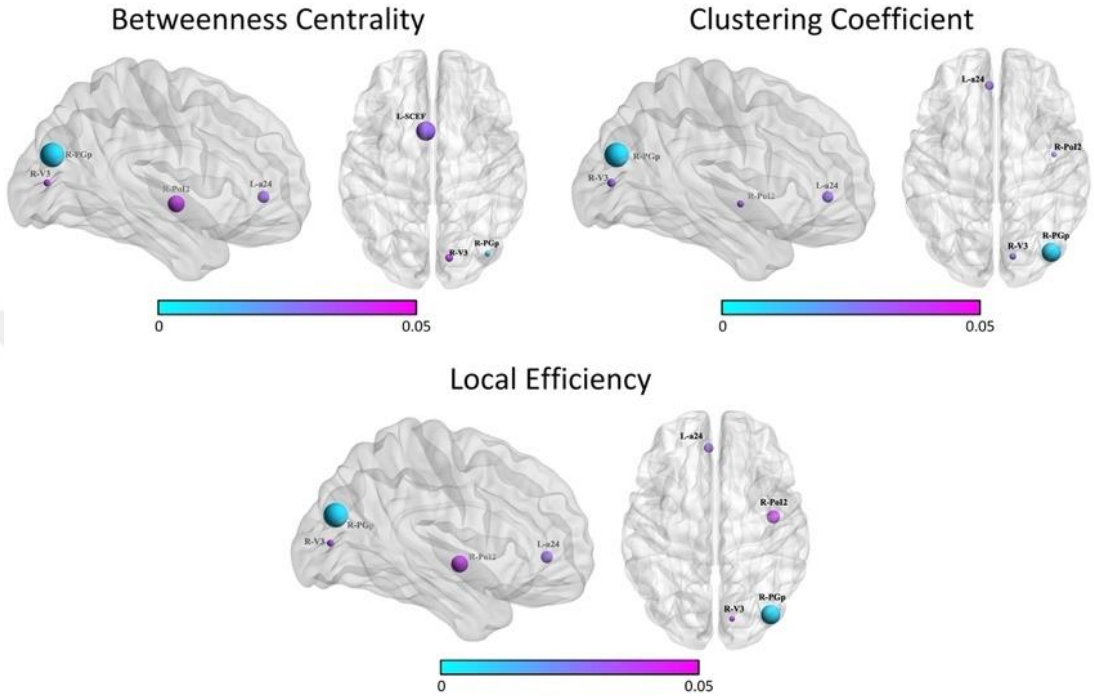


(b) Age at Disease-Onset

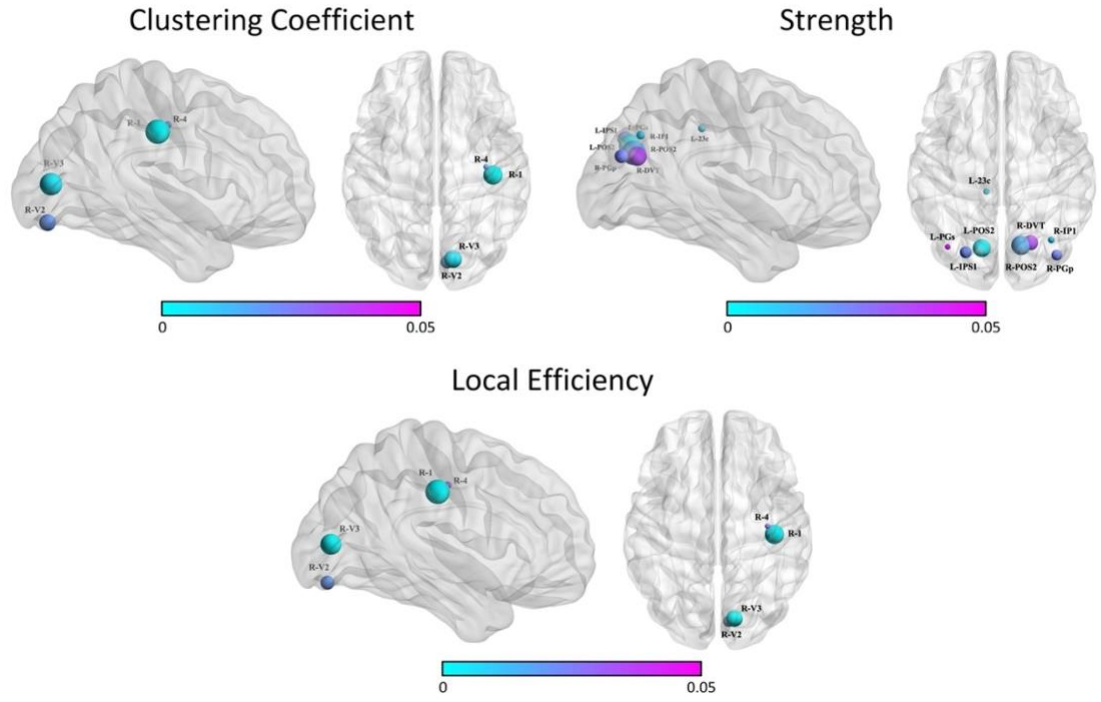

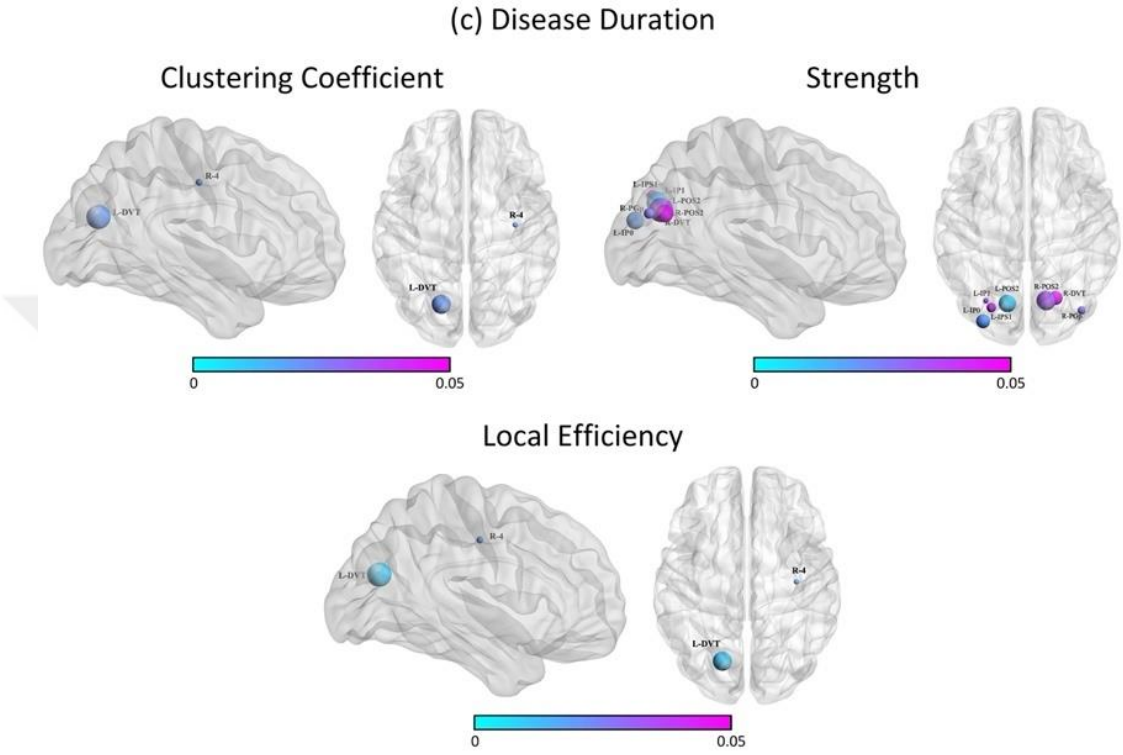


**Figure 3.8** - Structural brain hubs show the significant correlations between network metrics (a) age (b) age at disease onset (c) disease duration, in non-NPSLE patients and HCs. The color bars show the range of p-values. R for right, L for left; Figure prepared using BrainNet Viewer (https://www.nitrc.org/projects/bnv/).

### 3.6.2 Correlation with disease scores

The strength of the L_1 presented a significant positive correlation with the SLICC value (r = 0.58, p = 0.01). The CC of the L_6ma was also significantly positively correlated with the SLICC score (r = 0.56, p = 0.01).

Correlation coefficient analysis revealed that the strength of the right SFL and 8BL significantly negatively correlated with the STAI Trait score (r = -0.66, p = 0.003; r = -0.52, p = 0.029 respectively). The strength of the L_POS2, L_DVT, and L_IPS1also displayed a significant positive correlation with the STAI Trait score (r from 0.53 to 0.6 and p from 0.01 to 0.02). Similarly, the BC presented a significant negative

correlation with the STAI Trait value in L_V3, L_PoI2, R_SFL, R_8BM, and R_8BL hubs (r from -0.72 to -0.5 and p from 0.0008 to 0.03). The BC has also presented a significantly positive correlation with the STAI Trait score in L_POS2, L_p24, and L_TE1p (r from 0.51 to 0.57, and p from 0.016 to 0.03). Additionally, the CC presented a significantly positive correlation in L_V3, R_8BM, and R_8BL regions (r from 0.55 to 0.64, and p from 0.004 to 0.02) and a significant negative correlation in R_p24, L_TE1p, and L_9.46d hubs (r from -0.69 to -0.52, and p from 0.001 to 0.02) with STAI Trait value. Similarly, the LE presented a significant negative correlation with STAI Trait value in L_TE1p, and L_9.46d (r = -0.6, p = 0.01; r = -0.68, p = 0.002 respectively) and a significant positive correlation with STAI Trait value in L_V3, R_8BM, and R_8BL (r from 0.5 to 0.64 and p from 0.006 to 0.03). The strength presented a significant negative correlation in R_SFL, R_8BM, and L_SCEF areas (r from -0.66 to -0.51 and p from 0.003 to 0.033) and a significant positive correlation in L_POS2, L_DVT, L_IP0, L_V7, and L_9.46d regions (r from 0.49 to 0.64 and p from 0.005 to 0.04) with STAI State score. Correspondingly, the BC of the L_V3, L_SCEF, L_VVC, L_PoI2, R_8BM, and R_8BL regions were significantly negatively correlated with STAI State value (r from -0.7 to -0.53, and p from 0.001 to 0.02). The CC presented a significantly positive correlation with STAI State score in L_V3, L_SCEF, L_8BM, R_8BL, R_8BM regions (r from 0.51 to 0.76 and p from 0.0003 to 0.03) and a significant negative correlation in L_p24 (r = -0.48 and p = 0.04). Similarly, the LE showed a significant negative correlation in L_9m (r = -0.48, p = 0.04) and in L_V3, R_8BM, L_SCEF, L_8BM, and R_8BL regions (r from 0.51 to 0.72 and p from 0.0009 to 0.03) a significant positive correlation with STAI State score. BC had a significant positive correlation with NCD in L_10d, and L_9.46d areas (r = 0.52, p = 0.02; and r = 0.6, p = 0.009 respectively) and a significant negative correlation in L_23c and L_5mv regions (r = -0.63, p = 0.006; and r = -0.57, p = 0.01). There was a positive correlation between CC and NCD in L_23c and L_5mv areas (r = 0.6, p = 0.009; and r = 0.55, p = 0.02 respectively). Similarly, the LE presented a positive correlation in L_23c and L_5mv areas with NCD (r = 0.6, p = 0.009; and r = 0.52, p = 0.02 respectively). The results are summarized in Figure 3.9 and Table 3.9.

(a) SLEDAI

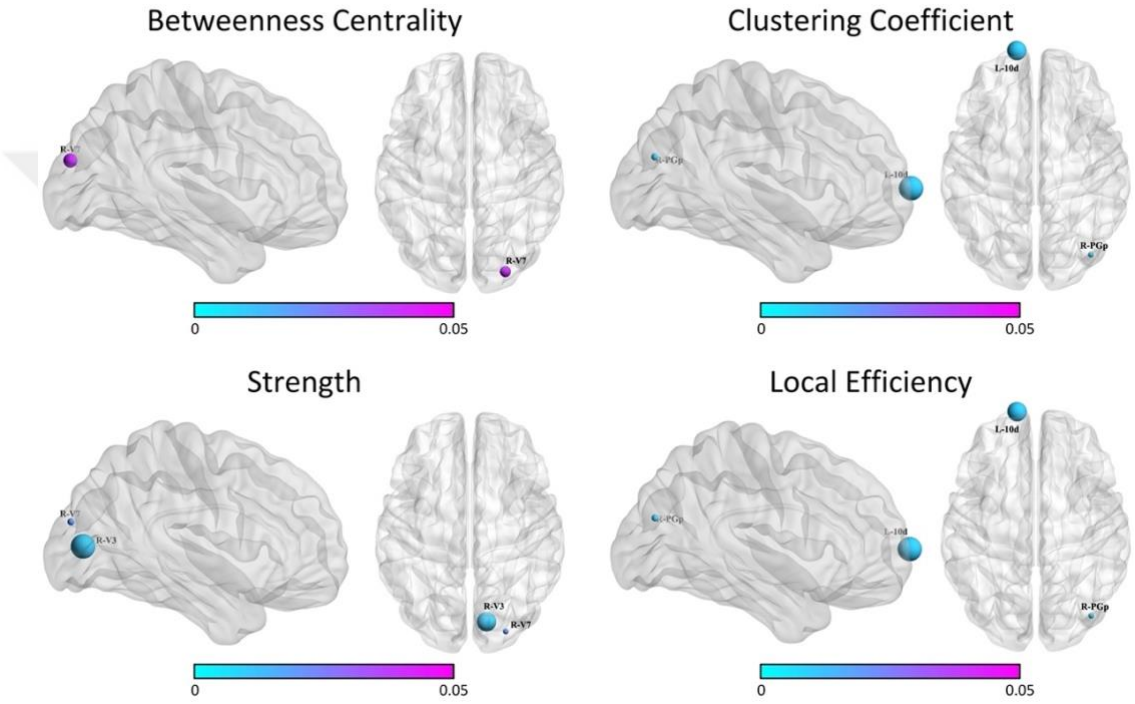


(b) SLICC

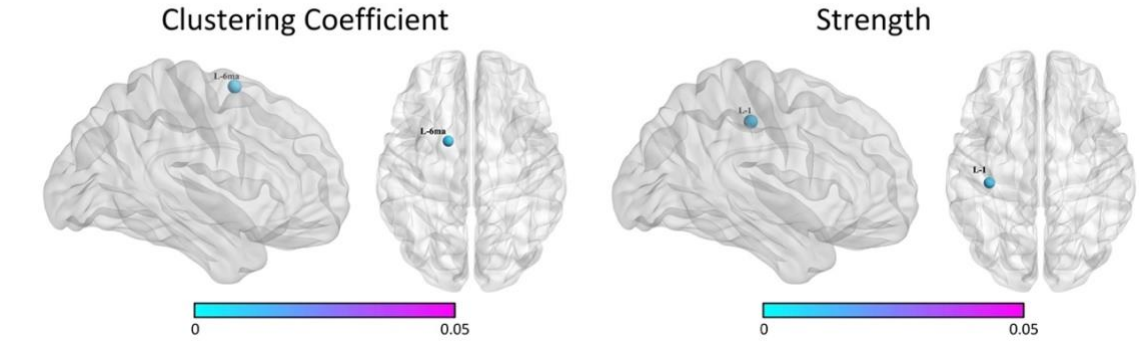

(c) STAI Trait

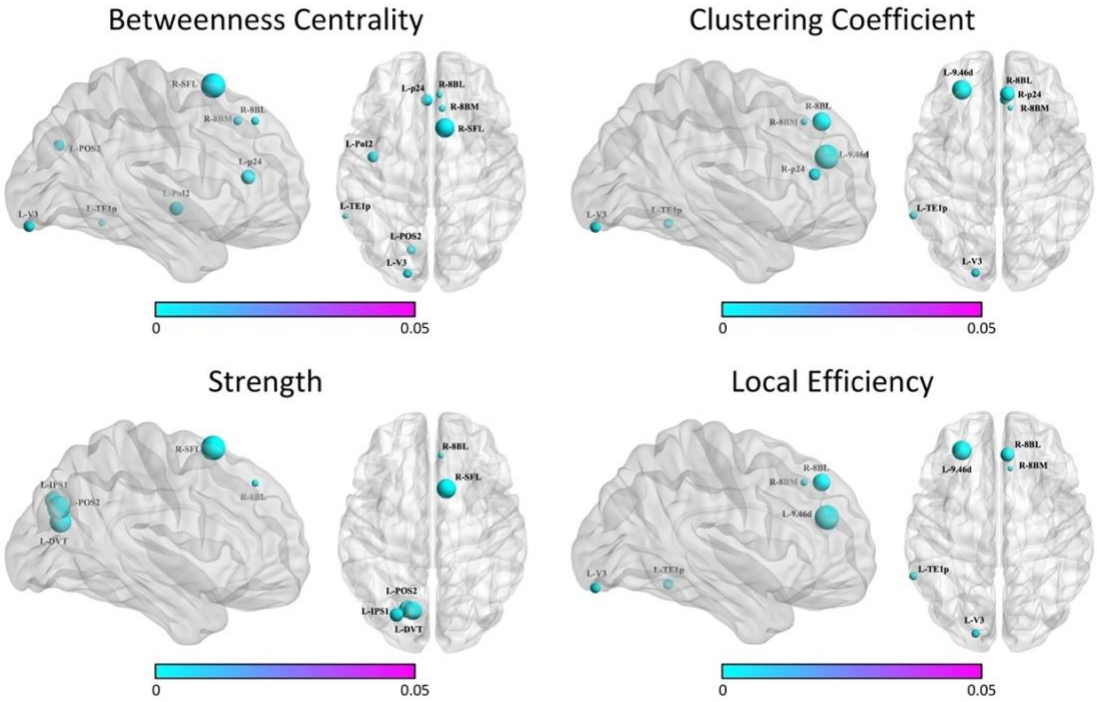


(d) STAI State

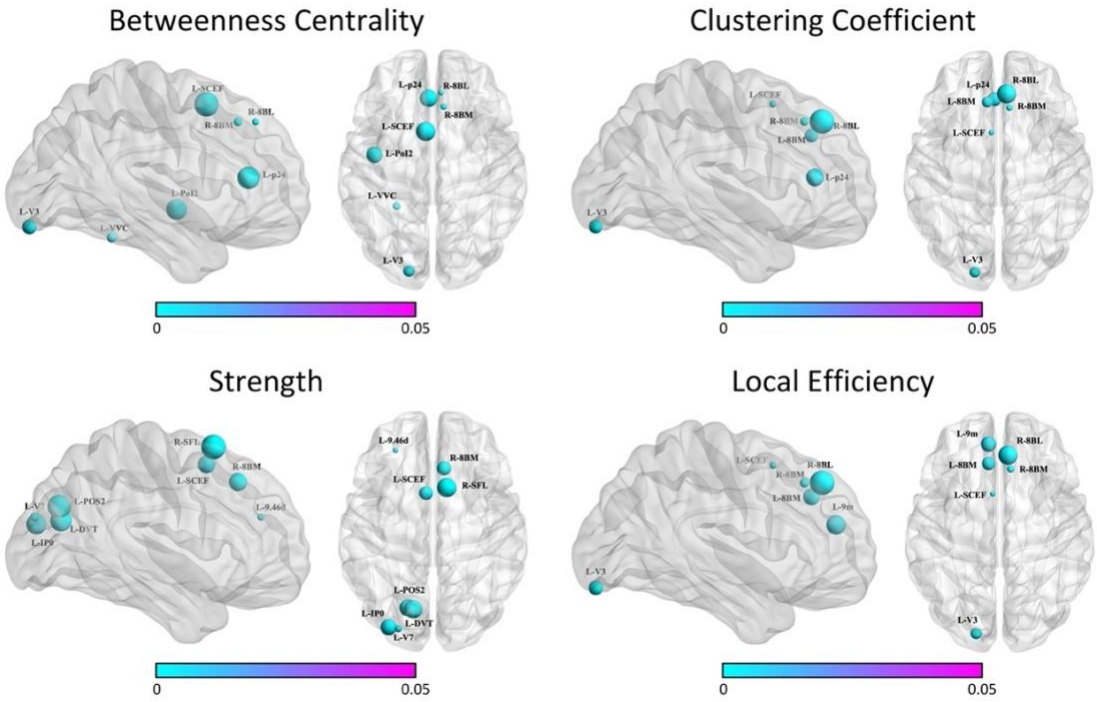

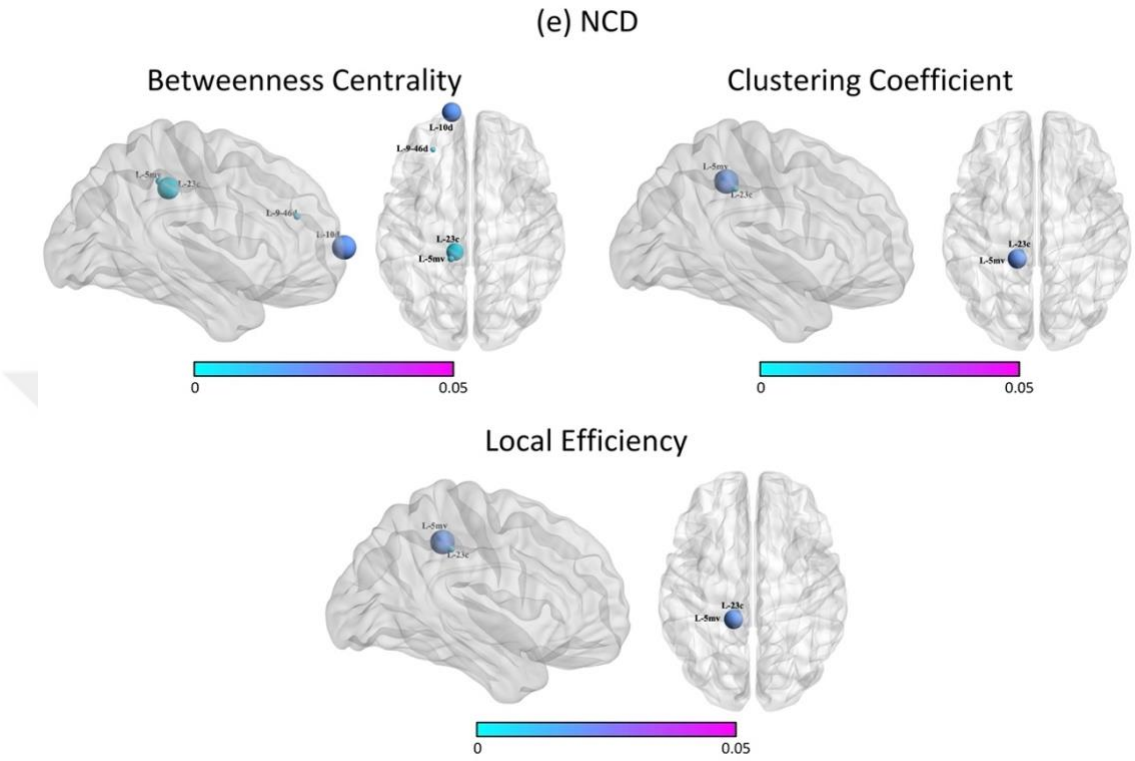


**Figure 3.9 -** Structural brain hubs show the significant correlations between network metrics (a) SLEDAI (b) SLICC (c) STAI-Trait (d) STAI-State (e) NCD, in non-NPSLE patients and HCs. The color bars show the range of p-values. R for right, L for left; Figure prepared using BrainNet Viewer (https://www.nitrc.org/projects/bnv/).

### 3.6.3 Correlation with WISC-IV scores

Results of correlation of connectivity metrics with WISC-IV scores are summarized in Table 3.11 and Figure 3.10. There was a positive correlation between BC and WISC-IV Verbal Comprehension index in R_V6, R_FFC, L_10d regions (r from 0.49 to 0.68, and p from 0.002 to 0.04), and a significant negative correlation in the L_PoI1 area (r = -0.49, p = 0.04). The CC of the R_FFC and L_10d were significantly negatively correlated with the WISCIVVC score (r = -0.53, p = 0.02; and r = -0.67, p = 0.003 respectively). The CC was also showed a significant positive correlation with the WISCIVVC score in the L_PoI1 and R_IPS1 (r = 0.53, p = 0.02; and r = 0.48, p = 0.04 respectively). Similarly, the LE of R_FFC and L_10d areas presented a negative correlation with the WISCIVVC score (r = -0.54, p = 0.02; and r = -0.67, p = 0.002

respectively). There was also positive correlation between LE and WISCIVVC index in L_PoI1 and R_IPS1 regions (r = 0.5, p = 0.03; and r = 0.49, p = 0.04 respectively).

The correlation analysis revealed that in the L_PoI1, L_PoI2, L_a24, and R_PoI2 regions there was a significant negative correlation between strength and WISC-IV Perceptual Reasoning index (WISCIVPR) (r from -0.63 to -0.49 and p from 0.006 to 0.04). Moreover, strength showed a significant positive correlation with WISCIVPR in L_IPS1, R_V7, and R_IPS1(r from 0.51 to 0.69 and p from 0.001 to 0.02). Additionally, the BC of the L_DVT, L_IPS1, L_V6, R_p24, L_6ma, L_V7, and L_9-46d hubs were significantly positively correlated with the WISCIVPR index (r from 0.49 to 0.72 and p from 0.0009 to 0.041). Both CC and LE showed a significant negative correlation with the WISCIVPR score in L_V6, L_6ma, and L_9-46d areas (r from 0.51 to 0.65 and p from 0.004 to 0.03).

The strength of the R_V3, L_SFL, L_V3, R_V2, L_SCEF, and L_6ma regions were significantly positively correlated with the WISC-IV Working Memory index (r from 0.5 to 0.65 and p from 0.004 to 0.037). The BC presented a significant negative correlation with the WISCIVWM in the R_PoI1, L_3b, and R_PoI2 regions (r from -0.55 to 0.5 and p from 0.02 to 0.04) and a significant positive correlation in the L_V6 and L_10d areas (r = 0.49, p = 0.04 and r = 0.48, p = 0.04 respectively). The CC and LE in the R_PoI1 showed a significant positive correlation (r = 0.49, p = 0.04 and r = 0.5, p = 0.03), and a significant negative correlation in L_IP0 (r = -0.52, p = 0.02).

The results of Spearman's rank correlation coefficient indicated that the strength of the R_V3, L_V3, R_V6, and L_V6 hubs presented a significantly positive correlation with WISCIVFS (r from 0.5 to 0.64, and p from 0.005 to 0.036), there was also a significant negative correlation in R_8BL hub (r = -0.49, p = 0.041). BC showed a significant positive correlation with WISCIVFS in L_V6, R_p24, R_FFC, L_10d, and L_6mp regions (r from 0.49 to 0.69 and p from 0.001 to 0.04). Moreover, CC presented a significant negative correlation in L_V6, R_p24, R_FFC, and L_10d with WISCIVFS (r from -0.64 to -0.52 and p from 0.005 to 0.03) and a significant positive correlation in L_PoI1 region (r = 0.52, p = 0.03). Additionally, LE showed a significant negative correlation with the WISCIVFS in the L_V6, R_p24, R_FFC, and L_10d regions (r from -0.65 to -0.52 and p from 0.004 to 0.02) and a significant positive

correlation in L_PoI1, and L_23c regions (r = 0.5, p = 0.03 and r = 0.5, p = 0.04 respectively).

The analysis results demonstrated that the strength in the R_V3, L_V3, R_V2, R_4, L_IP0, L_SCEF, L_6ma, L_V7, R_1, R_3b, and L_6mp hubs represented a significant positive correlation with WICSIVSN (r from 0.25 to 0.65 and p from 0.004 to 0.046). Furthermore, BC presented a significant negative correlation with WICSIVSN in R_PoI1 and R_PoI2 regions (r = -0.57, p = 0.01) and a significant positive correlation in L_IP0 and L_V6 (r = 0.51, p = 0.03 and r = 0.62, p = 0.007 respectively). The CC in the L_IP0 and L_V6 presented a negative correlation (r = -0.53, p = 0.02 and r = -0.63, p = 0.005) and in the R_PoI1 and R_PoI2 areas showed positive correlation (r = 0.51, p = 0.03 and r = 0.59, p = 0.01 respectively) with the WICSIVSN. In addition, LE presented a significant negative correlation with WICSIVSN in L_IP0 and L_V6 and a significant positive correlation in R_PoI1 (r = -0.53, p = 0.02; r = -0.63, p = 0.005; and r = 0.53, p = 0.02 respectively).

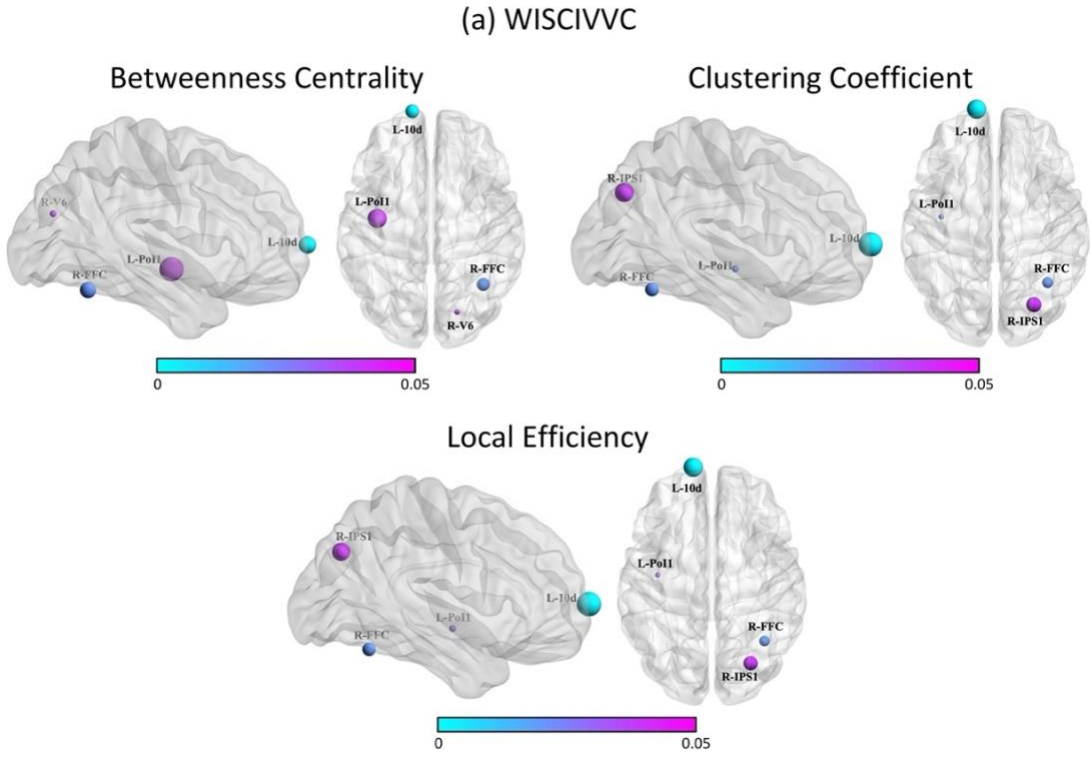

(b) WISCIVPR

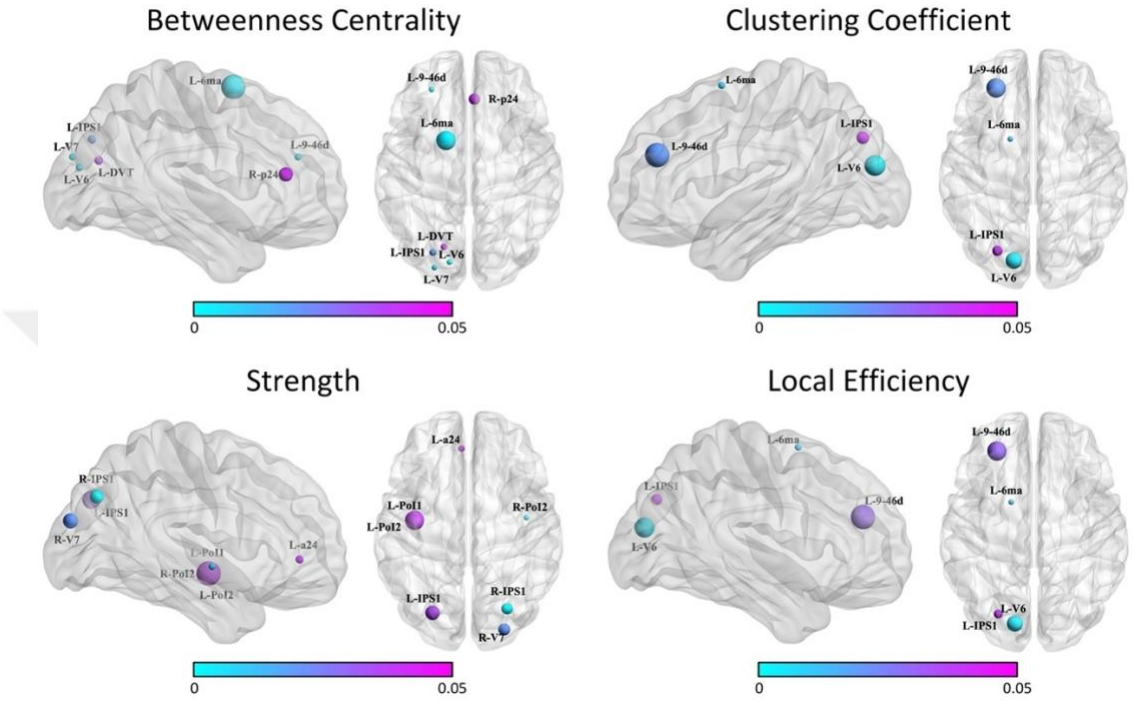


(c) WISCIVWM

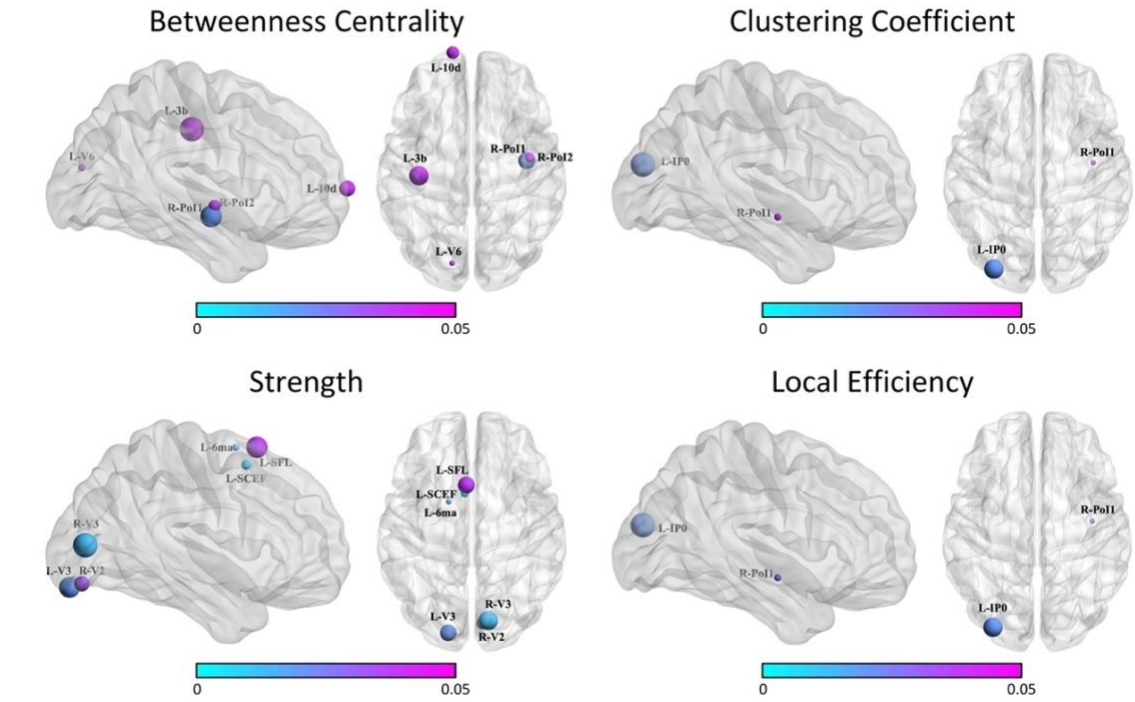

(d) WISCIVFS

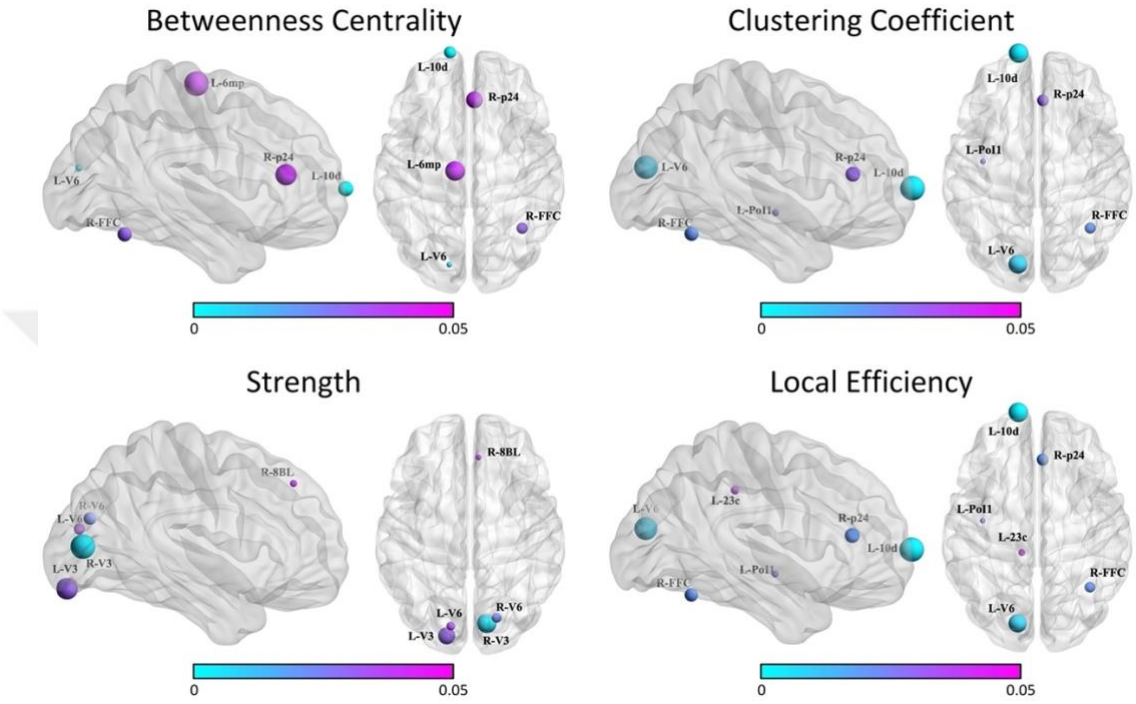


(e) WICSIVNS

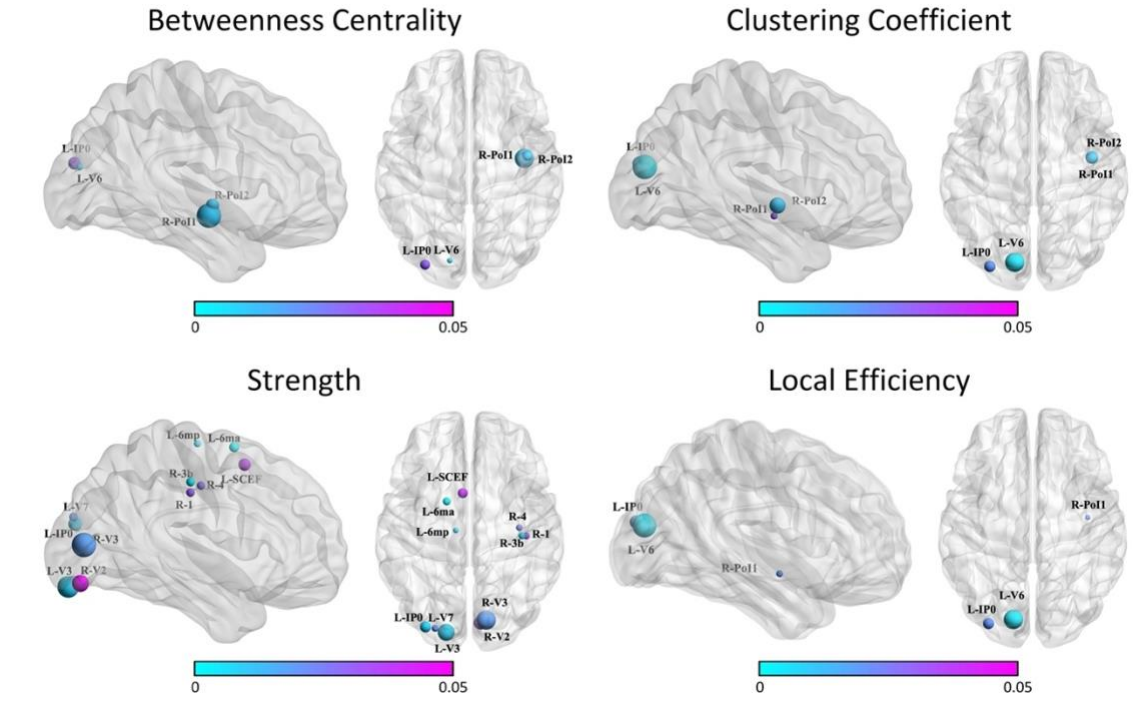

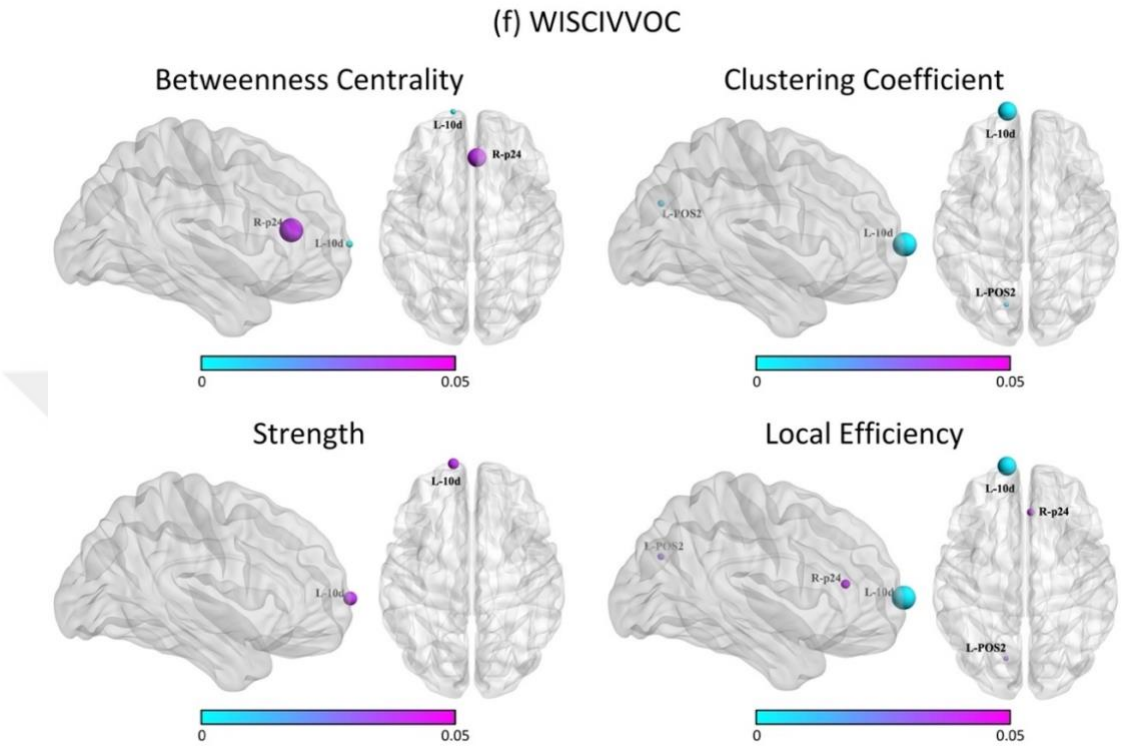


**Figure 3.10 -** Structural brain hubs show the significant correlations between network metrics and WISC-IV test scores in non-NPSLE patients and HCs, (a) WISCIVVC (b) WISCIVPR (c) WISCIVWM (d) WISCIVFS (e) WISCIVNS (f) WISCIVVOC. The color bars show the range of p-values. R for right, L for left; Figure prepared using BrainNet Viewer (https://www.nitrc.org/projects/bnv/).

**Table 3.9** - Significant correlations between clinical characteristics, WISC-IV test scores, and network properties in non-NPSLE patients.

| Variable | Strength | | | BC | | | CC | | | LE | | |
|---|---|---|---|---|---|---|---|---|---|---|---|---|
| | **Hubs** | **p value** | **r value** | **Hubs** | **p value** | **r value** | **Hubs** | **p value** | **r value** | **Hubs** | **p value** | **r value** |
| **Age** | ns | - | - | R_V3 | 0.04 | -0.48 | R_V3 | 0.03 | 0.5 | R_V3 | 0.04 | 0.49 |
| | | | | L_SCEF | 0.03 | -0.51 | R_PGp | 0.008 | 0.61 | R_PGp | 0.008 | 0.61 |
| | | | | R_PGp | 0.007 | -0.62 | L_a24 | 0.03 | 0.5 | L_a24 | 0.03 | 0.5 |
| | | | | | | | R_PoI2 | 0.04 | -0.49 | R_PoI2 | 0.04 | -0.49 |
| **Age at Disease-Onset** | R_POS2 | 0.015 | 0.57 | ns | - | - | R_V3 | 0.005 | 0.63 | R_V3 | 0.001 | 0.7 |
| | L_POS2 | 0.002 | 0.68 | | | | R_V2 | 0.02 | 0.54 | R_V2 | 0.02 | 0.54 |
| | R_DVT | 0.036 | 0.5 | | | | | | | | | |
| | L_IPS1 | 0.022 | 0.55 | | | | | | | | | |
| | R_PGp | 0.024 | 0.54 | | | | R_4 | 0.02 | 0.53 | R_4 | 0.03 | 0.52 |
| | R_IP1 | 0.009 | 0.6 | | | | | | | | | |
| | L_23c | 0.007 | 0.62 | | | | R_1 | 0.001 | 0.7 | R_1 | 0.001 | 0.7 |
| | L_PGs | 0.046 | 0.48 | | | | | | | | | |

| Variable | Strength | | | BC | | | CC | | | LE | | |
|---|---|---|---|---|---|---|---|---|---|---|---|---|
| | **Hubs** | **p value** | **r value** | **Hubs** | **p value** | **r value** | **Hubs** | **p value** | **r value** | **Hubs** | **p value** | **r value** |
| **Disease Duration** | R_POS2 | 0.033 | -0.51 | L_IP0 | 0.029 | -0.52 | R_4 | 0.02 | -0.53 | R_4 | 0.02 | -0.54 |
| | L_POS2 | 0.01 | -0.56 | | | | | | | | | |
| | L_IP0 | 0.019 | -0.56 | | | | | | | | | |
| | R_DVT | 0.046 | -0.48 | | | | | | | | | |
| | L_IPS1 | 0.04 | -0.49 | | | | L_DVT | 0.02 | -0.55 | L_DVT | 0.01 | -0.57 |
| | R_PGp | 0.025 | -0.53 | | | | | | | | | |
| | L_IP1 | 0.035 | -0.51 | | | | | | | | | |
| **SLEDAI** | R_V3 | 0.01 | 0.59 | R_V7 | 0.04 | 0.5 | R_PGp | 0.01 | -0.57 | R_PGp | 0.01 | -0.57 |
| | R_V7 | 0.021 | 0.55 | | | | L_10d | 0.01 | -0.55 | L_10d | 0.01 | -0.56 |
| **SLICC** | L_1 | 0.01 | 0.58 | ns | - | - | L_6ma | 0.01 | 0.56 | ns | - | - |
| **STAI Trait** | R_SFL | 0.003 | -0.66 | L_V3 | 0.01 | -0.56 | L_V3 | 0.004 | 0.64 | L_V3 | 0.005 | 0.64 |
| | L_POS2 | 0.01 | 0.58 | R_SFL | 0.03 | -0.52 | R_8BM | 0.02 | 0.55 | R_8BM | 0.03 | 0.5 |
| | L_DVT | 0.02 | 0.53 | L_POS2 | 0.02 | 0.55 | R_p24 | 0.02 | -0.52 | L_TE1p | 0.01 | -0.6 |
| | | | | R_8BM | 0.03 | -0.5 | L_TE1p | 0.009 | -0.6 | | | |
| | L_IPS1 | 0.01 | 0.6 | L_p24 | 0.03 | 0.51 | L_9.46d | 0.001 | -0.69 | L_9.46d | 0.002 | -0.68 |
| | | | | L_TE1p | 0.016 | 0.57 | | | | | | |
| | R_8BL | 0.029 | -0.52 | L_PoI2 | 0.03 | -0.52 | R_8BL | 0.006 | 0.63 | R_8BL | 0.006 | 0.62 |
| | | | | R_8BL | 0.0008 | -0.72 | | | | | | |
| **STAI State** | R_SFL | 0.003 | -0.66 | L_V3 | 0.02 | -0.53 | L_V3 | 0.001 | 0.69 | L_9m | 0.04 | -0.48 |
| | L_POS2 | 0.007 | 0.62 | R_8BM | 0.001 | -0.7 | R_8BM | 0.0003 | 0.76 | L_V3 | 0.002 | 0.69 |
| | L_DVT | 0.005 | 0.64 | L_SCEF | 0.02 | -0.53 | L_SCEF | 0.02 | 0.55 | R_8BM | 0.0009 | 0.72 |
| | L_IP0 | 0.04 | 0.49 | L_VVC | 0.01 | -0.57 | L_p24 | 0.04 | -0.48 | L_SCEF | 0.02 | 0.55 |
| | R_8BM | 0.015 | 40654 | L_p24 | 0.017 | 0.56 | L_8BM | 0.03 | 0.51 | L_8BM | 0.03 | 0.51 |
| | L_SCEF | 0.033 | -0.51 | L_PoI2 | 0.005 | -0.64 | R_8BL | 0.02 | 0.54 | R_8BL | 0.02 | 0.53 |
| | L_V7 | 0.019 | 0.55 | R_8BL | 0.009 | -0.6 | | | | | | |
| | L_9.46d | 0.032 | 0.51 | | | | | | | | | |
| **NCD** | ns | - | - | L_23c | 0.006 | -0.63 | L_23c | 0.009 | 0.6 | L_23c | 0.009 | 0.6 |
| | | | | L_10d | 0.02 | 0.52 | | | | | | |
| | | | | L_9.46d | 0.009 | 0.6 | L_5mv | 0.02 | 0.55 | L_5mv | 0.02 | 0.52 |
| | | | | L_5mv | 0.01 | -0.57 | | | | | | |
| **WISCIVVC** | ns | - | - | L_PoI1 | 0.04 | -0.49 | L_PoI1 | 0.02 | 0.53 | L_PoI1 | 0.03 | 0.5 |
| | | | | R_V6 | 0.04 | 0.49 | R_IPS1 | 0.04 | 0.48 | R_IPS1 | 0.04 | 0.49 |
| | | | | R_FFC | 0.02 | 0.54 | R_FFC | 0.02 | -0.53 | R_FFC | 0.02 | -0.54 |
| | | | | L_10d | 0.002 | 0.68 | L_10d | 0.003 | -0.67 | L_10d | 0.002 | -0.67 |
| **WISCIVPR** | L_PoI1 | 0.04 | -0.5 | L_DVT | 0.04 | 0.49 | L_IPS1 | 0.04 | -0.48 | L_IPS1 | 0.04 | -0.48 |
| | L_IPS1 | 0.035 | 0.51 | L_IPS1 | 0.018 | 0.56 | L_V6 | 0.004 | -0.65 | L_V6 | 0.004 | -0.65 |
| | R_V7 | 0.02 | 0.55 | L_V6 | 0.0009 | 0.72 | | | | | | |
| | R_IPS1 | 0.001 | 0.69 | R_p24 | 0.041 | 0.49 | L_6ma | 0.01 | -0.56 | L_6ma | 0.01 | -0.56 |
| | L_PoI2 | 0.04 | -0.49 | L_6ma | 0.004 | 0.64 | | | | | | |
| | L_a24 | 0.04 | -0.49 | L_V7 | 0.001 | 0.7 | L_9.46d | 0.02 | -0.55 | L_9.46d | 0.03 | -0.51 |
| | R_PoI2 | 0.006 | -0.63 | L_9.46d | 0.003 | 0.66 | | | | | | |

| Variable | Strength | | | BC | | | CC | | | LE | | |
|---|---|---|---|---|---|---|---|---|---|---|---|---|
| | **Hubs** | **p value** | **r value** | **Hubs** | **p value** | **r value** | **Hubs** | **p value** | **r value** | **Hubs** | **p value** | **r value** |
| **WISCIVWM** | R_V3 | 0.013 | 0.58 | R_PoI1 | 0.02 | -0.55 | R_PoI1 | 0.04 | 0.49 | R_PoI1 | 0.03 | 0.5 |
| | L_SFL | 0.037 | 0.5 | L_3b | 0.04 | -0.5 | | | | | | |
| | L_V3 | 0.02 | 0.55 | L_V6 | 0.04 | 0.49 | L_IP0 | 0.02 | -0.52 | L_IP0 | 0.02 | -0.52 |
| | R_V2 | 0.032 | 0.51 | L_10d | 0.04 | 0.48 | | | | | | |
| | L_SCEF | 0.004 | 0.65 | R_PoI2 | 0.04 | -0.5 | | | | | | |
| | L_6ma | 0.016 | 0.57 | | | | | | | | | |
| **WISCIVPS** | L_PGs | 0.01 | 0.6 | R_8BM | 0.03 | -0.51 | L_SCEF | 0.02 | 0.55 | R_8BM | 0.04 | 0.48 |
| | | | | L_SCEF | 0.04 | -0.48 | | | | L_SCEF | 0.01 | 0.58 |
| | | | | L_1 | 0.01 | 0.56 | | | | | | |
| **WISCIVFS** | R_V3 | 0.005 | 0.64 | L_V6 | 0.005 | 0.64 | l | 0.03 | 0.51 | L_PoI1 | 0.03 | 0.5 |
| | L_V3 | 0.03 | 0.52 | R_p24 | 0.04 | 0.48 | L_V6 | 0.009 | -0.6 | L_V6 | 0.009 | -0.6 |
| | R_V6 | 0.022 | 0.54 | R_FFC | 0.03 | 0.51 | R_p24 | 0.03 | -0.52 | R_p24 | 0.02 | -0.52 |
| | L_V6 | 0.036 | 0.5 | L_10d | 0.001 | 0.69 | R_FFC | 0.02 | -0.53 | L_23c | 0.04 | 0.5 |
| | R_8BL | 0.041 | -0.49 | L_6mp | 0.04 | 0.49 | L_10d | 0.005 | -0.64 | R_FFC | 0.02 | -0.54 |
| | | | | | | | | | | L_10d | 0.004 | -0.65 |
| **WICSIVSN** | R_V3 | 0.018 | 0.56 | R_PoI1 | 0.01 | -0.57 | R_PoI1 | 0.03 | 0.51 | R_PoI1 | 0.02 | 0.53 |
| | L_V3 | 0.008 | 0.61 | | | | | | | | | |
| | R_V2 | 0.046 | 0.48 | | | | | | | | | |
| | R_4 | 0.025 | 0.53 | L_IP0 | 0.03 | 0.51 | L_IP0 | 0.02 | -0.53 | L_IP0 | 0.02 | -0.53 |
| | L_IP0 | 0.008 | 0.61 | | | | | | | | | |
| | L_SCEF | 0.039 | 0.5 | | | | | | | | | |
| | L_6ma | 0.002 | 0.68 | L_V6 | 0.007 | 0.62 | L_V6 | 0.005 | -0.63 | L_V6 | 0.005 | -0.63 |
| | L_V7 | 0.02 | 0.55 | | | | | | | | | |
| | R_1 | 0.03 | 0.51 | | | | | | | | | |
| | R_3b | 0.004 | 0.65 | R_PoI2 | 0.01 | -0.57 | R_PoI2 | 0.01 | 0.59 | | | |
| | L_6mp | 0.008 | 0.25 | | | | | | | | | |
| **WISCIVVOC** | L_10d | 0.04 | 0.49 | R_p24 | 0.04 | 0.48 | L_POS2 | 0.01 | 0.56 | L_POS2 | 0.03 | 0.5 |
| | | | | L_10d | 0.0004 | 0.75 | L_10d | 0.005 | -0.64 | R_p24 | 0.04 | -0.49 |
| | | | | | | | | | | L_10d | 0.005 | -0.64 |

BC: Betweenness Centrality, CC: Clustering Coefficient, LE: Local Efficiency, ns: non-significant, SLEDAI: systemic lupus disease activity index, SLICC: Systemic Lupus International Collaborating Clinics' damage index score, NCD: Neurocognitive Dysfunction score, WISCIVVC: Verbal Comprehension score, WISCIVPR: Perceptual Reasoning score, WISCIVWM: Working Memory score, WISCIVPS: Processing Speed score, WISCIVFS: Full-Scale score, WICSIVSN: Serial Number score, WISCIVVOC: Vocabulary score, R: Right, L: Left. For abbreviations, see page xiv.

*p-value and r-value calculated according to Spearman's rank correlation coefficient.

# Chapter 4

# Discussion

Normal behavior and cognition are dependent on the dynamic interactions and synchronization between various brain regions [97]. The brain has complex structural and functional networks, where any disruption caused by systemic illnesses affecting the nervous system like SLE, or neurologic diseases like multiple sclerosis (MS) may result in cognitive and behavioral abnormalities [98].

This study aimed to investigate the structural connectivity modifications of the white matter networks between healthy controls and pediatric-onset SLE patients prior to neuropsychiatric manifestations. Using connectivity and tractography-based analysis, we were able to demonstrate that patients with pediatric-onset non-NPSLE had extensive local and global abnormalities in the structural brain network compared to healthy controls.

The main findings of our study are: 1) When the hubs were selected according to the strength of the nodes, their structure and distribution were changed in the patients. 2) Patients presented higher network characteristic path length and assortativity, and lower density and global efficiency than healthy controls. The other measured characteristics of the structural network also showed different connectivity patterns between healthy controls and patients. 3) Non-NPSLE patients showed significantly lower scores according to WISC-IV score components compared to healthy controls. From a network and connectivity perspective, our research demonstrated that pediatric-onset non-NPSLE patients had altered topological structure of the brain.

In graph theory, there are three kinds of networks: regular networks, random networks, and small-world networks. Whenever a network combines the benefits of regular and random networks, it is referred to as a small-world network. This indicates that the network has higher LE while also having a comparatively higher global efficiency. In parallel information processing, a network's small-world features often represent an appropriate balance of local specialization and global integration [99]. In our investigation, both the patient and HC groups' brain WM structural networks revealed small-worldness characteristics. This finding demonstrated that the fundamental structure of the brain is retained in non-NPSLE patient, implying that the small-world network can endure some structural changes [100][101].

## 4.1 Global network structural disruption

A few studies employing graph theory to evaluate the structural network discovered abnormalities in global network features in adult patients with non-NPSLE. According to Xu et al.'s investigation, patients with non-NPSLE had considerably lower local and global efficiency and a higher shortest path length and assortativity than HCs [102]. Regarding network efficiency, our findings demonstrated a reduction in global efficiency and density in patients compared to healthy controls.

Reduced global efficiency and density in our young patients indicate a less effective interaction as well as less neural information transmission between remote cortical regions. Reduced LE points out diminished local specialization that facilitates modular information processing between nearby cortical regions [103]. The changes in network efficiency seen in patients suggest a breakdown in the topological structure caused by disease.

Remarkably, the alterations in all these characteristics show that in WM structural networks of non-NPSLE patients' brain, the capability of parallel information processing may have diminished for global integration and local specialization. This observation is consistent with Mikdashi's analysis of fMRI [104] results in SLE patients, which demonstrated a lack of efficient integration and coordination capabilities across various brain regions in SLE patients. Reduction in global and LE suggests a long and short range connection loss, respectively.

Our results show an increase in the network characteristic path length and assortativity of patients compared to HCs. Furthermore, non-NPSLE patients showed a reduction in CC and LE in 33/59 of shared hubs while showing increments in 22/59 hubs compared to HCs.

An increment in the length of short path characteristics reflects lesser optimum connections between neurons, although the optimum interactions are required for functional cognitive processes both inside and across the regions of the brain [105]. Furthermore, the imbalance between integration and functional segregation of structural connectivity may also occur as shown by reduction in CC.

Loss of integrity in the WM is commonly accepted as a reason for enhancement in the shortest path length among the patient group. Earlier DTI investigations demonstrated fiber tract degradation, as seen by dramatically reduced FA and elevated MD values in various tracts of the brains of non-NPSLE and NPSLE individuals [106][30][32]. In particular, Jung et al. [31] found that adult NPSLE patients had substantial alterations in the MD and FA of the corpus callosum body, left anterior corona radiata, and left forceps major. Despite the fact that our patients were younger and free of any radiological abnormality on brain MRI by our more strict inclusion criteria, our TBSS maps revealed significantly reduced FA in areas common, but elevated MD in more extensively than Jung et al. 's patient cohorts. Disease onset at a younger age, particularly in childhood and adolescence where intensive synaptic connections form in the brain might have resulted in more extensive changes in terms of both damage and repair mechanisms [8][107].

## 4.2 Hub distribution and structure disruption

Our structural-based connectivity analysis showed that pediatric-onset non-NPSLE patients had significantly different global brain structural connectivity features from matched HCs. Moreover, the distribution of structural hubs in non-NPSLE patients was different. Twenty hubs identified in HCs were not retrieved while 15 additional hubs appeared in the patients. The majority (14/20; 70%) of the disappeared hubs were from the left hemisphere. Regarding the nodal strength, all newly added hubs presented a higher nodal strength while all the disappeared hubs showed a lower nodal

strength in the patients compared with HCs. The variations in the hub distribution seen in non-NPSLE patients may be a result of the brain network changing over the course of the illness. These modifications may have an effect on the channels used to transmit brain information optimally [108]. Consequently, several brain regions may become less or more integrated, and which in turn, represented by a reduction or an increase in nodal strength [102].

Brain topology around the nodes can be reconstructed according to strength alterations among the appeared and disappeared hubs in our non-NPSLE patients. Hub strengthening can lead to a higher dependency on that node which can cause remodeling of the local peri-nodal topology in the brain. Same sort of adaptive alterations can also occur with reduced hub strength. Consequently, we noticed a higher reliance mostly on subdivisions of cingulate cortex region, parietal cortex area, intraparietal cortex area, auditory cortex, seventh visual area, prefrontal cortical area, lateral frontal lobe, medial auditory belt cortex, and middle temporal gyrus hubs and a decreased reliance on part of the premotor cortex, parainsular area, frontal cortex, hippocampus, medial auditory belt cortex, insular granular cortex, parahippocampal area, primary visual cortex and some other visual areas, ventral visual complex, and dorsal anterior cingulate hubs in non-NPSLE patients.

Based on the altered nodal strength and degree, BC, CC, and LE's significant modifications between non-NPSLE patients and HCs along with TBSS findings, the altered regions can be categorized into language, visual, auditory, and motor-related areas.

Increased strength in superior longitudinal fasciculus and significantly decreased CC and LE in this area in addition to higher MD value based on our TBSS analysis than HCs may be linked to language comprehension and visual processing in our patients. SLF has a significant impact on attention, emotion, memory, and language [109]. As demonstrated in Table 3.9 there is a significant positive correlation at SLF between WISC-IV WMI and strength which shows that any alteration in this region may have a direct impact on WISC-IV WMI which means a low WMI score indicates attention impairments.

In addition, compared to healthy controls non-NPSLE patients presented a significant reduction in CC and LE of fusiform face complex area which is in the inferior temporal cortex, and relates to the human visual system. Also, the disappearance and appearance of hubs, which are essential regions in visual processing could be due to reactive structural plasticity in WM in patients with pediatric-onset non-NPSLE. This is also supported with another TBSS finding, that bilateral inferior fronto-occipital fasciculus, one of the most essential regions for visual processing, showed higher MD and RD values in the patients than HCs. This means that structural plasticity could help the brain compensate for connection disruptions and reorganization of brain functionality.

In analysis of the patients vs HCs, TBSS maps exhibited a significant decrease in FA and increase in MD and RD in the body and genu of corpus callosum and left anterior corona radiata. This suggests abnormalities in the inter-hemispheric motor region connections. Also, a significant nodal strength increment in the left 5mv region (subdivision of the parietal cortex), and a significant CC and LE, plus a significant decrease in nodal degree in L_10d (part of the prefrontal cortical area) were observed in non-NPSLE patients compared to HCs. The prefrontal cortex has several connections with motor areas which let it transfer a huge amount of information to these hubs [110]. As a consequence, changes in the structural connectivity of the prefrontal cortex hub may cause many abnormalities in patients' motor system [31]. As indicated in previous fMRI studies, the parietal cortex is implicated in the processing of somatosensory inputs as well as the planning and execution of movements [111][112]. Therefore, later addition of the left 5mv hub in our patients can result from reactive plasticity to overcome mentioned weaknesses in motor-related areas [113].

## 4.3 Clinical relevance

The strength and BC of the network presented a significant positive correlation with SLEDAI of the patients at some of the visual areas while the CC and LE presented a significant negative correlation in the prefrontal cortical area and posterior parietal area of G. These findings suggested that the SLEDAI score can impact the characteristics and the topological arrangement of the network even in the early stages

of the disease. It may be concluded that changes in these areas (R_V7, R_V3, R_PGp and L_10) play an important role in the development of SLE.

The strength of the left primary somatosensory cortex and the CC of the left anterior supplementary motor area presented a significant positive correlation with the SLICC score. These findings propose that network features could provide measures to better characterize disease effects on the brain. Many other studies reported a correlation between connectivity features and SLEDAI and SLICC in NPSLE and SLE patients [26][102][114][115].

## 4.4 Behavioral and neuropsychiatric test relevance

According to our analysis, SPL presented a positive correlation between all the WISC-IV components, and HCs while SPL presented a negative correlation with WISCIVVC, WISCIWWM, WISCIVFS, and WISCIVVOC in patients. As earlier discussed, increment in SPL leads to a more effective data transformation between neurons which is required for the proper functioning of cognitive processes both inside and across the brain. The abovementioned finding shows a higher intelligence is highly related to SPL. Due to a negative correlation between SPL and WISC-IV scores, we can conclude that in patients the structural organization may have abnormalities that lead to a less number of SPL. Since we worked on pediatric non-NPSLE patients who do not have many disease manifestations, based on abnormalities in structural topology we can expect more additional manifestations.

## 4.5 Limitations

This study presents a few limitations that must be addressed. First is small number of participants which is mainly due to the relative rarity of pediatric-onset SLE. Our patient cohort was obtained from the tertiary care reference center at Hacettepe University Pediatric Rheumatology Clinics. The second drawback of our study is the age of our participants which started from pediatric age, but some patients exceeded 18 years old at the time of the examination. The last one is, our images were acquired at a 3T. With a 7T scanner, our connectivity matrix would be more precise leading to

a better understanding of the structural network and its connections and therefore probable abnormalities.

## 4.6 Conclusions

Existing literature on lupus focuses on adult-onset patients, studies using connectivity analysis did so on adults. Taking the advantage of HCP atlas, which provided us more detailed brain parcellations, our findings demonstrated that pediatric-onset SLE patients without neuropsychiatric clinical symptoms faced alterations in white matter connectivity network.

Language, visual, auditory, and motor systems are affected. Using the nodal strength to identify the brain hubs, non-NPSLE patients showed changed hub distribution in the brain. Connectivity metrics showed a correlation with disease activity and severity, neurocognitive dysfunction score, trait, and state anxiety inventory scores, neurocognitive scores, assessed by WISC-IV. Even in the absence of neuropsychiatric symptoms, our data indicated modifications in the white matter connectome of pediatric-onset SLE patients. Structural alterations driving functional and neurocognitive abnormalities in the absence of clinical manifestations have been better understood.

There is an elevated risk of central nervous system impairment in pediatric-onset NPSLE because of disease onset age, the cumulative effect of the disease in a longer expected life-time, and other probable pathogenic causes. So, understanding the timing and severity of nervous tissue alterations by DTI connectivity may help developing new and more appropriate treatment strategies.

# Bibliography


[1] J. J. Manson and A. Rahman, “Systemic lupus erythematosus,” *Orphanet J. Rare Dis.*, vol. 1, no. 1, p. 6, 2006, doi: 10.1186/1750-1172-1-6.

[2] M. Molokhia and P. McKeigue, “Risk for rheumatic disease in relation to ethnicity and admixture.,” *Arthritis Res.*, vol. 2, no. 2, pp. 115–125, 2000, doi: 10.1186/ar76.

[3] R. Cervera *et al.*, “Morbidity and mortality in systemic lupus erythematosus during a 10-year period: a comparison of early and late manifestations in a cohort of 1,000 patients.,” *Medicine (Baltimore).*, vol. 82, no. 5, pp. 299–308, Sep. 2003, doi: 10.1097/01.md.0000091181.93122.55.

[4] A. E. Johnson, C. Gordon, R. G. Palmer, and P. A. Bacon, “The prevalence and incidence of systemic lupus erythematosus in Birmingham, England. Relationship to ethnicity and country of birth.,” *Arthritis Rheum.*, vol. 38, no. 4, pp. 551–558, Apr. 1995, doi: 10.1002/art.1780380415.

[5] B. Livingston, A. Bonner, and J. Pope, “Differences in clinical manifestations between childhood-onset lupus and adult-onset lupus: a meta-analysis.,” *Lupus*, vol. 20, no. 13, pp. 1345–1355, Nov. 2011, doi: 10.1177/0961203311416694.

[6] C. A. Silva, T. Avcin, and H. I. Brunner, “Taxonomy for systemic lupus erythematosus with onset before adulthood.,” *Arthritis Care Res. (Hoboken).*, vol. 64, no. 12, pp. 1787–1793, Dec. 2012, doi: 10.1002/acr.21757.

[7] S. Kamphuis and E. D. Silverman, “Prevalence and burden of pediatric-onset systemic lupus erythematosus.,” *Nat. Rev. Rheumatol.*, vol. 6, no. 9, pp. 538–546, Sep. 2010, doi: 10.1038/nrrheum.2010.121.

[8] D. M. Levy and S. Kamphuis, “Systemic lupus erythematosus in children and adolescents.,” *Pediatr. Clin. North Am.*, vol. 59, no. 2, pp. 345–364, Apr. 2012,

doi: 10.1016/j.pcl.2012.03.007.

[9] C. Malattia and A. Martini, “Paediatric-onset systemic lupus erythematosus.,” *Best Pract. Res. Clin. Rheumatol.*, vol. 27, no. 3, pp. 351–362, Jun. 2013, doi: 10.1016/j.berh.2013.07.007.

[10] T. Tarr *et al.*, “Similarities and differences between pediatric and adult patients with systemic lupus erythematosus.,” *Lupus*, vol. 24, no. 8, pp. 796–803, Jul. 2015, doi: 10.1177/0961203314563817.

[11] R. C. Gomes *et al.*, “Features of 847 Childhood-Onset Systemic Lupus Erythematosus Patients in Three Age Groups at Diagnosis: A Brazilian Multicenter Study.,” *Arthritis Care Res. (Hoboken).*, vol. 68, no. 11, pp. 1736–1741, Nov. 2016, doi: 10.1002/acr.22881.

[12] B. Bader-Meunier *et al.*, “Initial presentation of childhood-onset systemic lupus erythematosus: a French multicenter study.,” *J. Pediatr.*, vol. 146, no. 5, pp. 648–653, May 2005, doi: 10.1016/j.jpeds.2004.12.045.

[13] J. G. Hanly, “Neuropsychiatric lupus.,” *Rheum. Dis. Clin. North Am.*, vol. 31, no. 2, pp. 273–98, vi, May 2005, doi: 10.1016/j.rdc.2005.01.007.

[14] J. Seguí *et al.*, “Psychiatric and psychosocial disorders in patients with systemic lupus erythematosus: a longitudinal study of active and inactive stages of the disease.,” *Lupus*, vol. 9, no. 8, pp. 584–588, 2000, doi: 10.1191/096120300678828730.

[15] L. N. Moorthy, M. J. Harrison, M. Peterson, K. B. Onel, and T. J. A. Lehman, “Relationship of quality of life and physical function measures with disease activity in children with systemic lupus erythematosus.,” *Lupus*, vol. 14, no. 4, pp. 280–287, 2005, doi: 10.1191/0961203305lu2075oa.

[16] G. K. Bertsias and D. T. Boumpas, “Pathogenesis, diagnosis and management of neuropsychiatric SLE manifestations.,” *Nat. Rev. Rheumatol.*, vol. 6, no. 6, pp. 358–367, Jun. 2010, doi: 10.1038/nrrheum.2010.62.

[17] “The American College of Rheumatology nomenclature and case definitions for neuropsychiatric lupus syndromes.,” *Arthritis Rheum.*, vol. 42, no. 4, pp. 599–608, Apr. 1999, doi: 10.1002/1529-0131(199904)42:4<599::AID-ANR2>3.0.CO;2-F.

[18] M. C. Hollander *et al.*, “International consensus for provisions of quality-driven care in childhood-onset systemic lupus erythematosus.,” *Arthritis Care Res. (Hoboken).*, vol. 65, no. 9, pp. 1416–1423, Sep. 2013, doi: 10.1002/acr.21998.

[19] M. H. Lee, U. Sriram, M. Chakhtoura, R. W. Chain, R. Caricchio, and S. Gallucci, “The effects of Estrogen on the IFN signature in Lupus,” *J. Immunol.*, vol. 196, no. 1 Supplement, pp. 118.18--118.18, 2016, [Online]. Available: https://www.jimmunol.org/content/196/1_Supplement/118.18.

[20] G. J. Pons-Estel, G. S. Alarcón, L. Scofield, L. Reinlib, and G. S. Cooper, “Understanding the epidemiology and progression of systemic lupus erythematosus.,” *Semin. Arthritis Rheum.*, vol. 39, no. 4, pp. 257–268, Feb. 2010, doi: 10.1016/j.semarthrit.2008.10.007.

[21] E. Muscal and R. L. Brey, “Neurologic manifestations of systemic lupus erythematosus in children and adults.,” *Neurol. Clin.*, vol. 28, no. 1, pp. 61–73, Feb. 2010, doi: 10.1016/j.ncl.2009.09.004.

[22] W. L. J. Sibbitt *et al.*, “The incidence and prevalence of neuropsychiatric syndromes in pediatric onset systemic lupus erythematosus.,” *J. Rheumatol.*, vol. 29, no. 7, pp. 1536–1542, Jul. 2002.

[23] G. S. Ross *et al.*, “A proposed framework to standardize the neurocognitive assessment of patients with pediatric systemic lupus erythematosus.,” *Arthritis Care Res. (Hoboken).*, vol. 62, no. 7, pp. 1029–1033, Jul. 2010, doi: 10.1002/acr.20152.

[24] E. Kozora, S. G. West, B. L. Kotzin, L. Julian, S. Porter, and E. Bigler, “Magnetic resonance imaging abnormalities and cognitive deficits in systemic lupus erythematosus patients without overt central nervous system disease.,” *Arthritis Rheum.*, vol. 41, no. 1, pp. 41–47, Jan. 1998, doi: 10.1002/1529-0131(199801)41:1<41::AID-ART6>3.0.CO;2-7.

[25] I. Shapira-Lichter *et al.*, “Learning and memory-related brain activity dynamics are altered in systemic lupus erythematosus: a functional magnetic resonance imaging study.,” *Lupus*, vol. 22, no. 6, pp. 562–573, May 2013, doi: 10.1177/0961203313480399.

[26] J. Hou *et al.*, “Abnormalities of frontal-parietal resting-state functional connectivity are related to disease activity in patients with systemic lupus erythematosus,” *PLoS One*, vol. 8, no. 9, pp. e74530–e74530, Sep. 2013, doi:

10.1371/journal.pone.0074530.

[27] M. Mackay *et al.*, “Differences in regional brain activation patterns assessed by functional magnetic resonance imaging in patients with systemic lupus erythematosus stratified by disease duration.,” *Mol. Med.*, vol. 17, no. 11–12, pp. 1349–1356, 2011, doi: 10.2119/molmed.2011.00185.

[28] M. W. DiFrancesco *et al.*, “Functional neuronal network activity differs with cognitive dysfunction in childhood-onset systemic lupus erythematosus.,” *Arthritis Res. Ther.*, vol. 15, no. 2, p. R40, Mar. 2013, doi: 10.1186/ar4197.

[29] R. E. Jung, J. M. Segall, R. G. Grazioplene, C. Qualls, W. L. Sibbitt, and C. A. Roldan, “Cortical thickness and subcortical gray matter reductions in neuropsychiatric systemic lupus erythematosus.,” *PLoS One*, vol. 5, no. 3, p. e9302, Mar. 2010, doi: 10.1371/journal.pone.0009302.

[30] B. J. Emmer, I. M. Veer, G. M. Steup-Beekman, T. W. J. Huizinga, J. van der Grond, and M. A. van Buchem, “Tract-based spatial statistics on diffusion tensor imaging in systemic lupus erythematosus reveals localized involvement of white matter tracts.,” *Arthritis Rheum.*, vol. 62, no. 12, pp. 3716–3721, Dec. 2010, doi: 10.1002/art.27717.

[31] R. E. Jung *et al.*, “Diffusion tensor imaging in neuropsychiatric systemic lupus erythematosus.,” *BMC Neurol.*, vol. 10, p. 65, Jul. 2010, doi: 10.1186/1471-2377-10-65.

[32] T. Schmidt-Wilcke *et al.*, “Diminished white matter integrity in patients with systemic lupus erythematosus.,” *NeuroImage. Clin.*, vol. 5, pp. 291–297, 2014, doi: 10.1016/j.nicl.2014.07.001.

[33] Z. Wang, Z. Dai, G. Gong, C. Zhou, and Y. He, “Understanding structural-functional relationships in the human brain: a large-scale network perspective.,” *Neurosci. a Rev. J. bringing Neurobiol. Neurol. psychiatry*, vol. 21, no. 3, pp. 290–305, Jun. 2015, doi: 10.1177/1073858414537560.

[34] W. L. J. Sibbitt, R. R. Sibbitt, and W. M. Brooks, “Neuroimaging in neuropsychiatric systemic lupus erythematosus.,” *Arthritis Rheum.*, vol. 42, no. 10, pp. 2026–2038, Oct. 1999, doi: 10.1002/1529-0131(199910)42:10<2026::AID-ANR2>3.0.CO;2-J.

[35] S. G. West, W. Emlen, M. H. Wener, and B. L. Kotzin, “Neuropsychiatric lupus erythematosus: a 10-year prospective study on the value of diagnostic tests.,” *Am. J. Med.*, vol. 99, no. 2, pp. 153–163, Aug. 1995, doi: 10.1016/s0002-9343(99)80135-1.

[36] V. P. B. Grover, J. M. Tognarelli, M. M. E. Crossey, I. J. Cox, S. D. Taylor-Robinson, and M. J. W. McPhail, “Magnetic Resonance Imaging: Principles and Techniques: Lessons for Clinicians.,” *J. Clin. Exp. Hepatol.*, vol. 5, no. 3, pp. 246–255, Sep. 2015, doi: 10.1016/j.jceh.2015.08.001.

[37] R. Brown, “XXVII. A brief account of microscopical observations made in the months of June, July and August 1827, on the particles contained in the pollen of plants; and on the general existence of active molecules in organic and inorganic bodies,” *Philos. Mag.*, vol. 4, no. 21, pp. 161–173, Sep. 1828, doi: 10.1080/14786442808674769.

[38] D. C. Alexander *et al.*, “Orientationally invariant indices of axon diameter and density from diffusion MRI.,” *Neuroimage*, vol. 52, no. 4, pp. 1374–1389, Oct. 2010, doi: 10.1016/j.neuroimage.2010.05.043.

[39] D. Le Bihan, E. Breton, D. Lallemand, P. Grenier, E. Cabanis, and M. Laval-Jeantet, “MR imaging of intravoxel incoherent motions: application to diffusion and perfusion in neurologic disorders.,” *Radiology*, vol. 161, no. 2, pp. 401–407, Nov. 1986, doi: 10.1148/radiology.161.2.3763909.

[40] P. J. Basser, J. Mattiello, and D. Lebihan, “Estimation of the Effective Self-Diffusion Tensor from the NMR Spin Echo,” *J. Magn. Reson. Ser. B*, vol. 103, no. 3, pp. 247–254, 1994, doi: https://doi.org/10.1006/jmrb.1994.1037.

[41] P. J. Basser, J. Mattiello, and D. LeBihan, “MR diffusion tensor spectroscopy and imaging.,” *Biophys. J.*, vol. 66, no. 1, pp. 259–267, Jan. 1994, doi: 10.1016/S0006-3495(94)80775-1.

[42] C. Pierpaoli, P. Jezzard, P. J. Basser, A. Barnett, and G. Di Chiro, “Diffusion tensor MR imaging of the human brain.,” *Radiology*, vol. 201, no. 3, pp. 637–648, Dec. 1996, doi: 10.1148/radiology.201.3.8939209.

[43] C. Pierpaoli and P. J. Basser, “Toward a quantitative assessment of diffusion anisotropy.,” *Magn. Reson. Med.*, vol. 36, no. 6, pp. 893–906, Dec. 1996, doi: 10.1002/mrm.1910360612.

[44] L. J. O'Donnell and C.-F. Westin, "An introduction to diffusion tensor image analysis.," *Neurosurg. Clin. N. Am.*, vol. 22, no. 2, pp. 185–96, viii, Apr. 2011, doi: 10.1016/j.nec.2010.12.004.

[45] T. A. G. M. Huisman, "Diffusion-weighted and diffusion tensor imaging of the brain, made easy," *Cancer Imaging*, vol. 10 Spec no, no. 1A, pp. S163–S171, Oct. 2010, doi: 10.1102/1470-7330.2010.9023.

[46] M. D. Budde, M. Xie, A. H. Cross, and S.-K. Song, "Axial diffusivity is the primary correlate of axonal injury in the experimental autoimmune encephalomyelitis spinal cord: a quantitative pixelwise analysis," *J. Neurosci.*, vol. 29, no. 9, pp. 2805–2813, Mar. 2009, doi: 10.1523/JNEUROSCI.4605-08.2009.

[47] T. Engelhorn *et al.*, "Changes of Radial Diffusivity and Fractional Anisotopy in the Optic Nerve and Optic Radiation of Glaucoma Patients," *Sci. World J.*, vol. 2012, p. 849632, 2012, doi: 10.1100/2012/849632.

[48] L. R. Ranzenberger and T. Snyder, "Diffusion Tensor Imaging.," Treasure Island (FL), 2022.

[49] G. P. T. Bosma, T. W. J. Huizinga, S. P. Mooijaart, and M. A. Van Buchem, "Abnormal brain diffusivity in patients with neuropsychiatric systemic lupus erythematosus.," *AJNR. Am. J. Neuroradiol.*, vol. 24, no. 5, pp. 850–854, May 2003.

[50] M. Hughes *et al.*, "Diffusion tensor imaging in patients with acute onset of neuropsychiatric systemic lupus erythematosus: a prospective study of apparent diffusion coefficient, fractional anisotropy values, and eigenvalues in different regions of the brain.," *Acta Radiol.*, vol. 48, no. 2, pp. 213–222, Mar. 2007, doi: 10.1080/02841850601105825.

[51] R. C. Welsh, H. Rahbar, B. Foerster, M. Thurnher, and P. C. Sundgren, "Brain diffusivity in patients with neuropsychiatric systemic lupus erythematosus with new acute neurological symptoms.," *J. Magn. Reson. Imaging*, vol. 26, no. 3, pp. 541–551, Sep. 2007, doi: 10.1002/jmri.21036.

[52] L. Zhang *et al.*, "Diffusion changes in patients with systemic lupus erythematosus.," *Magn. Reson. Imaging*, vol. 25, no. 3, pp. 399–405, Apr. 2007, doi: 10.1016/j.mri.2006.09.037.

[53] B. J. Emmer, J. van der Grond, G. M. Steup-Beekman, T. W. J. Huizinga, and M. A. van Buchem, “Selective involvement of the amygdala in systemic lupus erythematosus,” *PLoS Med.*, vol. 3, no. 12, pp. e499–e499, Dec. 2006, doi: 10.1371/journal.pmed.0030499.

[54] D. S. Tuch, T. G. Reese, M. R. Wiegell, and V. J. Wedeen, “Diffusion MRI of complex neural architecture.,” *Neuron*, vol. 40, no. 5, pp. 885–895, Dec. 2003, doi: 10.1016/s0896-6273(03)00758-x.

[55] S. Mori, B. J. Crain, V. P. Chacko, and P. C. van Zijl, “Three-dimensional tracking of axonal projections in the brain by magnetic resonance imaging.,” *Ann. Neurol.*, vol. 45, no. 2, pp. 265–269, Feb. 1999, doi: 10.1002/1531-8249(199902)45:2<265::aid-ana21>3.0.co;2-3.

[56] G. J. M. Parker, H. A. Haroon, and C. A. M. Wheeler-Kingshott, “A framework for a streamline-based probabilistic index of connectivity (PICo) using a structural interpretation of MRI diffusion measurements.,” *J. Magn. Reson. Imaging*, vol. 18, no. 2, pp. 242–254, Aug. 2003, doi: 10.1002/jmri.10350.

[57] T. E. J. Behrens, H. J. Berg, S. Jbabdi, M. F. S. Rushworth, and M. W. Woolrich, “Probabilistic diffusion tractography with multiple fibre orientations: What can we gain?,” *Neuroimage*, vol. 34, no. 1, pp. 144–155, Jan. 2007, doi: 10.1016/j.neuroimage.2006.09.018.

[58] G. J. M. Parker and D. C. Alexander, “Probabilistic anatomical connectivity derived from the microscopic persistent angular structure of cerebral tissue.,” *Philos. Trans. R. Soc. London. Ser. B, Biol. Sci.*, vol. 360, no. 1457, pp. 893–902, May 2005, doi: 10.1098/rstb.2005.1639.

[59] S. Mori and P. C. M. van Zijl, “Fiber tracking: principles and strategies - a technical review.,” *NMR Biomed.*, vol. 15, no. 7–8, pp. 468–480, 2002, doi: 10.1002/nbm.781.

[60] T. E. Conturo *et al.*, “Tracking neuronal fiber pathways in the living human brain.,” *Proc. Natl. Acad. Sci. U. S. A.*, vol. 96, no. 18, pp. 10422–10427, Aug. 1999, doi: 10.1073/pnas.96.18.10422.

[61] T. E. J. Behrens *et al.*, “Non-invasive mapping of connections between human thalamus and cortex using diffusion imaging,” *Nat. Neurosci.*, vol. 6, no. 7, pp. 750–757, 2003, doi: 10.1038/nn1075.

[62] D. K. Jones, T. R. Knösche, and R. Turner, “White matter integrity, fiber count, and other fallacies: the do’s and don’ts of diffusion MRI.,” *Neuroimage*, vol. 73, pp. 239–254, Jun. 2013, doi: 10.1016/j.neuroimage.2012.06.081.

[63] P. Fillard *et al.*, “Quantitative evaluation of 10 tractography algorithms on a realistic diffusion MR phantom.,” *Neuroimage*, vol. 56, no. 1, pp. 220–234, May 2011, doi: 10.1016/j.neuroimage.2011.01.032.

[64] O. Sporns, G. Tononi, and R. Kötter, “The human connectome: A structural description of the human brain.,” *PLoS Comput. Biol.*, vol. 1, no. 4, p. e42, Sep. 2005, doi: 10.1371/journal.pcbi.0010042.

[65] B. George, “Graph Theory, Konigsberg Problem BT - Encyclopedia of GIS,” S. Shekhar, H. Xiong, and X. Zhou, Eds. Cham: Springer International Publishing, 2015, pp. 1–6.

[66] O. Sporns, “Graph theory methods: applications in brain networks,” *Dialogues Clin. Neurosci.*, vol. 20, no. 2, pp. 111–121, Jun. 2018, doi: 10.31887/DCNS.2018.20.2/osporns.

[67] R. Diestel, “The Basics BT - Graph Theory,” R. Diestel, Ed. Berlin, Heidelberg: Springer Berlin Heidelberg, 2017, pp. 1–34.

[68] A. Fornito, A. Zalesky, and E. T. B. T.-F. of B. N. A. Bullmore, Eds., “Chapter 4 - Node Degree and Strength,” San Diego: Academic Press, 2016, pp. 115–136.

[69] O. Sporns, “Structure and function of complex brain networks.,” *Dialogues Clin. Neurosci.*, vol. 15, no. 3, pp. 247–262, Sep. 2013, doi: 10.31887/DCNS.2013.15.3/osporns.

[70] P. Babaeeghazvini, L. M. Rueda-Delgado, J. Gooijers, S. P. Swinnen, and A. Daffertshofer, “Brain Structural and Functional Connectivity: A Review of Combined Works of Diffusion Magnetic Resonance Imaging and Electro-Encephalography ,” *Frontiers in Human Neuroscience* , vol. 15. 2021, [Online]. Available: https://www.frontiersin.org/article/10.3389/fnhum.2021.721206.

[71] D. S. Bassett and E. T. Bullmore, “Human brain networks in health and disease.,” *Curr. Opin. Neurol.*, vol. 22, no. 4, pp. 340–347, Aug. 2009, doi:

10.1097/WCO.0b013e32832d93dd.

[72] M. Rubinov and O. Sporns, “Complex network measures of brain connectivity: uses and interpretations.,” *Neuroimage*, vol. 52, no. 3, pp. 1059–1069, Sep. 2010, doi: 10.1016/j.neuroimage.2009.10.003.

[73] M. J. Paldino, W. Zhang, Z. D. Chu, and F. Golriz, “Metrics of brain network architecture capture the impact of disease in children with epilepsy,” *NeuroImage. Clin.*, vol. 13, pp. 201–208, Dec. 2016, doi: 10.1016/j.nicl.2016.12.005.

[74] M. L. Stanley, S. L. Simpson, D. Dagenbach, R. G. Lyday, J. H. Burdette, and P. J. Laurienti, “Changes in brain network efficiency and working memory performance in aging,” *PLoS One*, vol. 10, no. 4, pp. e0123950–e0123950, Apr. 2015, doi: 10.1371/journal.pone.0123950.

[75] N. Masuda, M. Sakaki, T. Ezaki, and T. Watanabe, “Clustering Coefficients for Correlation Networks,” *Front. Neuroinform.*, vol. 12, p. 7, Mar. 2018, doi: 10.3389/fninf.2018.00007.

[76] E. Bullmore and O. Sporns, “Complex brain networks: graph theoretical analysis of structural and functional systems.,” *Nat. Rev. Neurosci.*, vol. 10, no. 3, pp. 186–198, Mar. 2009, doi: 10.1038/nrn2575.

[77] H. Kwon, Y.-H. Choi, and J.-M. Lee, “A Physarum Centrality Measure of the Human Brain Network,” *Sci. Rep.*, vol. 9, no. 1, p. 5907, 2019, doi: 10.1038/s41598-019-42322-7.

[78] M. E. J. Newman, “Assortative Mixing in Networks,” *Phys. Rev. Lett.*, vol. 89, no. 20, p. 208701, Oct. 2002, doi: 10.1103/PhysRevLett.89.208701.

[79] K. E. Joyce, P. J. Laurienti, J. H. Burdette, and S. Hayasaka, “A new measure of centrality for brain networks,” *PLoS One*, vol. 5, no. 8, pp. e12200–e12200, Aug. 2010, doi: 10.1371/journal.pone.0012200.

[80] C. C. Hilgetag and M. Kaiser, “Clustered organization of cortical connectivity.,” *Neuroinformatics*, vol. 2, no. 3, pp. 353–360, 2004, doi: 10.1385/NI:2:3:353.

[81] O. Sporns, C. J. Honey, and R. Kötter, “Identification and classification of hubs

in brain networks.," *PLoS One*, vol. 2, no. 10, p. e1049, Oct. 2007, doi: 10.1371/journal.pone.0001049.

[82] M. P. van den Heuvel and O. Sporns, "Rich-club organization of the human connectome.," *J. Neurosci.*, vol. 31, no. 44, pp. 15775–15786, Nov. 2011, doi: 10.1523/JNEUROSCI.3539-11.2011.

[83] D. Wahlstrom, K. C. Breaux, J. Zhu, and L. G. Weiss, "the Wechsler Intelligence Scale for Children—Fourth Edition," *Contemporary intellectual assessment: Theories, tests, and issues,The Guilford Press.*, pp. 224–248, 2012.

[84] I. S. Baron, "Test review: Wechsler Intelligence Scale for Children-Fourth Edition (WISC-IV).," *Child Neuropsychol. a J. Norm. Abnorm. Dev. Child. Adolesc.*, vol. 11, no. 5, pp. 471–475, Oct. 2005, doi: 10.1080/09297040590951587.

[85] M. C. Hochberg, "Updating the American College of Rheumatology revised criteria for the classification of systemic lupus erythematosus.," *Arthritis and rheumatism*, vol. 40, no. 9. United States, p. 1725, Sep. 1997, doi: 10.1002/art.1780400928.

[86] J. L. R. Andersson and S. N. Sotiropoulos, "An integrated approach to correction for off-resonance effects and subject movement in diffusion MR imaging.," *Neuroimage*, vol. 125, pp. 1063–1078, Jan. 2016, doi: 10.1016/j.neuroimage.2015.10.019.

[87] A. Leemans and D. K. Jones, "The B-matrix must be rotated when correcting for subject motion in DTI data.," *Magn. Reson. Med.*, vol. 61, no. 6, pp. 1336–1349, Jun. 2009, doi: 10.1002/mrm.21890.

[88] E. O. Stejskal and J. E. Tanner, "Spin Diffusion Measurements: Spin Echoes in the Presence of a Time-Dependent Field Gradient," *J. Chem. Phys.*, vol. 42, no. 1, pp. 288–292, Jan. 1965, doi: 10.1063/1.1695690.

[89] F. Yeh, "DSI Studio," Jun. 2021, doi: 10.5281/ZENODO.4978980.

[90] F.-C. Yeh and W.-Y. I. Tseng, "NTU-90: a high angular resolution brain atlas constructed by q-space diffeomorphic reconstruction.," *Neuroimage*, vol. 58, no. 1, pp. 91–99, Sep. 2011, doi: 10.1016/j.neuroimage.2011.06.021.

[91] F.-C. Yeh, V. J. Wedeen, and W.-Y. I. Tseng, “Generalized q-sampling imaging.,” *IEEE Trans. Med. Imaging*, vol. 29, no. 9, pp. 1626–1635, Sep. 2010, doi: 10.1109/TMI.2010.2045126.

[92] F. C. Yeh, T. D. Verstynen, Y. Wang, J. C. Fernández-Miranda, and W. Y. I. Tseng, “Deterministic diffusion fiber tracking improved by quantitative anisotropy,” *PLoS One*, 2013, doi: 10.1371/journal.pone.0080713.

[93] P. J. Basser, S. Pajevic, C. Pierpaoli, J. Duda, and A. Aldroubi, “In vivo fiber tractography using DT-MRI data.,” *Magn. Reson. Med.*, vol. 44, no. 4, pp. 625–632, Oct. 2000, doi: 10.1002/1522-2594(200010)44:4<625::aid-mrm17>3.0.co;2-o.

[94] O. Sporns and C. J. Honey, “The human connectome: a structural description of the human brain, volume 1,” *Proc. Natl. Acad. Sci. U. S. A.*, vol. 103, no. 51, pp. 19219–19220, Dec. 2006, doi: 10.1073/pnas.0609523103.

[95] D. S. Bassett and E. Bullmore, “Small-world brain networks.,” *Neurosci. a Rev. J. bringing Neurobiol. Neurol. psychiatry*, vol. 12, no. 6, pp. 512–523, Dec. 2006, doi: 10.1177/1073858406293182.

[96] T. Rstudio, “RStudio: Integrated Development for R.,” *Rstudio Team, PBC, Boston, MA URL http://www.rstudio.com/*. 2020, doi: 10.1145/3132847.3132886.

[97] L. Pessoa, “On the relationship between emotion and cognition.,” *Nat. Rev. Neurosci.*, vol. 9, no. 2, pp. 148–158, Feb. 2008, doi: 10.1038/nrn2317.

[98] E. Bullmore and O. Sporns, “The economy of brain network organization.,” *Nat. Rev. Neurosci.*, vol. 13, no. 5, pp. 336–349, Apr. 2012, doi: 10.1038/nrn3214.

[99] O. Sporns, G. Tononi, and G. M. Edelman, “Theoretical neuroanatomy: relating anatomical and functional connectivity in graphs and cortical connection matrices.,” *Cereb. Cortex*, vol. 10, no. 2, pp. 127–141, Feb. 2000, doi: 10.1093/cercor/10.2.127.

[100] Y. He *et al.*, “Impaired small-world efficiency in structural cortical networks in multiple sclerosis associated with white matter lesion load.,” *Brain*, vol. 132, no. Pt 12, pp. 3366–3379, Dec. 2009, doi: 10.1093/brain/awp089.

[101] K. Supekar, M. Musen, and V. Menon, “Development of large-scale functional brain networks in children.,” *PLoS Biol.*, vol. 7, no. 7, p. e1000157, Jul. 2009, doi: 10.1371/journal.pbio.1000157.

[102] M. Xu *et al.*, “Alterations of white matter structural networks in patients with non-neuropsychiatric systemic lupus erythematosus identified by probabilistic tractography and connectivity-based analyses.,” *NeuroImage. Clin.*, vol. 13, pp. 349–360, 2017, doi: 10.1016/j.nicl.2016.12.021.

[103] V. Latora and M. Marchiori, “Efficient behavior of small-world networks.,” *Phys. Rev. Lett.*, vol. 87, no. 19, p. 198701, Nov. 2001, doi: 10.1103/PhysRevLett.87.198701.

[104] J. A. Mikdashi, “Altered functional neuronal activity in neuropsychiatric lupus: A systematic review of the fMRI investigations.,” *Semin. Arthritis Rheum.*, vol. 45, no. 4, pp. 455–462, Feb. 2016, doi: 10.1016/j.semarthrit.2015.08.002.

[105] O. Sporns and J. D. Zwi, “The small world of the cerebral cortex.,” *Neuroinformatics*, vol. 2, no. 2, pp. 145–162, 2004, doi: 10.1385/NI:2:2:145.

[106] E. Ercan *et al.*, “A multimodal MRI approach to identify and characterize microstructural brain changes in neuropsychiatric systemic lupus erythematosus,” *NeuroImage Clin.*, vol. 8, pp. 337–344, 2015, doi: https://doi.org/10.1016/j.nicl.2015.05.002.

[107] R. Mina and H. I. Brunner, “Pediatric lupus--are there differences in presentation, genetics, response to therapy, and damage accrual compared with adult lupus?,” *Rheum. Dis. Clin. North Am.*, vol. 36, no. 1, pp. 53–80, vii–viii, Feb. 2010, doi: 10.1016/j.rdc.2009.12.012.

[108] M. Mackay, C. C. Tang, and A. Vo, “Advanced neuroimaging in neuropsychiatric systemic lupus erythematosus.,” *Curr. Opin. Neurol.*, vol. 33, no. 3, pp. 353–361, Jun. 2020, doi: 10.1097/WCO.0000000000000822.

[109] A. Kamali, A. E. Flanders, J. Brody, J. V Hunter, and K. M. Hasan, “Tracing superior longitudinal fasciculus connectivity in the human brain using high resolution diffusion tensor tractography.,” *Brain Struct. Funct.*, vol. 219, no. 1, pp. 269–281, Jan. 2014, doi: 10.1007/s00429-012-0498-y.

[110] P. S. Goldman-Rakic, “Motor control function of the prefrontal cortex.,” *Ciba*

*Found. Symp.*, vol. 132, pp. 187–200, 1987, doi: 10.1002/9780470513545.ch12.

[111] M. A. Rocca *et al.*, "An fMRI study of the motor system in patients with neuropsychiatric systemic lupus erythematosus," *Neuroimage*, vol. 30, no. 2, pp. 478–484, 2006, doi: https://doi.org/10.1016/j.neuroimage.2005.09.047.

[112] Y. E. Cohen and R. A. Andersen, "A common reference frame for movement plans in the posterior parietal cortex," *Nat. Rev. Neurosci.*, vol. 3, no. 7, pp. 553–562, 2002, doi: 10.1038/nrn873.

[113] B. Audoin *et al.*, "Structure of WM bundles constituting the working memory system in early multiple sclerosis: a quantitative DTI tractography study.," *Neuroimage*, vol. 36, no. 4, pp. 1324–1330, Jul. 2007, doi: 10.1016/j.neuroimage.2007.04.038.

[114] J. Xu *et al.*, "White-matter volume reduction and the protective effect of immunosuppressive therapy in systemic lupus erythematosus patients with normal appearance by conventional magnetic resonance imaging.," *J. Rheumatol.*, vol. 37, no. 5, pp. 974–986, May 2010, doi: 10.3899/jrheum.090967.

[115] L. Podrazilová *et al.*, "Magnetic resonance volumetry of pathological brain foci in patients with systemic lupus erythematosus.," *Clin. Exp. Rheumatol.*, vol. 26, no. 4, pp. 604–610, 2008.